材料电热输运计算原理、方法及热电应用

杨炯

jiongy@t.shu.edu.cn

上海大学

材料基因组工程研究院

个人经历

教育经历：

华东师范大学化学系　　化学 学士学位　　09/2000-07/2004

中国科学院上海硅酸盐研究所

材料科学与工程 博士学位 （导师：张文清） 08/2004-07/2009

工作经历：

中国科学院上海硅酸盐研究所　　助理研究员　　08/2009-01/2012

美国华盛顿大学 材料科学与工程系　　博士后　　02/2012-04/2015

上海大学 材料基因组工程研究院　　教授　　05/2015-

热电材料应用 —发电

热电偶

野外应急灯

汽车电座椅加热

……

余（废）热回收

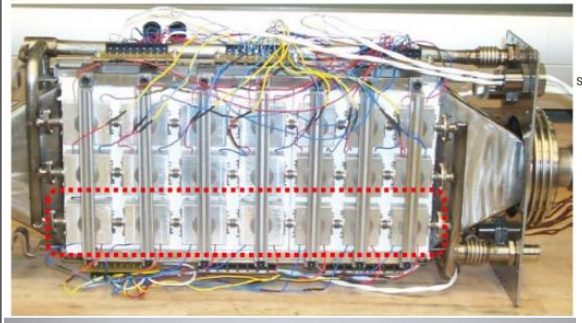

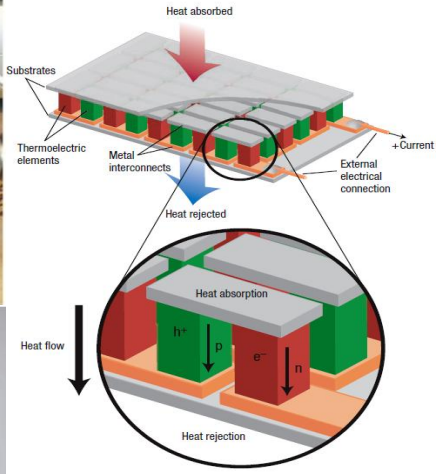

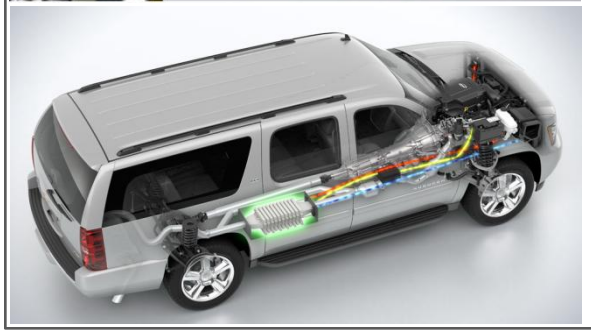

太阳能热电发电

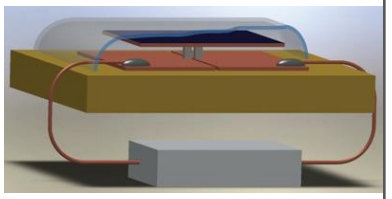

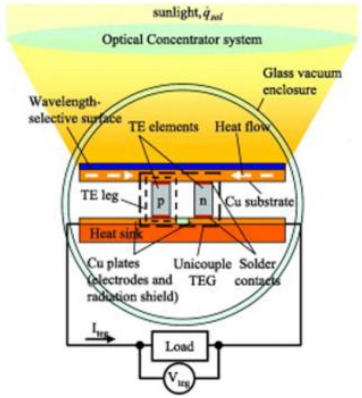

清洁能源

减少环境污染

减少温室效应

热电材料应用 —制冷

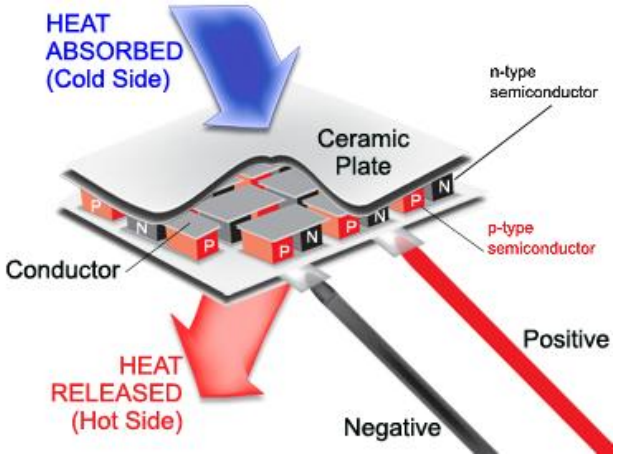

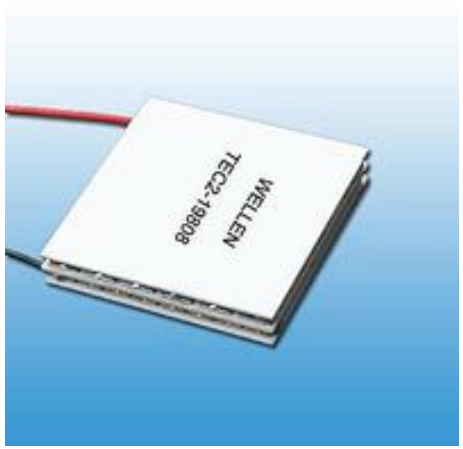

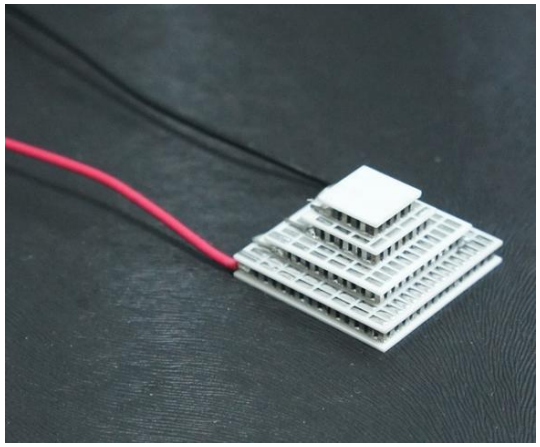

无运动部件

无磨损

无噪音

无污染

体积小

重量轻

结构简单

坚固耐用

热电微观机理

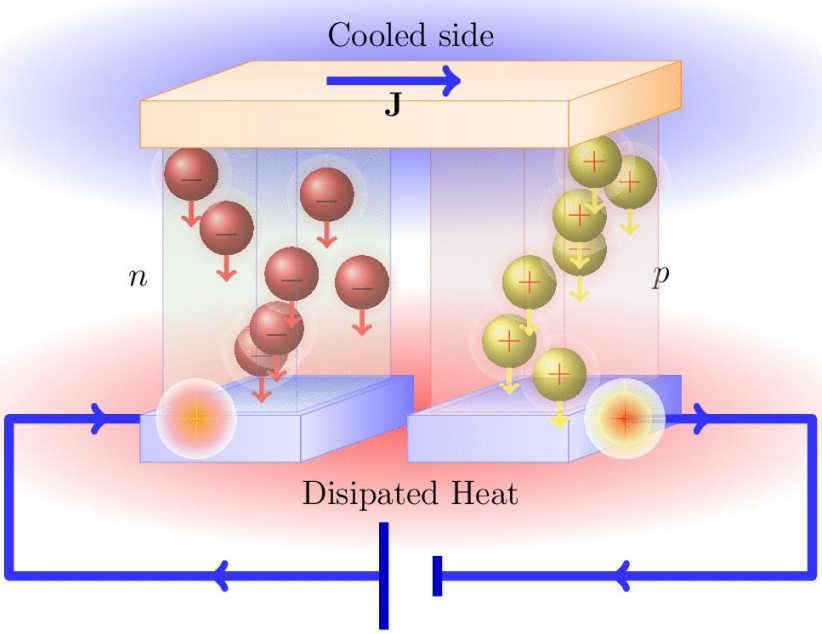

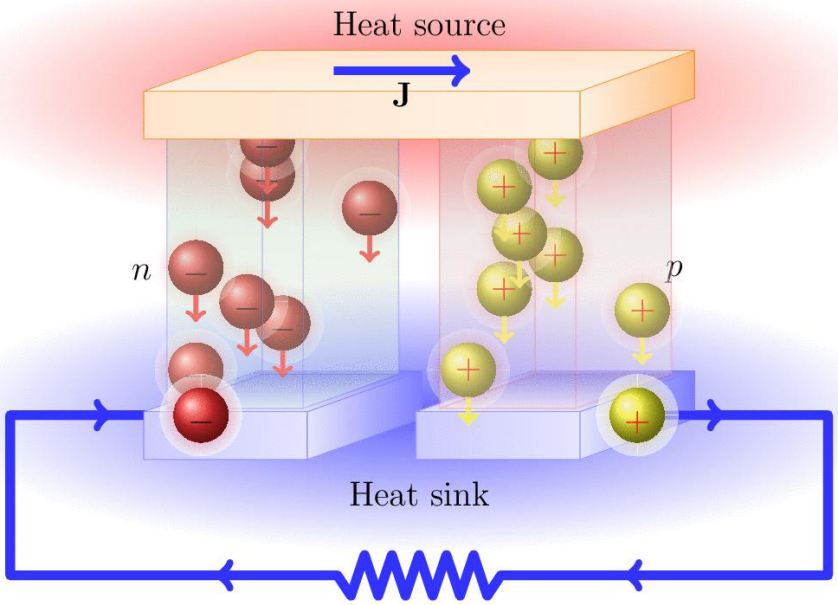

$$ZT = \frac{S^2 \sigma T}{\kappa}$$

$$\kappa = \kappa_e + \kappa_L \qquad \kappa_e = L\sigma T$$

电输运性质

- 电输运理论及概念理解
- 电输运及相关程序使用
- 电输运计算的应用

材料的电导率

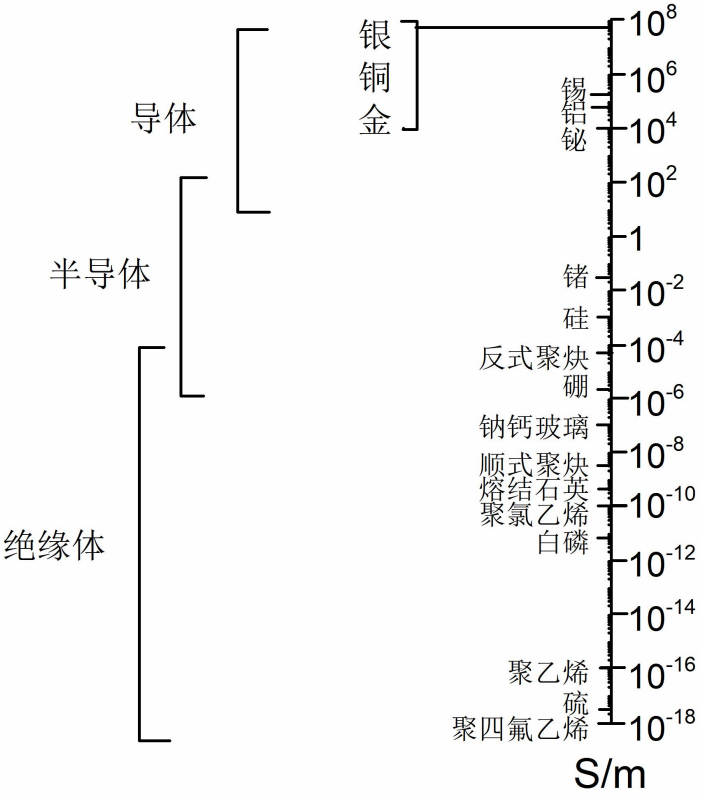

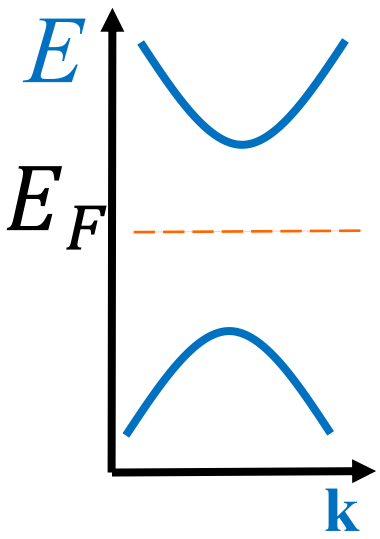

绝缘体

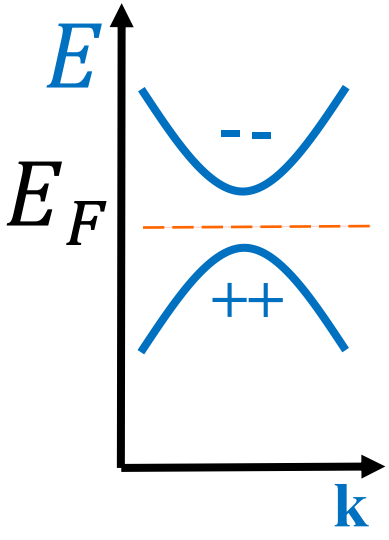

半导体

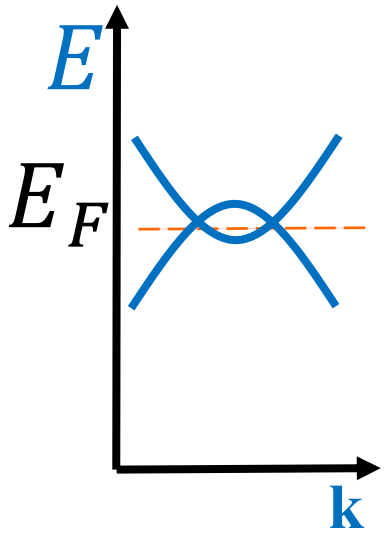

金属

电荷传输理论模型

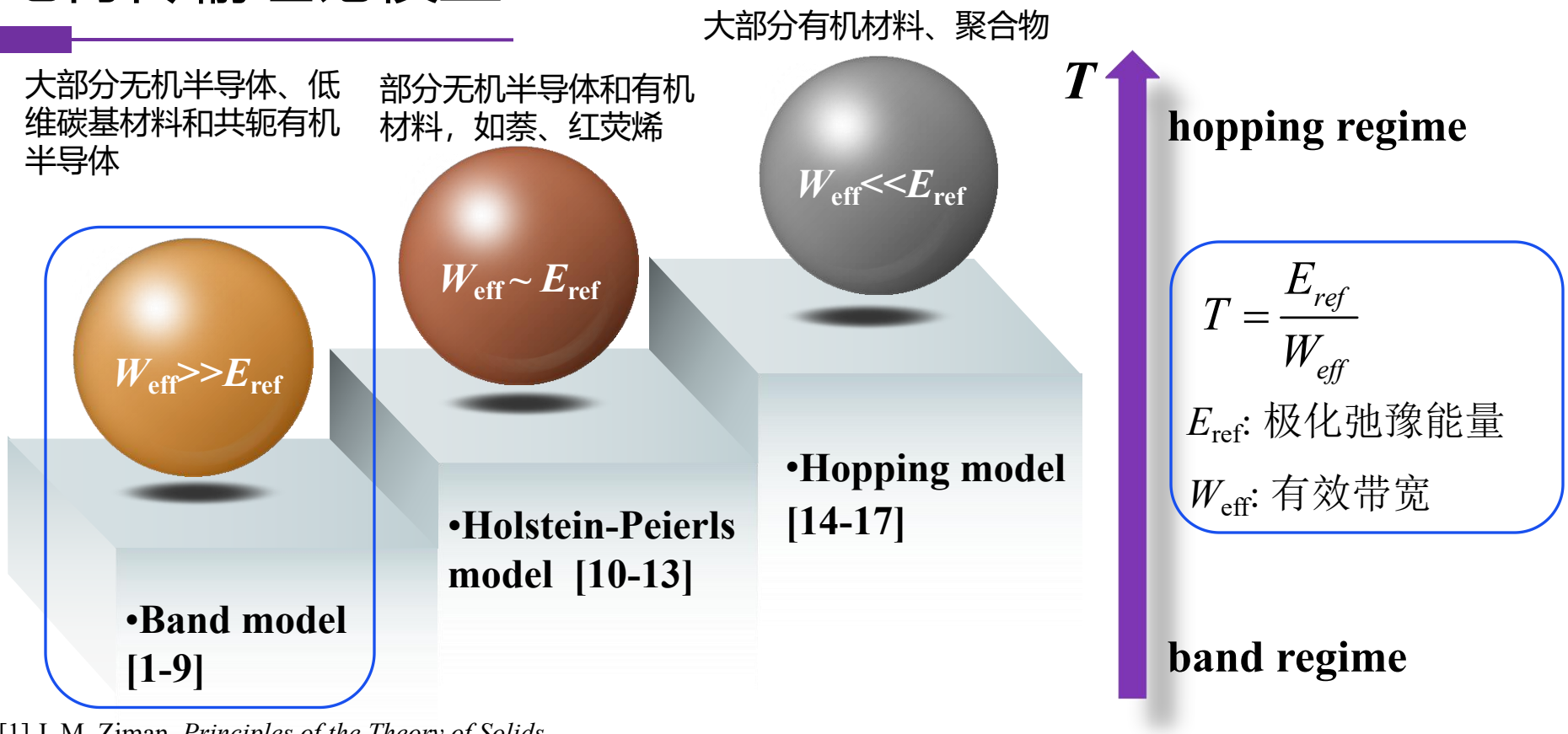

[1] J. M. Ziman, *Principles of the Theory of Solids* (Cambridge University, London, 2nd, 1972);
[2] M. Q. Long *et al, J. Am. Chem. Soc*., 2009, **131**, 17728-17729;
[3] M. Q. Long *et al*, *ACS Nano*, 2011, **5**, 2593-2600;
[4] J. M. Chen *et al*, *J. Phys. Chem. Lett*., 2013, **4**, 1443;
[5] J. E. Northrup, *Appl. Phys. Lett*., 2011, **99**, 62111–62113;
[6] G. Wang and Y. Huang, *J. Phys. Chem. Solids*, 2007, **68**, 2003–2007;
[7] L. Tang *et al*, *Sci. China, Ser. B: Chem*., 2009, **52**, 1646–1652;
[8] J. Y. Xi *et al*, *Nanoscale*, 2012, **4**, 4348-4369;
[9] W. Shi *et al*, Chem. Mater., 2014, 26, 2669-2677;
[10] T. Holstein, *Ann. Phys*., 1959, **8**, 343–389;
[11] K. Hannewald and P. A. Bobbert, *Phys. Rev. B: Condens. Matter Mater. Phys*., 2004, **69**, 75212;
[12] L. J. Wang *et al, J. Chem. Phys*., 2007, **127**, 044506;
[13] F. Ortmann and S. Roche, *Phys. Rev. B: Condens. Matter Mater. Phys*., 2011, **84**, 180302(R);
[14] H. Bassler, *Phys. Status Solidi B,* 1993, **175**, 15–56;
[15] V. Coropceanu *et al*, *Chem. Rev*., 2007, **107**, 926–952;
[16] G. J. Nan *et al*, *Phys. Rev. B* 2009, **79**, 115203;
[17] L. J. Wang *et al, Chem. Soc. Rev*. 2010, **39**, 423;
[18] Z. G. Shuai *et al*, *Adv. Mater*., 2011, **23**, 1145–1153.

电输运性质的计算公式

$$\sigma = ne\mu$$

$$ZT = \frac{S^2\sigma T}{\kappa}$$

$$\sigma(T) = \frac{1}{\Omega}\int N(\varepsilon)\mathbf{v}^2\tau\left[-\frac{\partial f_0(T,\varepsilon_F)}{\partial\varepsilon}\right]d\varepsilon$$

$$S(T) = \frac{1}{eT\Omega\sigma}\int N(\varepsilon)\mathbf{v}^2\tau\,(\varepsilon_F-\varepsilon)\left[-\frac{\partial f_0(T,\varepsilon_F)}{\partial\varepsilon}\right]d\varepsilon$$

$f_0 = \frac{1}{\exp(\varepsilon-\varepsilon_F)+1}$ 费米-狄拉克分布　　τ 载流子驰豫时间

能带，态密度，波函数

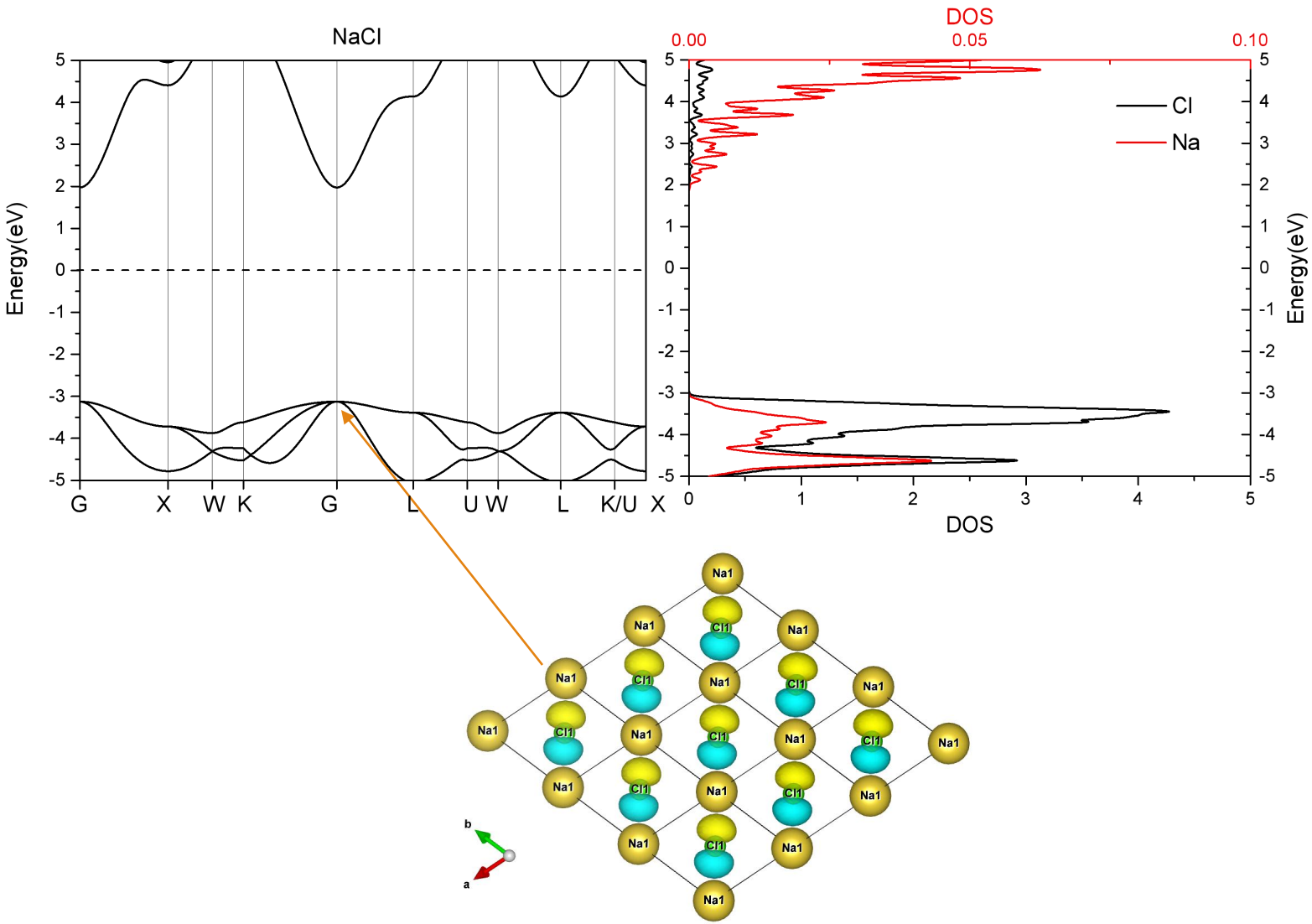
NaCl
Energy(eV)
G
X
W
K
G
L
U
W
L
K/U
X
DOS
0.00
0.05
0.10
Cl
Na
DOS
Energy(eV)
Na1
Cl1
b
a

能带，态密度的关系

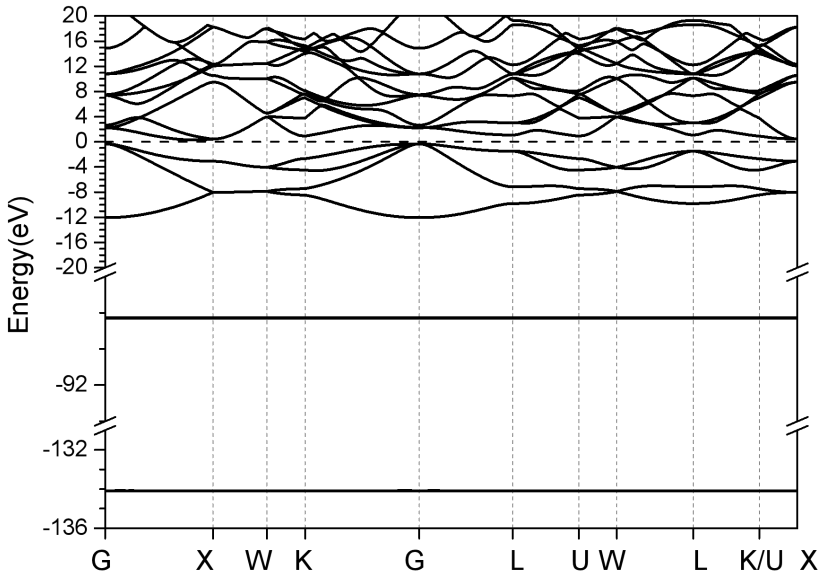

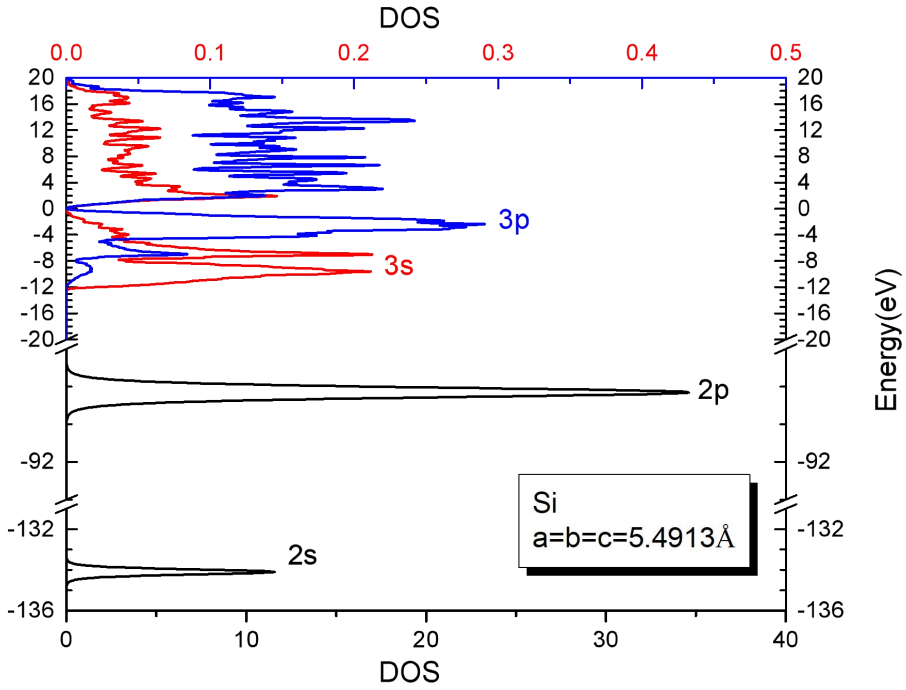

- 能带是倒空间布里渊区一定高对称点之间的原子间相互作用的能量变化关系。并不能代表整个布里渊区的性质。
- 态密度能代表布里渊区整体情况。态密度的积分为电子数。

玻尔兹曼输运理论

$$\sigma = ne\mu$$

$$\sigma = \frac{1}{\Omega}\int N(E)\mathbf{v}^2\tau\left[-\frac{\partial f_0(T,E_F)}{\partial E}\right]dE$$

v 电子群速度

Ω 体积

$N(E)$ 电子态密度

τ 电子驰豫时间，f_0费米-狄拉克分布

乘积变积分，所有电子态参与贡献！

电子态作用范围

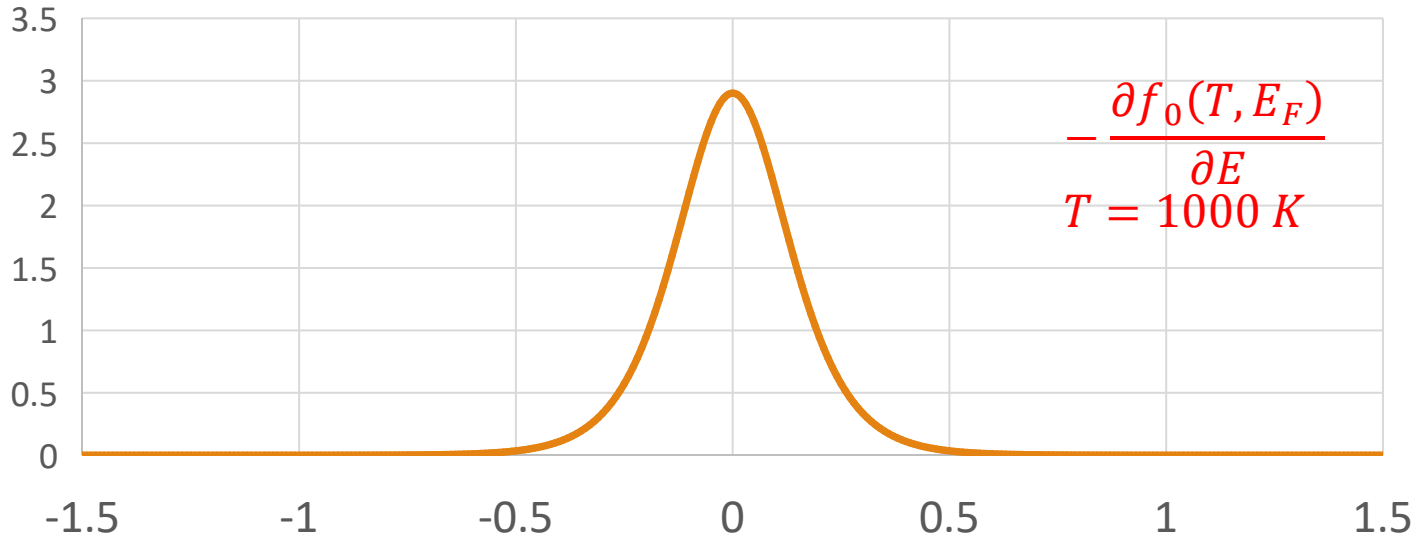

- 仅E_F周围几个k_BT范围的电子态对输运有重要贡献；
- 远离E_F的电子态重要性指数级下降；
- 温度上升有效范围加大 。

金属导电性根源--费米能级处大的费米面

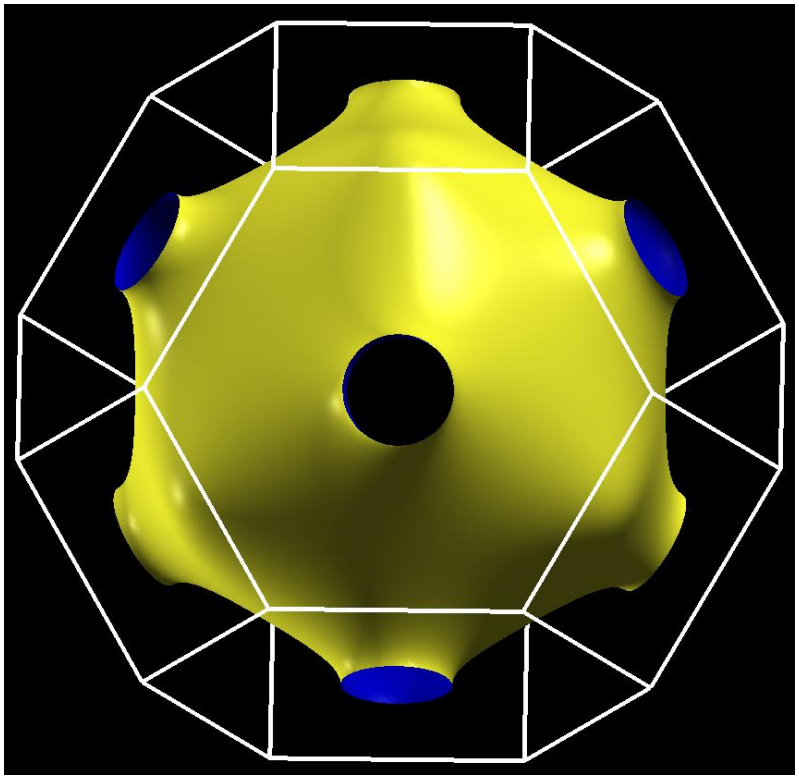

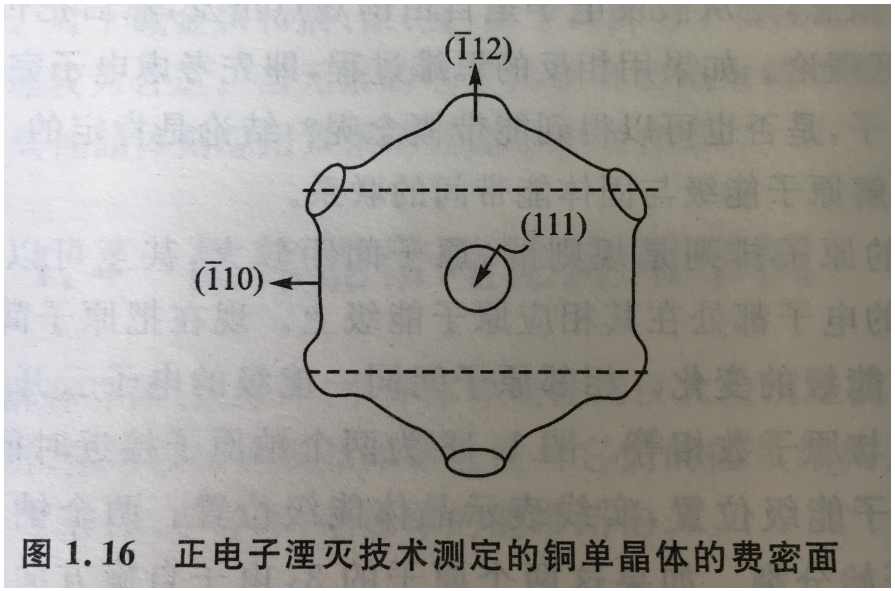

图 1.16　正电子湮灭技术测定的铜单晶体的费密面

金属在E_F周围存在电子态, $N(E_F)>0$, 载流子浓度大

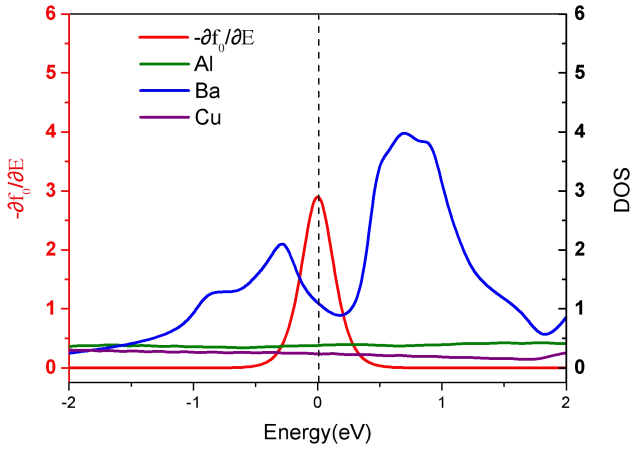

金属，绝缘体，半导体差异

$$\sigma = \frac{1}{\Omega}\int N(E)\mathbf{v}^2\tau\left[-\frac{\partial f_0(T,E_F)}{\partial E}\right]dE \qquad n = \frac{1}{\Omega}\int N(E)\left[-\frac{\partial f_0(T,E_F)}{\partial E}\right]dE$$

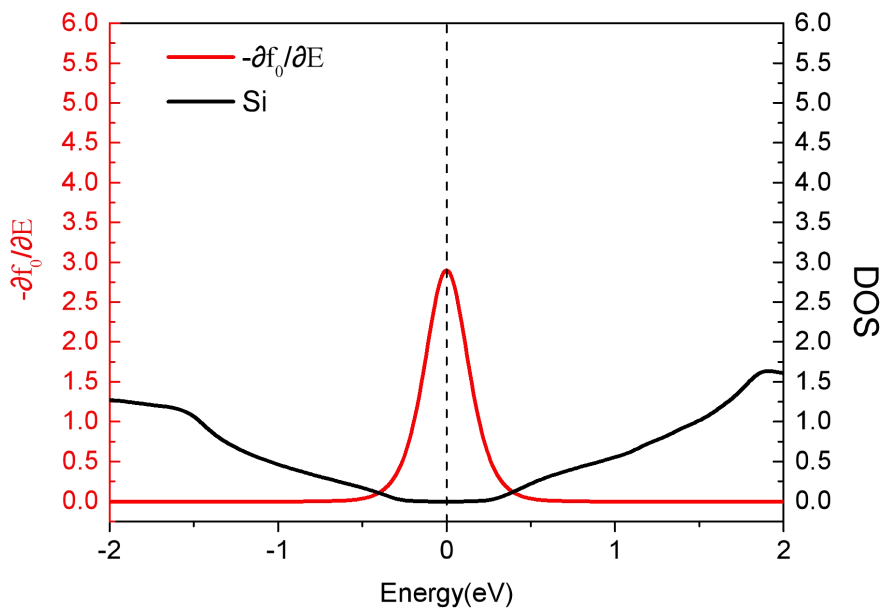

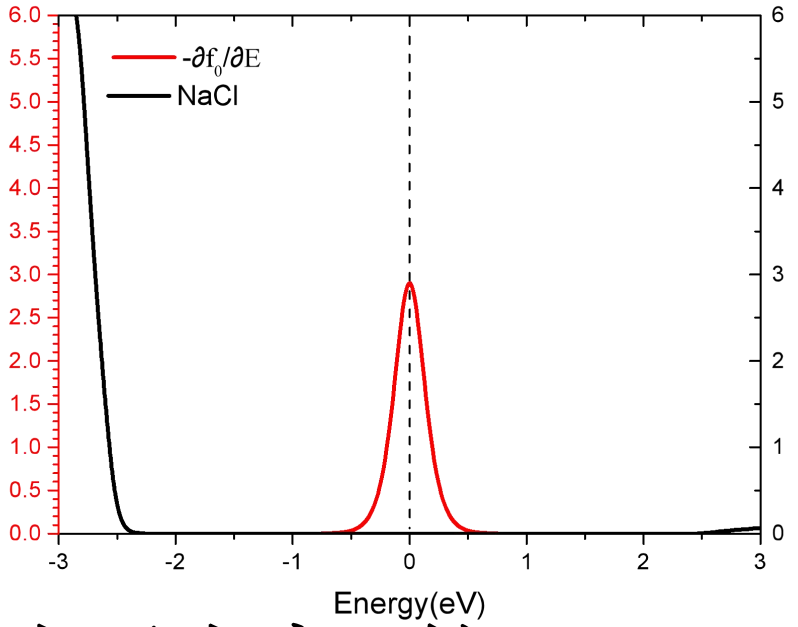

半导体，绝缘体的带边电子态离E_F较远，
决定电导率的电子态随着带隙指数级下降

电子群速度(v)

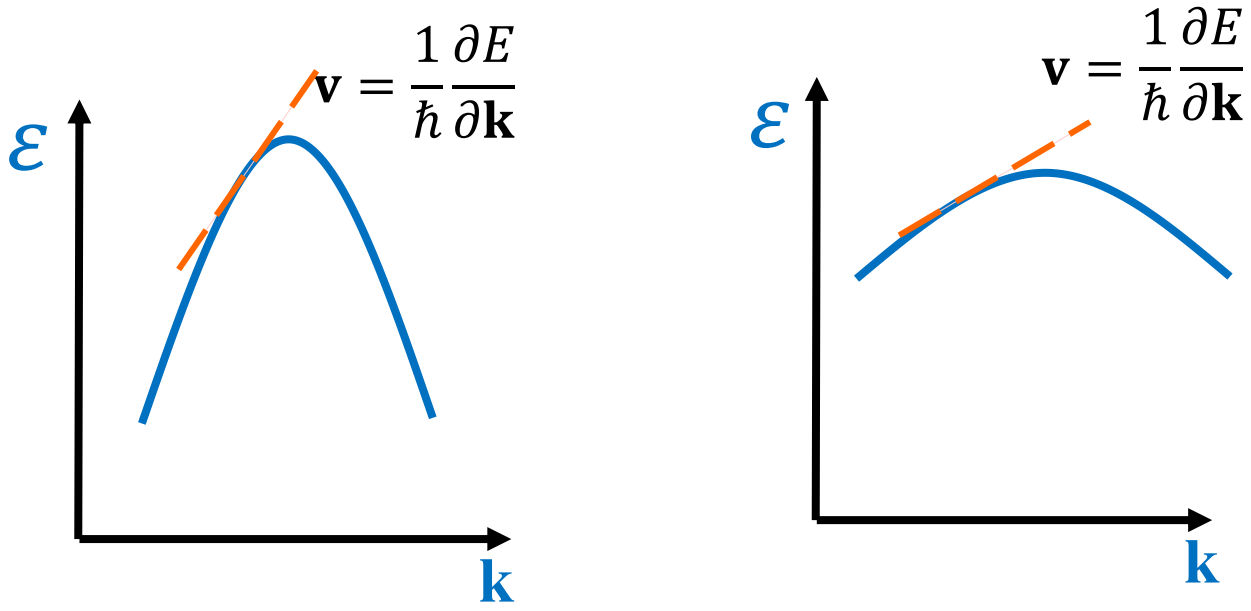

平均电子群速度 10^4~ 10^5 m/s

迁移率与电子驰豫时间

$$\sigma = \frac{1}{\Omega}\int N(E)\mathbf{v}^2\tau\left[-\frac{\partial f_0(T,E_F)}{\partial E}\right]dE \qquad n = \frac{1}{\Omega}\int N(E)\left[-\frac{\partial f_0(T,E_F)}{\partial E}\right]dE$$

$$\mu = \frac{1}{\Omega}\int \mathbf{v}^2\tau\left[-\frac{\partial f_0(T,E_F)}{\partial E}\right]dE \qquad \tau\ 10^{-15}\sim10^{-14}\ s$$

马西森定律(Matthiessen Rule)

$$\frac{1}{\tau_{n\mathbf{k}}} = \frac{1}{\tau_{e-p}} + \frac{1}{\tau_{imp}} + \ldots$$

泽贝克系数相关—载流子浓度优化

$$S(T) = \frac{1}{eT\Omega\sigma}\int N(E)\mathbf{v}^2\tau\,(E_F - E)\left[-\frac{\partial f_0(T,E_F)}{\partial E}\right]dE$$

$$\sigma(T) = \frac{1}{\Omega}\int N(E)\mathbf{v}^2\tau\left[-\frac{\partial f_0(T,E_F)}{\partial E}\right]dE$$

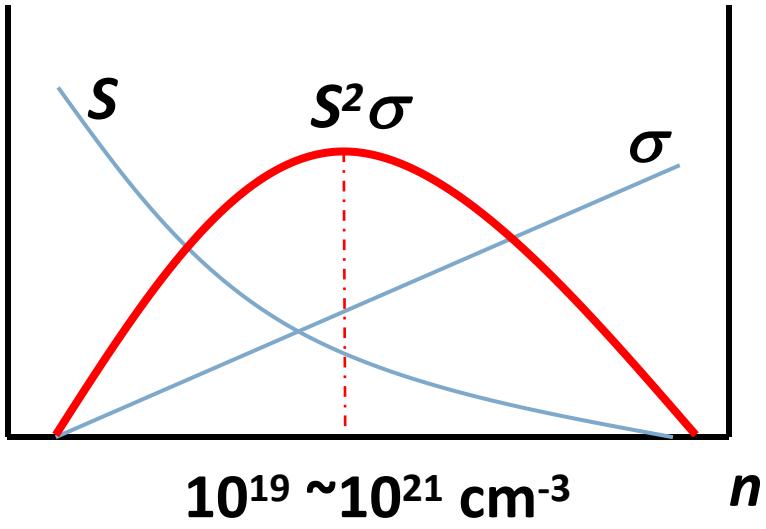

- 载流子浓度优化是热电材料电性能优化最重要的一环

泽贝克系数相关—双极扩散

$$S(T) = \frac{1}{eT\Omega\sigma}\int N(E)\mathbf{v}^2\tau\,(E_F - E)\left[-\frac{\partial f_0(T, E_F)}{\partial E}\right]dE$$

$(E_F - E)$ 决定了Seebeck系数的正负

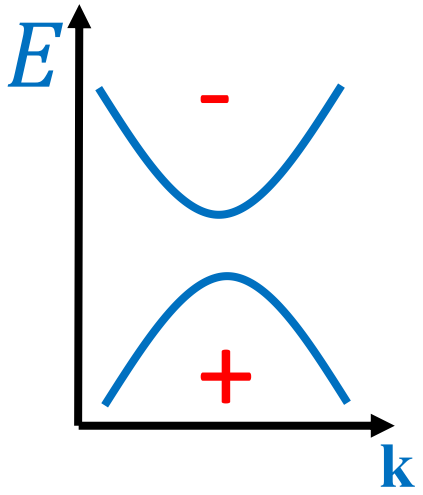

泽贝克系数特点

$$S(T)=\frac{1}{eT\Omega}\frac{\int N(E)\mathbf{v}^2\tau\,(E_F-E)\left[-\dfrac{\partial f_0(T,E_F)}{\partial E}\right]dE}{\int N(E)\mathbf{v}^2\tau\left[-\dfrac{\partial f_0(T,E_F)}{\partial E}\right]dE}$$

Seebeck系数与态密度，群速度，驰豫时间关系不大？

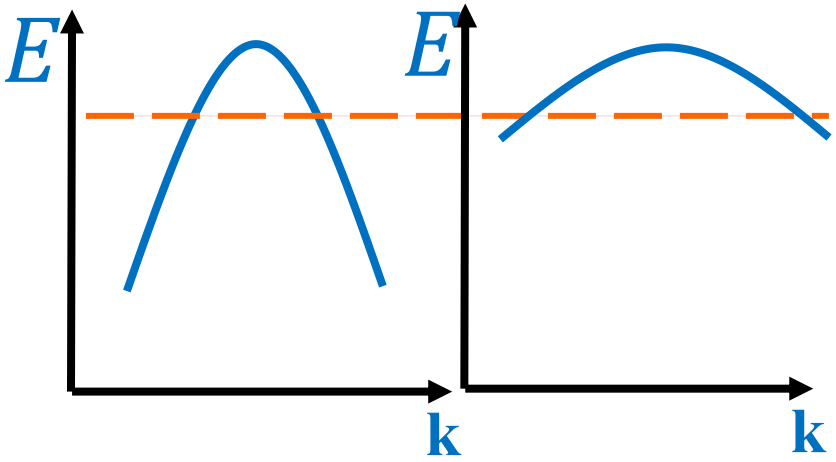

Seebeck系数基本只与费米能级位置有关

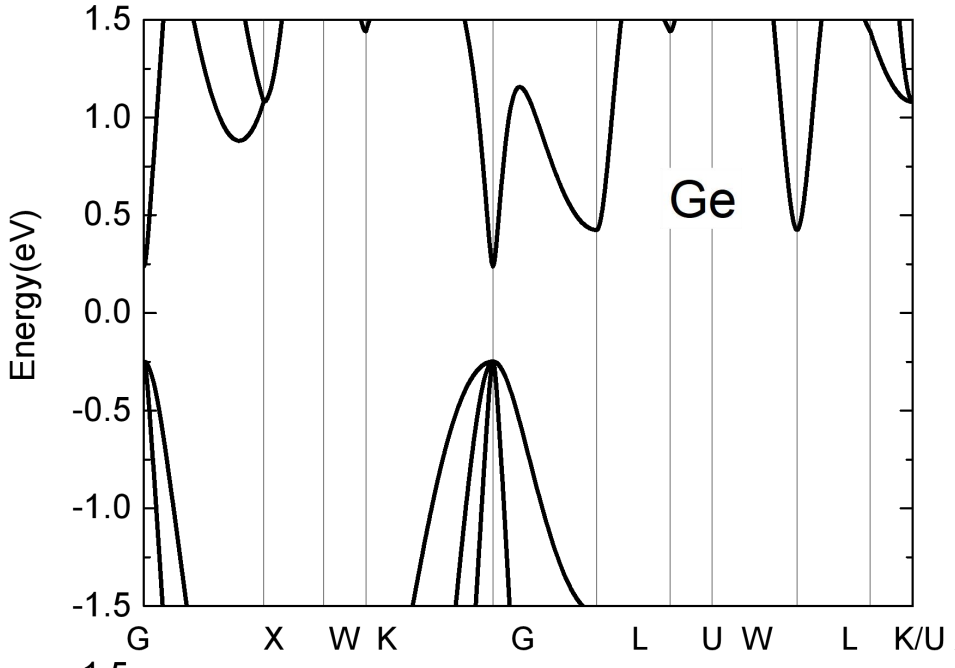
Energy(eV)
1.5
1.0
0.5
0.0
-0.5
-1.0
-1.5
Ge
G
X
W
K
G
L
U
W
L
K/U
X

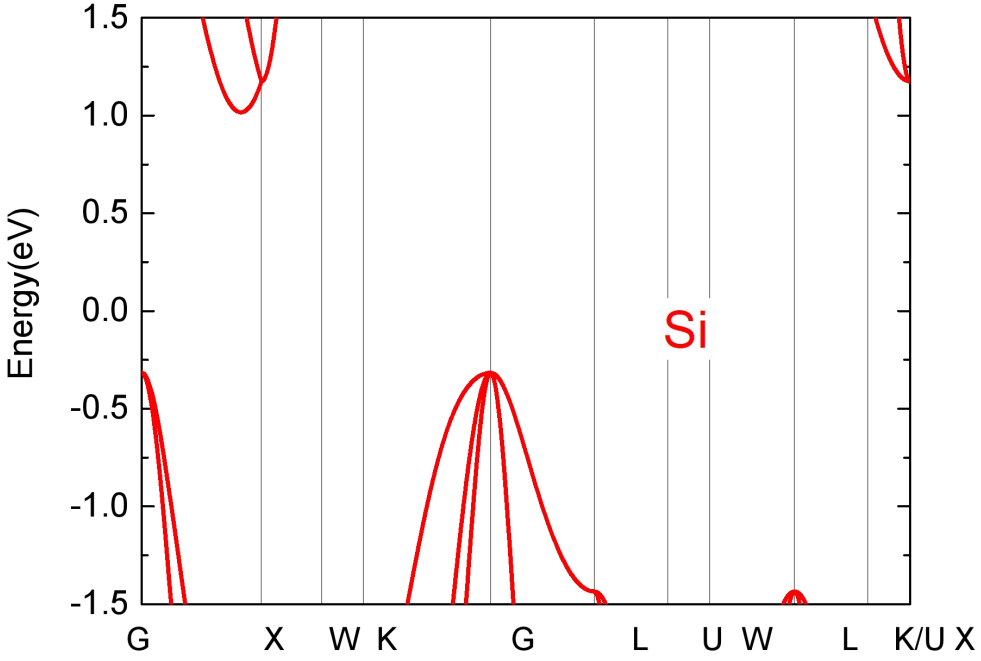
Energy(eV)
1.5
1.0
0.5
0.0
-0.5
-1.0
-1.5
Si
G
X
W
K
G
L
U
W
L
K/U
X

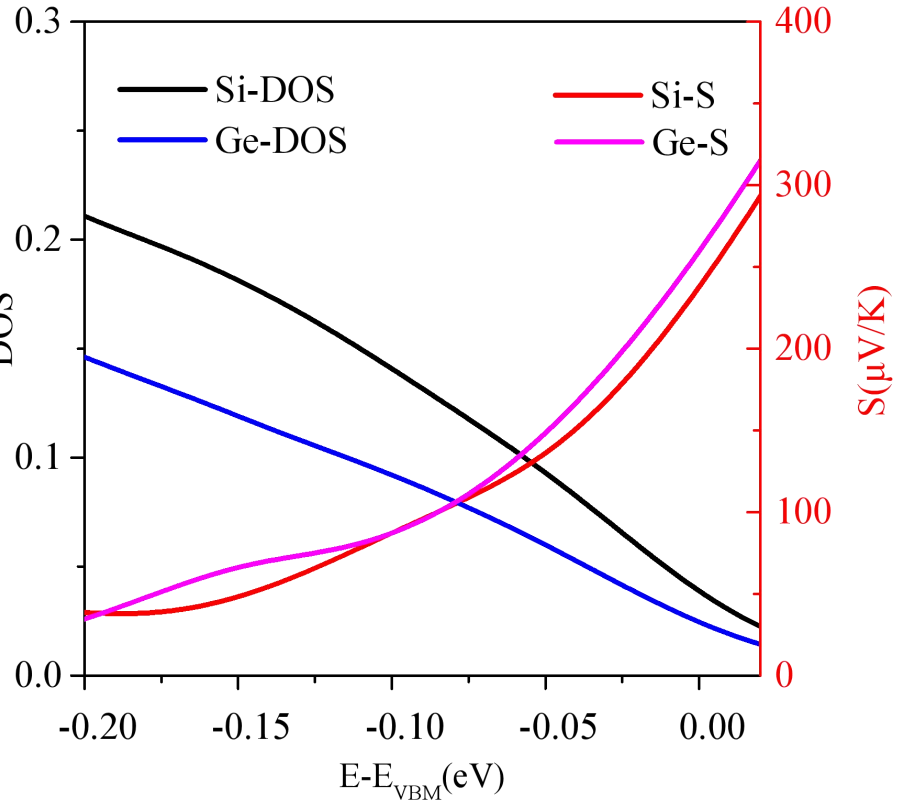
0.3
0.2
0.1
0.0
DOS
400
300
200
100
0
S(μV/K)
Si-DOS
Ge-DOS
Si-S
Ge-S
-0.20
-0.15
-0.10
-0.05
0.00
E-E$_{VBM}$(eV)

能带简并实例--四方黄铜矿

- 四方黄铜矿结构众多（上千），如何筛选？

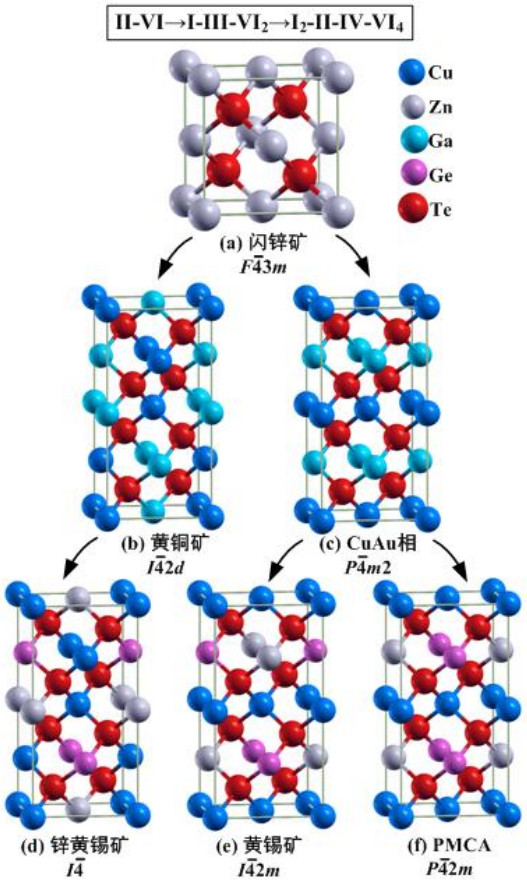

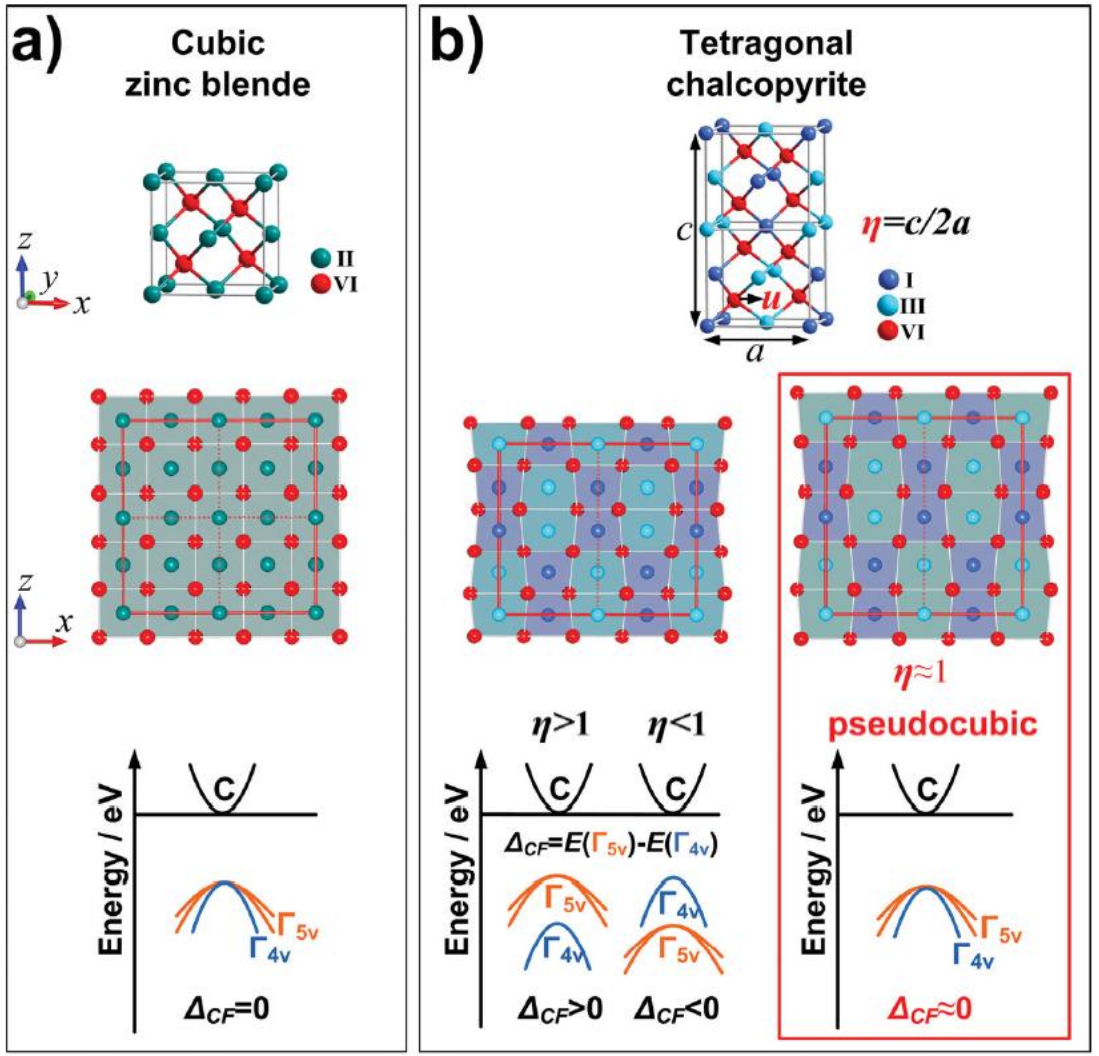

The Unity-η Rule

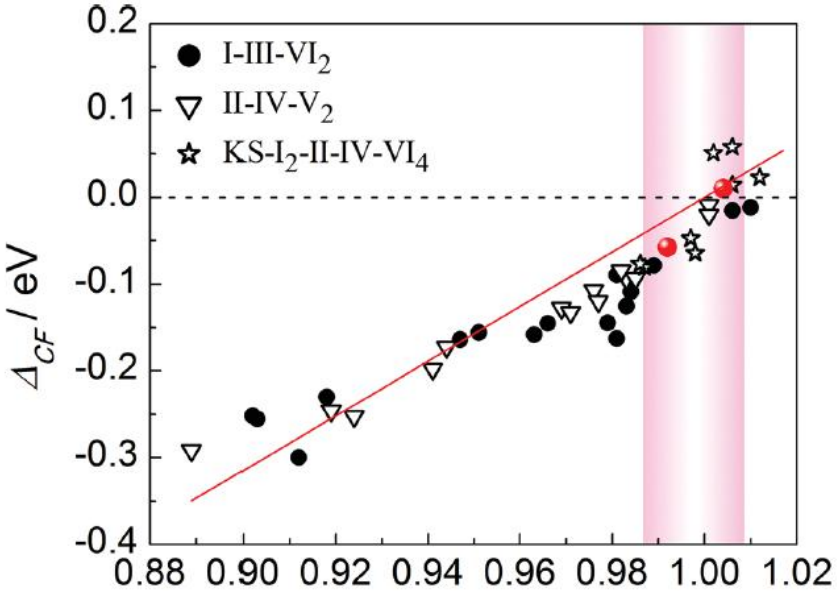

$\eta = c/2a$

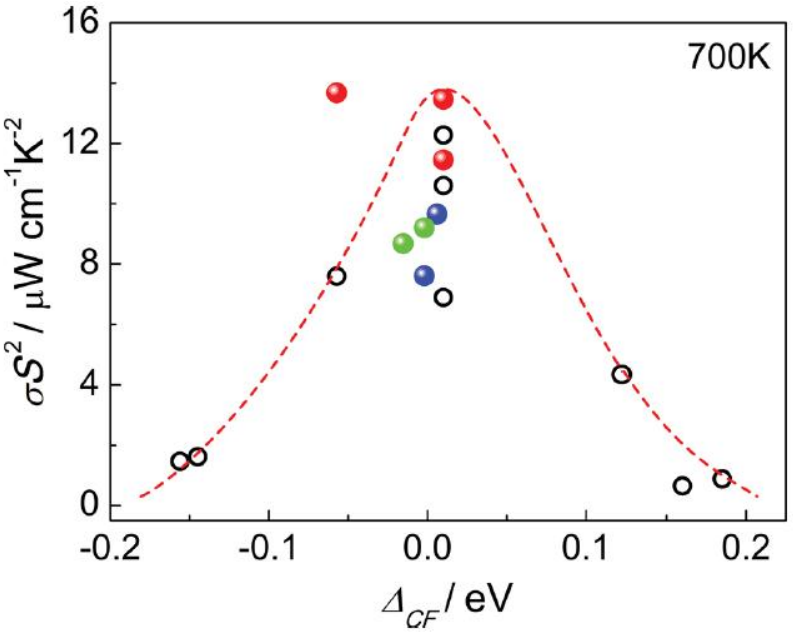

- η=1 对应于最佳的功率因子;
- $CuInTe_2$、$CuGaTe_2$, η~1;
- 如何设计 η~1的体系?

“赝立方设计”: 从非立方结构设计立方结构

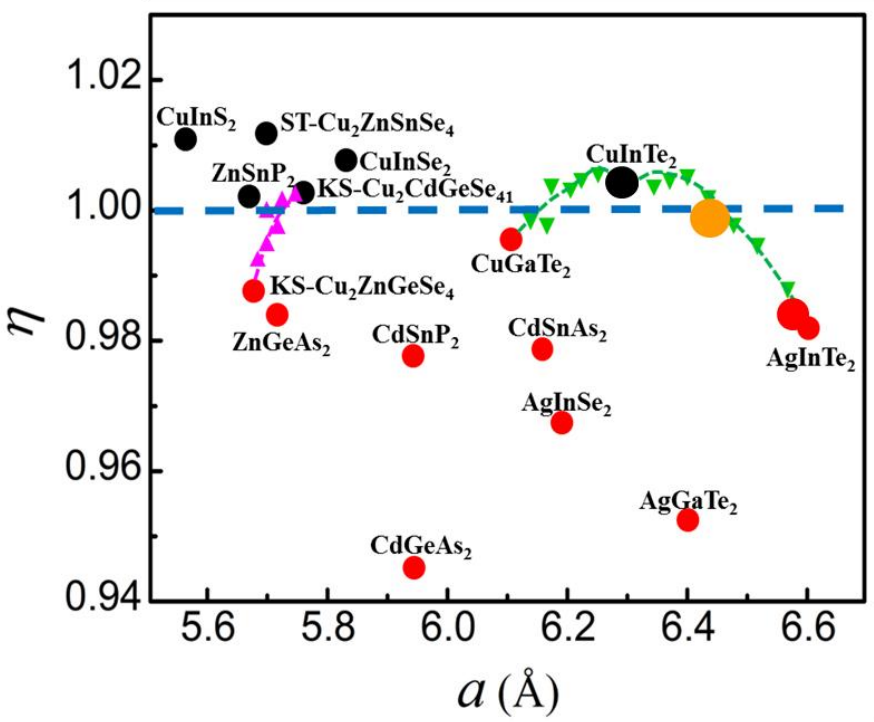

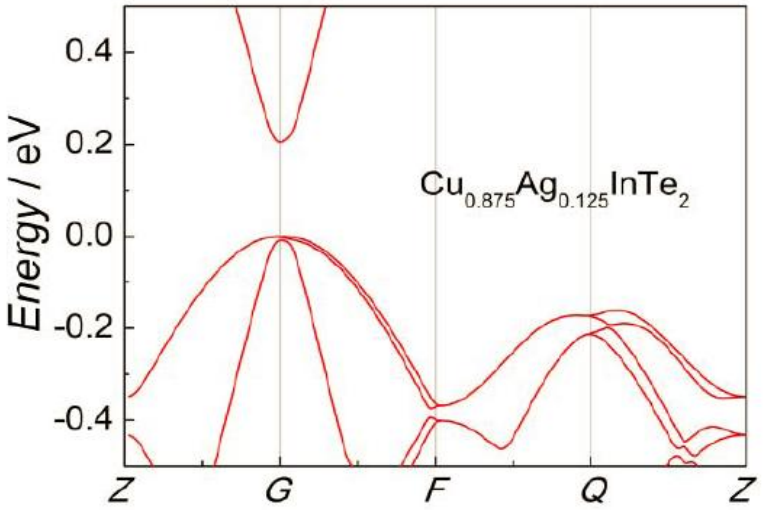

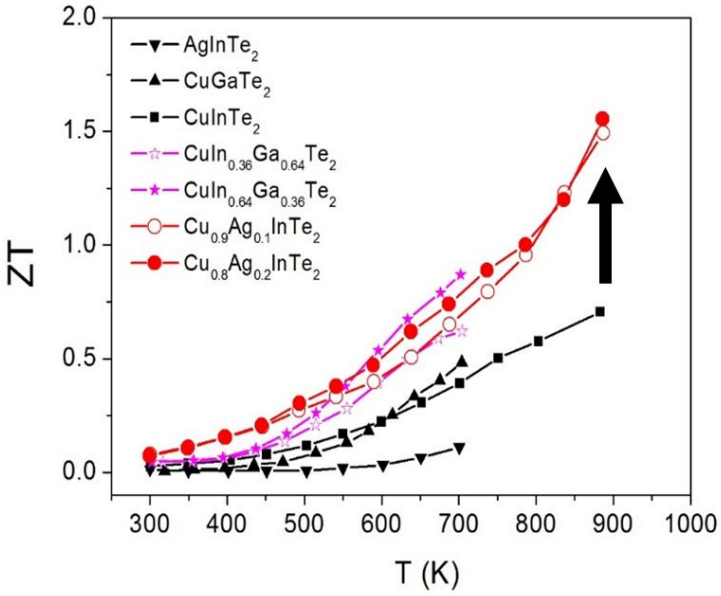

- 赝立方: 把两个非立方的材料结构，使固溶体变成立方结构

J. W. Zhang, W. Zhang, et. al , Adv. Mater. 26, 3848 (2014)

电输运性质

- 电输运理论及概念理解
- 电输运及相关程序使用
- 电输运计算的应用

关键计算参量

密网格的态密度计算E_{nk}

电子群速度v_{nk}

电子驰豫时间τ_{nk}

常见程序

Quantum Espresso （v_{nk} 矩阵元；τ_{nk}精确电声相互作用；无泽贝克等）

BoltzTrap （v_{nk} 能带梯度；τ_{nk}常数驰豫时间；Wien2k & VASP-based）

TransOpt（v_{nk} 能带梯度&矩阵元；τ_{nk}形变势方法，电离杂质散射；QE & VASP-based）

Quantum Espresso

- 精确电声相互作用下的电子驰豫时间；
- 程序不自带泽贝克系数等输运计算；
- 第三方后处理程序可得到输运结果

PHYSICAL REVIEW B **92**, 075405 (2015)

Electrical transport limited by electron-phonon coupling from Boltzmann transport equation: An *ab initio* study of Si, Al, and MoS_2

Wu Li*
Scientific Computing & Modelling NV, De Boelelaan 1083, 1081 HV Amsterdam, The Netherlands
(Received 24 March 2015; published 4 August 2015)

Case study—ZnS, ZnSe

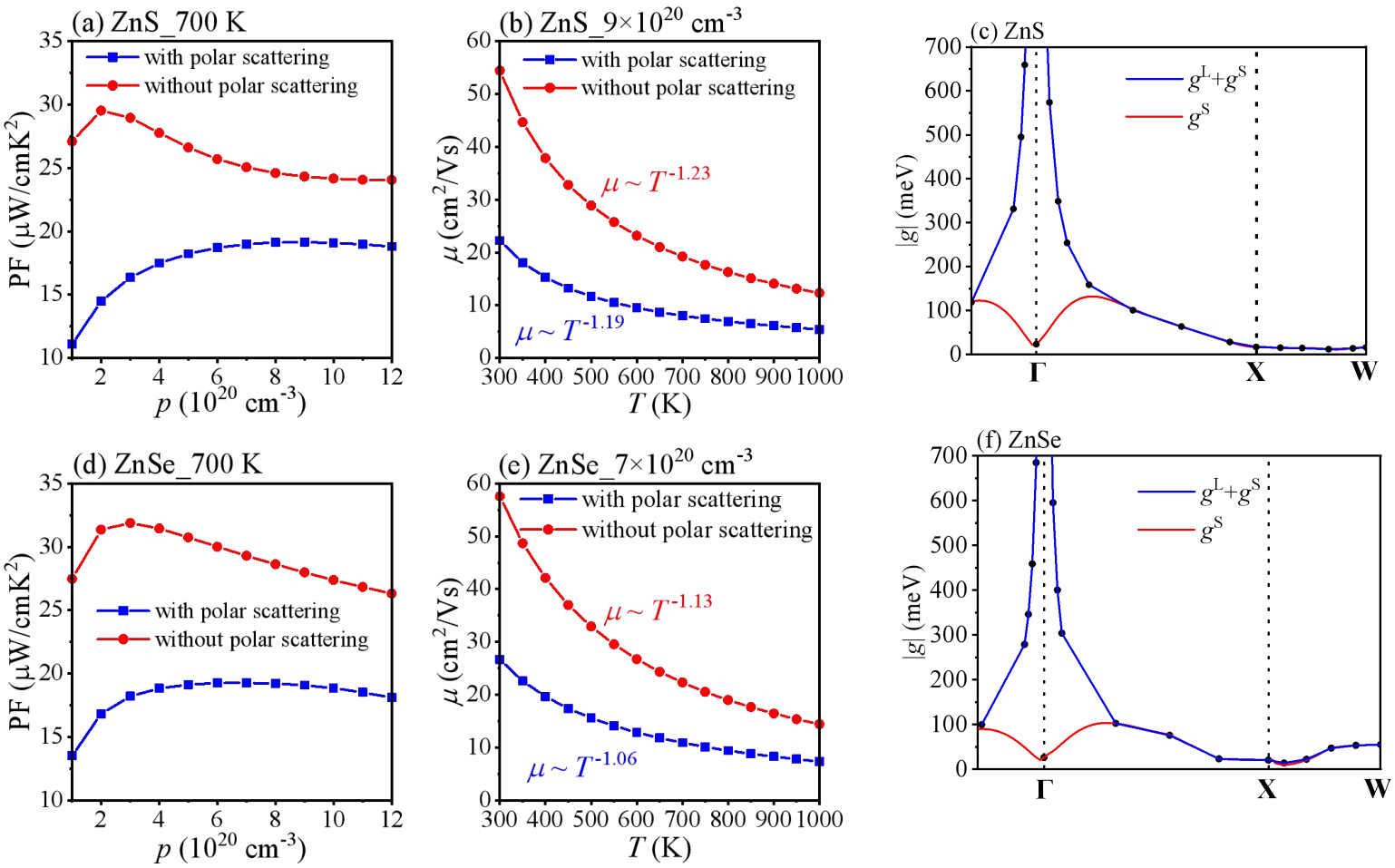

- Agreements with experiments are good.
- The scatterings of polar optical phonons are nonnegligible.

Ding, Xi, Yang, et al., J. Materiomics, 7, 310 (2021)

BoltzTrap

Available online at www.sciencedirect.com
SCIENCE DIRECT
Computer Physics Communications 175 (2006) 67–71
Computer Physics Communications
www.elsevier.com/locate/cpc

BoltzTraP. A code for calculating band-structure dependent quantities ☆

Georg K.H. Madsen [a,*], David J. Singh [b]

[a] Department of Chemistry, University of Aarhus, DK-8000 Århus C, Denmark
[b] Condensed Matter Sciences Division, Oak Ridge National Laboratory, Oak Ridge, TN 37831-6032, USA

Received 25 September 2005; accepted 3 March 2006
Available online 2 May 2006

Computer Physics Communications 231 (2018) 140–145

Contents lists available at ScienceDirect
Computer Physics Communications
journal homepage: www.elsevier.com/locate/cpc

BoltzTraP2, a program for interpolating band structures and calculating semi-classical transport coefficients☆

Georg K.H. Madsen [a,*], Jesús Carrete [a], Matthieu J. Verstraete [b,c]

[a] Institute of Materials Chemistry, TU Wien, A-1060 Vienna, Austria
[b] nanomat/QMAT/CESAM and Department of Physics, Université de Liège, allée du 6 août, 19, B-4000 Liège, Belgium
[c] European Theoretical Spectroscopy Facility, Belgium

- 发布早，可计算泽贝克系数等，应用广泛，常数电子驰豫时间；
- 适用于高通量；
- 第三方后处理程序可得到近似下的驰豫时间

TransOpt

两大改进（相比于BoltzTrap）：

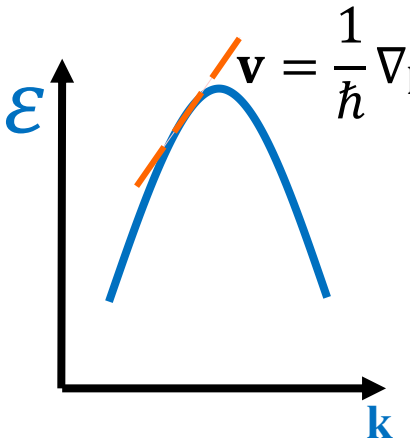

电子群速度

群速度的处理

1. 能带梯度Gradient: $\mathbf{v}_{n\mathbf{k}} = \frac{1}{\hbar}\nabla_{\mathbf{k}}\varepsilon_{n\mathbf{k}}$

2. 动量矩阵元Momentum matrix： $\mathbf{v}_{n\mathbf{k}} = \frac{1}{m_e} < \psi_{n\mathbf{k}}|\hat{\mathbf{p}}|\psi_{n\mathbf{k}} >$

动量矩阵元方法可以解决能带交叉问题

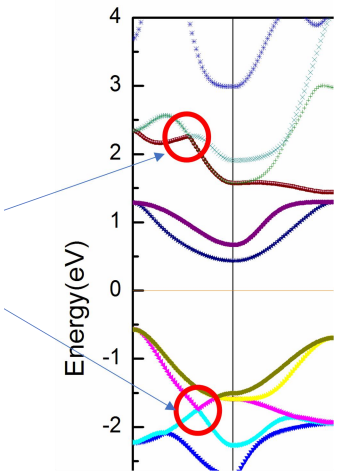

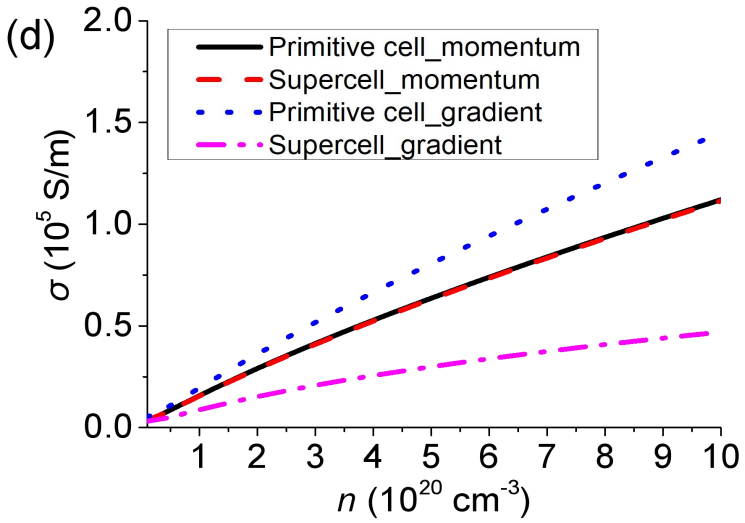

J. Electron. Mater., 38, 1397 (2009)　Comp. Mater. Sci. 186, 110074 (2021)

TransOpt对于弛豫时间的处理

$$\frac{1}{\tau_{n\mathbf{k}}} = \frac{2\pi}{\hbar}\sum_{m\mathbf{k}'\lambda} |g^{\lambda}_{m\mathbf{k}',n\mathbf{k}}|^2 \{[f_{m\mathbf{k}'} + n_{\mathbf{q}\lambda}]\delta(\varepsilon_{m\mathbf{k}'} - \varepsilon_{n\mathbf{k}} - \hbar\omega_{\mathbf{q}\lambda})\delta_{\mathbf{k}+\mathbf{q},\mathbf{k}'} + [1 + n_{\mathbf{q}\lambda} - f_{m\mathbf{k}'}]\delta(\varepsilon_{m\mathbf{k}'} - \varepsilon_{n\mathbf{k}} + \hbar\omega_{\mathbf{q}\lambda})\delta_{\mathbf{k}-\mathbf{q},\mathbf{k}'}\}(1 - \frac{\mathbf{v}_{\mathbf{k}'}\cdot\mathbf{v}_{\mathbf{k}}}{|\mathbf{v}_{\mathbf{k}'}|\cdot|\mathbf{v}_{\mathbf{k}}|})$$

Elastic scattering

$$\frac{1}{\tau_{nk}} = \frac{2\pi}{\hbar}\sum_{mk'\lambda} |g^{\lambda}_{mk',nk}|^2 \cdot 2n_{q\lambda}\delta(\varepsilon_{nk} - \varepsilon_{mk'})\delta_{k+q,k'}$$

Constant electron-phonon coupling approximation

常数电声耦合近似：处理驰豫时间中的能带部分

$$\frac{1}{\tau_{nk}} = \frac{CT}{V}\sum_{m\mathbf{k}'} \delta(\varepsilon_{n\mathbf{k}} - \varepsilon_{m\mathbf{k}'})$$

C substituted by E_n^2/G

进一步用形变势方法处理可以得到输运参数绝对值

$$\frac{1}{\tau_{nk}} = \frac{2\pi k_B T E_n^2}{V\hbar G}\sum_{mk'} \delta(\varepsilon_{nk} - \varepsilon_{mk'})$$

J. Electron. Mater., 38, 1397 (2009) Comp. Mater. Sci. 186, 110074 (2021)

电离杂质散射

$$\frac{1}{\tau_{imp}} = \sum_{m,\mathbf{k}'} \frac{2\pi\, n_{ion} Z_{ion}^2 e^4}{V\hbar(\varepsilon_r\varepsilon_0)^2 (L_D^{-2} + |\mathbf{k}' - \mathbf{k}|^2)^{-2}} \delta(\varepsilon_{n,\mathbf{k}} - \varepsilon_{m,\mathbf{k}'})$$

$$L_D = \sqrt{\varepsilon_r \varepsilon_0 k_B T / e^2 N_0}$$ Debye screening length

$$\frac{1}{\tau} = \frac{1}{\tau_{DP}} + \frac{1}{\tau_{imp}}$$ 马西森规则

Rev. Mod. Phys., 1981, 53, 745
Sci. Rep., 2016, 6, 19968

TransOpt案例

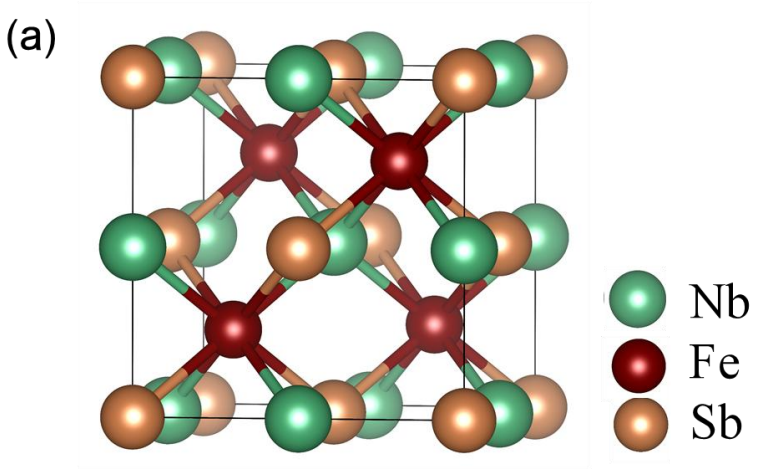

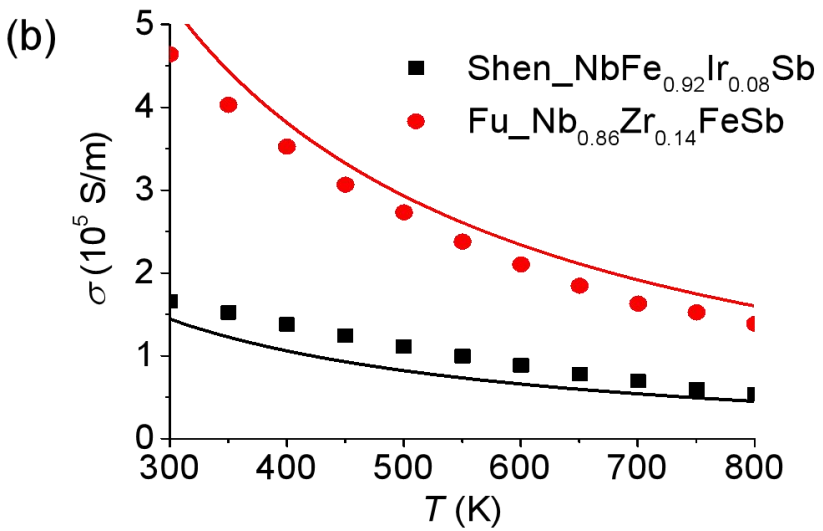

Deformation potential: 2.11 eV for p type (Fe 1s); 4.41eV for n type (Nb 1s)
Young's modulus: 209.70 GPa

https://github.com/yangjio4849/TransOpt.git

Materials Today Physics **2019,** *8*, 62-70.
Nature Communications **2015**, 6， 68144.

J. Electron. Mater., 38, 1397 (2009)　Comp. Mater. Sci. 186, 110074 (2021)

TransOpt案例

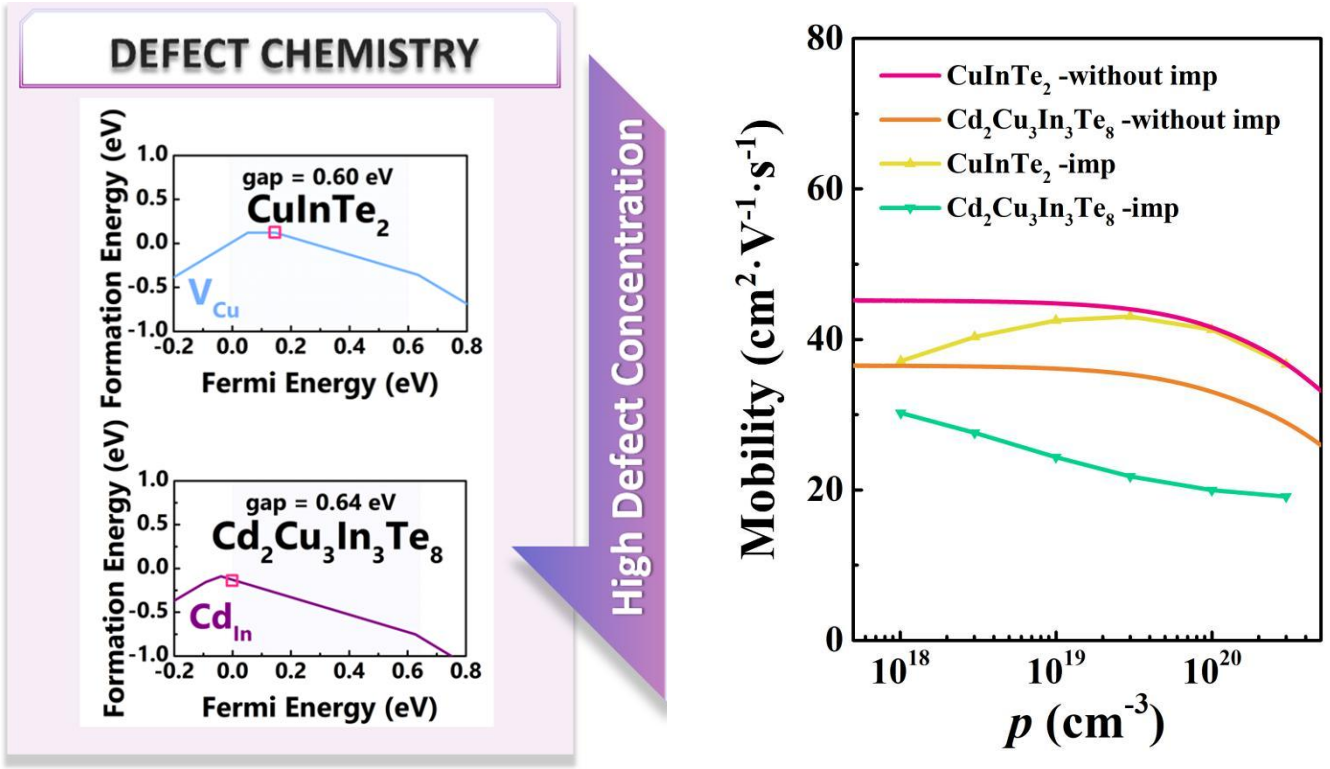

- 四元类金刚石化合物的杂质形成能较三元低-->杂质浓度高；
- 高电离杂质浓度的四元类金刚石化合物的迁移率在10^{20} cm^{-3}空穴浓度下依然受到电离杂质的影响。

J. Materiomics, DOI:10.1016/j.jmat.2022.05.003 (2022)

TransOpt程序使用

安装

兼容vasp 4.6、vasp 5.4.4和vasp 6.3.0

具体安装方式与v_{nk}求解有关：

1. 能带梯度方法：将main.F_for_symm替换main.F，重新编译即可。

2. 动量矩阵元法：将main.F_for_vk替换main.F，复制getnabij.F，.objects至src，重新编译vasp。

https://github.com/yangjio4849/TransOpt.git

J. Electron. Mater., 38, 1397 (2009)　Comp. Mater. Sci. 186, 110074 (2021)

TransOpt程序使用

程序使用说明：

- 两种方法都可以计算常数电声耦合下的驰豫时间。
- 能带梯度方法：使用无限制，可处理SOI下的电输运，并考虑对称性。
- 动量矩阵元法：修改于optics.F，需要INCAR中NPAR=1，并且不支持SOI计算。

https://github.com/yangjio4849/TransOpt.git

J. Electron. Mater., 38, 1397 (2009)　Comp. Mater. Sci. 186, 110074 (2021)

电输运计算方法发展

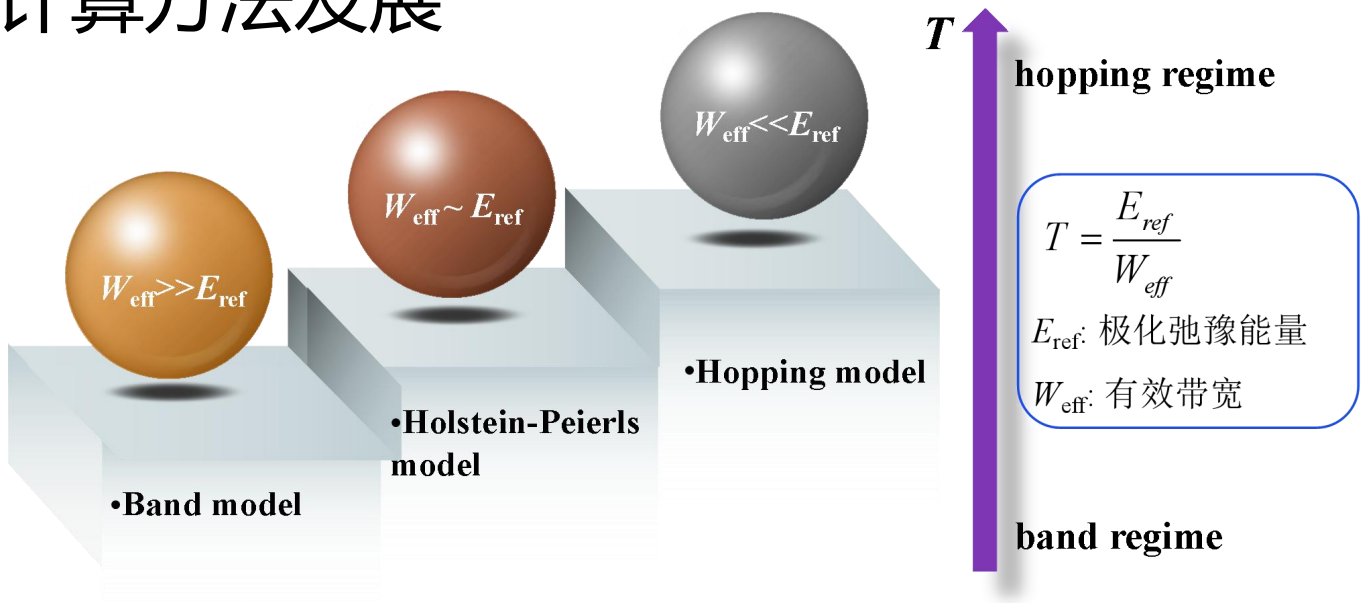

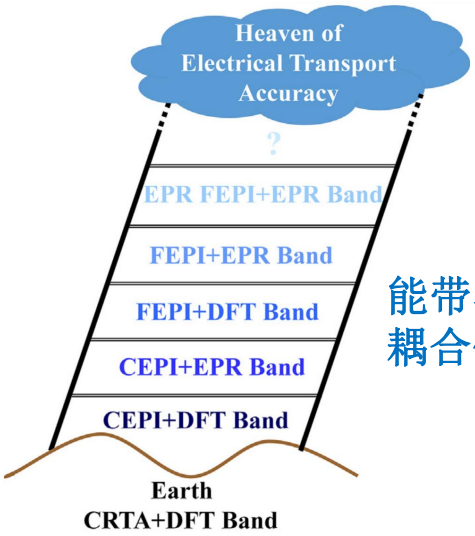

能带与电声耦合修正

$$\frac{1}{\tau_{n\mathbf{k}}} = \frac{1}{\tau_{e-p}} + \frac{1}{\tau_{imp}} + others$$

FIG. 4. Jacob's ladder of the electrical transport calculation accuracy.

Appl. Phys. Lett. 120, 190503 (2022)

电输运计算材料应用

- 能带的理解与应用——能带简并等

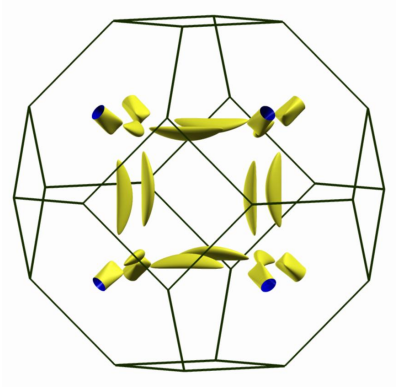

- 能带变化化学键理解

J. Comput. Chem. 40 (2019) 1693
Materials Today Physics 25 (2022) 100702
J. Mater. Chem. A, 10 (2022) 11039

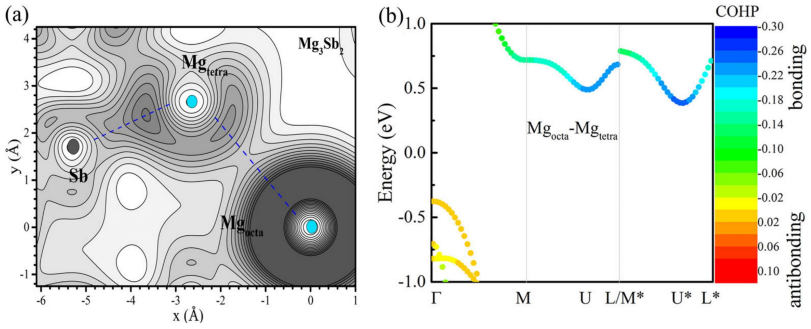

- 材料基因与高通量

电输运性质

- 电输运理论及概念理解
- 电输运及相关程序使用
- 电输运计算的应用——材料基因相关

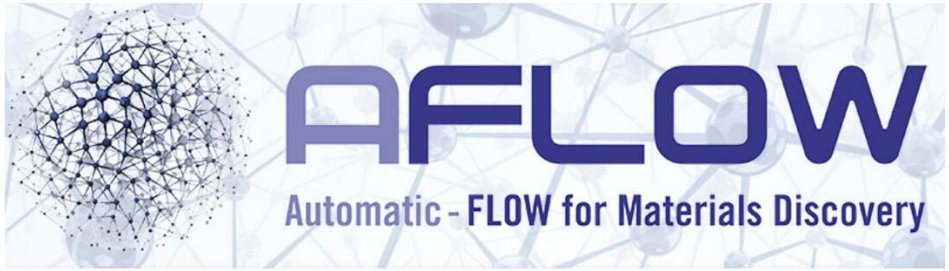

©MaterialGo
为科研提供知识服务

材料基因数据库

Database of electrical transport on MP

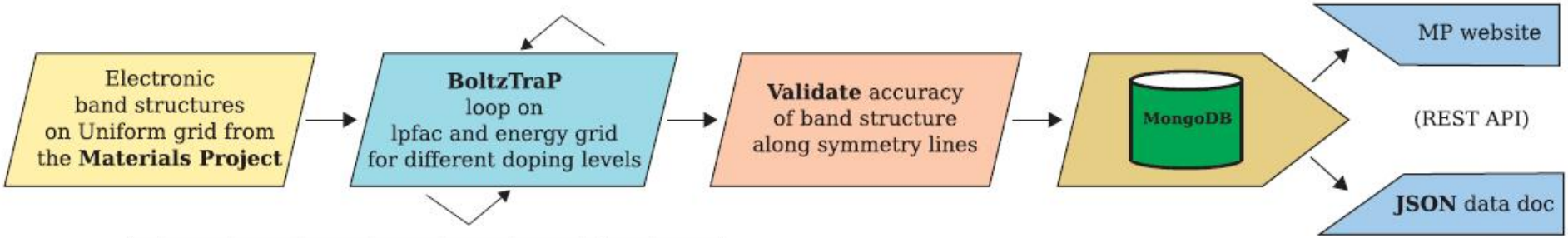

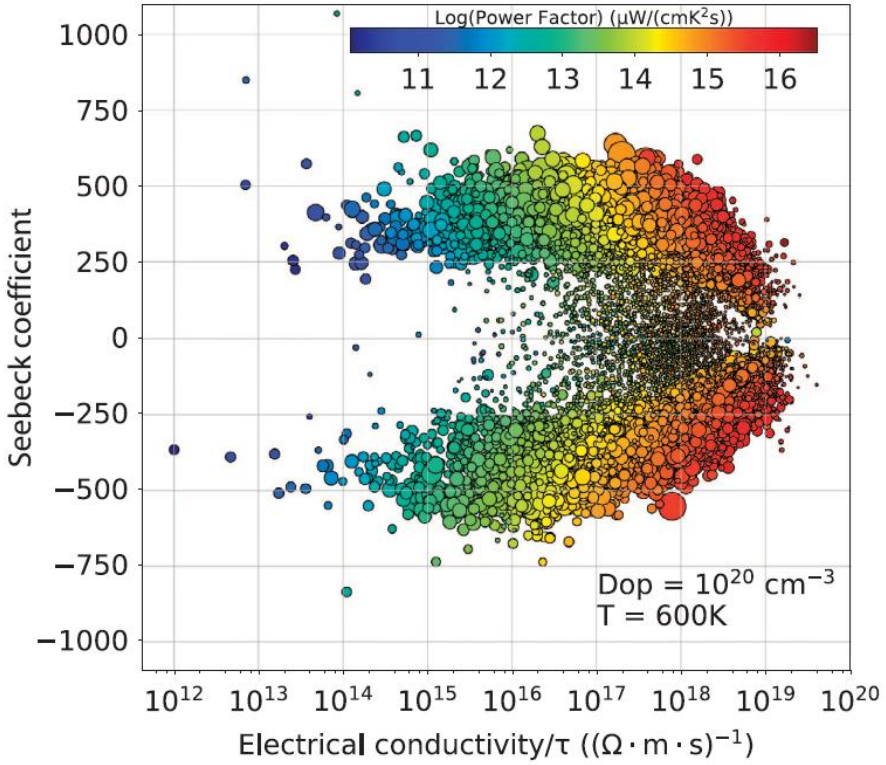

Ricci et al., Scientific Data 4, 170085 (2017)

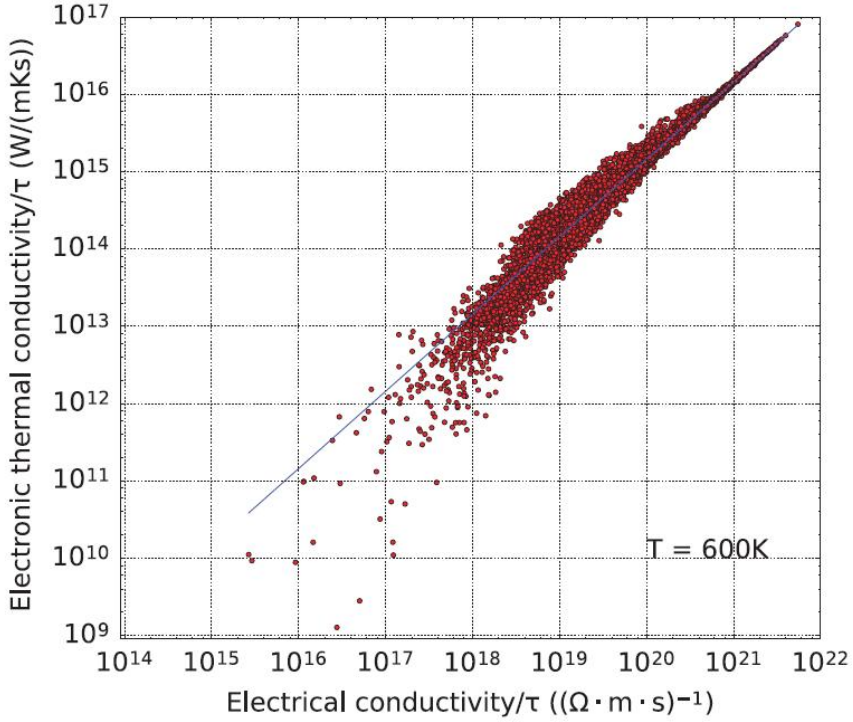

高通量通常τ处理方法：常数驰豫时间

Materials Hub (MatHub)

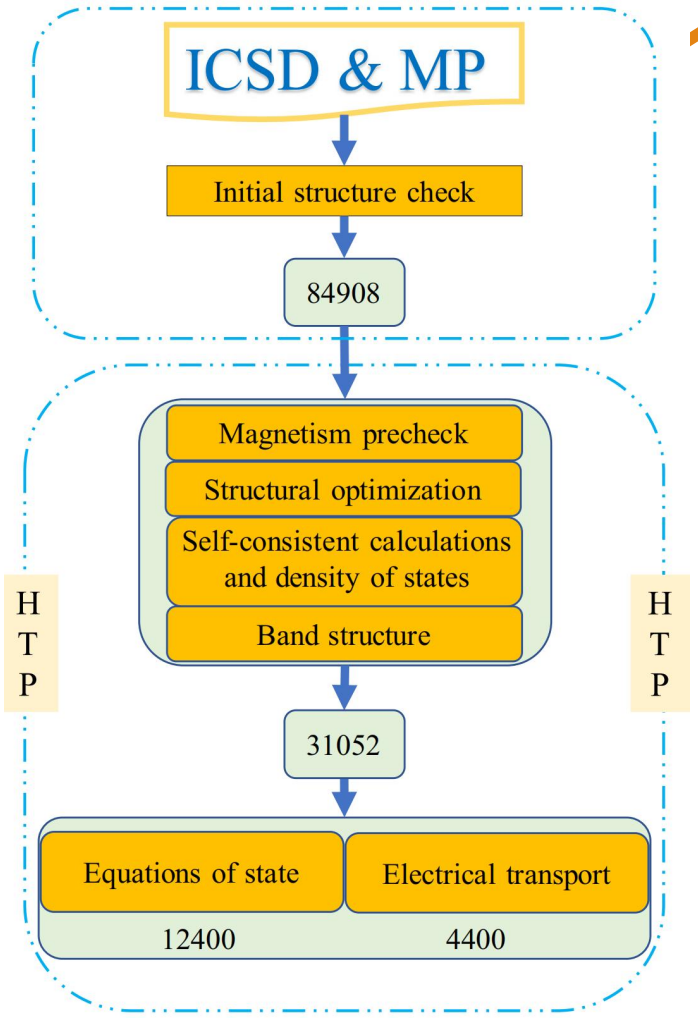

MatHub-3D
www.mathub3d.net

数据统计：
晶体结构：~ 85000
电子结构：> 33000
电输运性质：~ 10200
形变势常数(p,n)：~ 10200
状态方程与体模量：> 12000

Sci. Data 8, 236 (2021)

Fe1Nb1Sb1

MatHub3d-84427-FeNbSb

Basic properties

Property	Value
Space group	(216, "'F-43m'")
Magnetic	FALSE
Band gap (PBE) (eV)	0.55
Total energy (eV)	-23.648
Total energy / atom (eV)	-7.883

Lattice Parameters(from the source)

a, b, c (Å):	5.920	5.920	5.920
α, β, γ(°):	90.0	90.0	90.0

Lattice Parameters(computed)

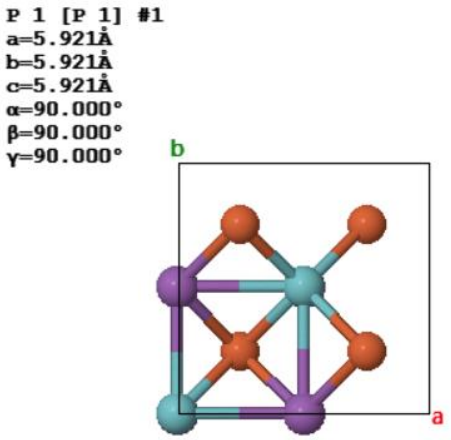

JSmol

Unit cell

Download input files

- 计算软件：VASP
- 泛函：PBE+U
- 截断能：520 eV
- 电输运计算软件：TransOpt

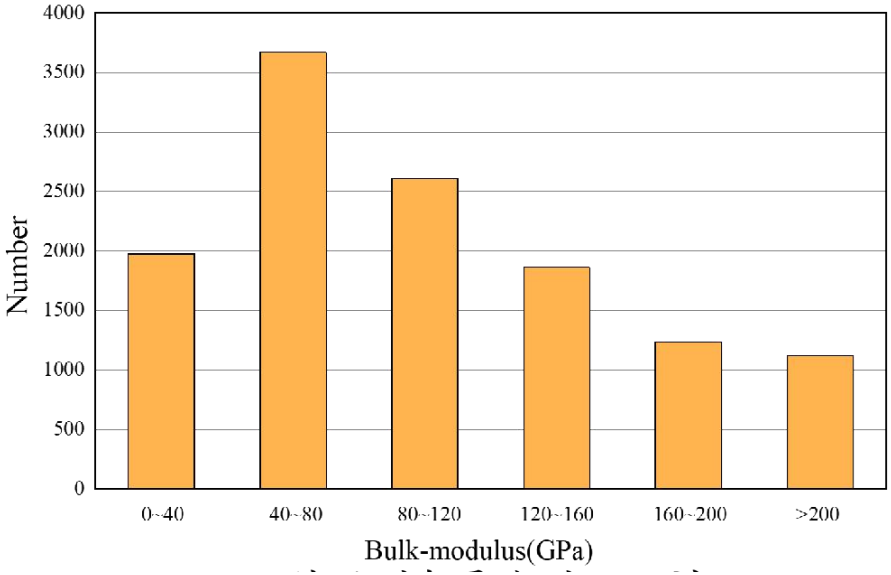

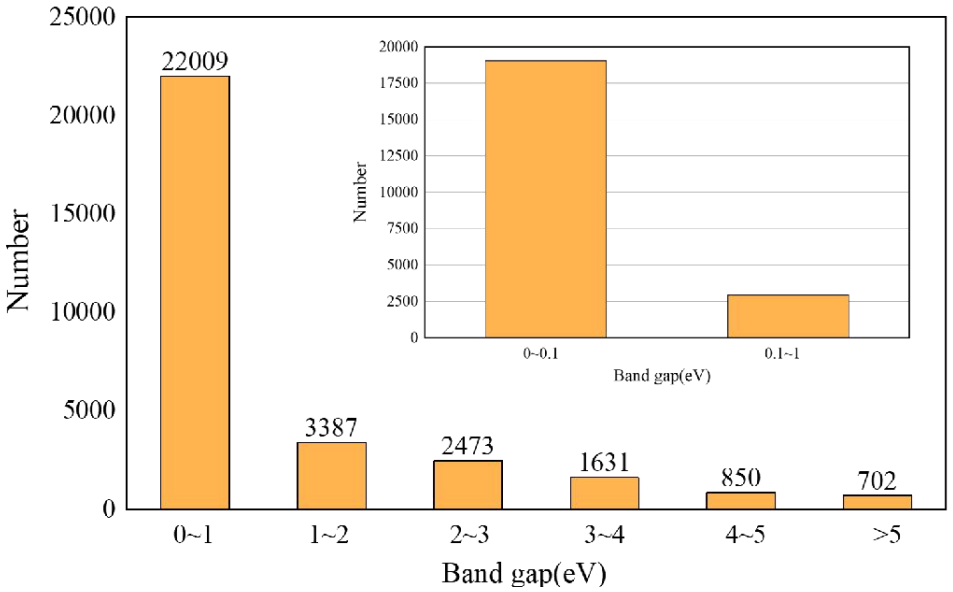

投影能带

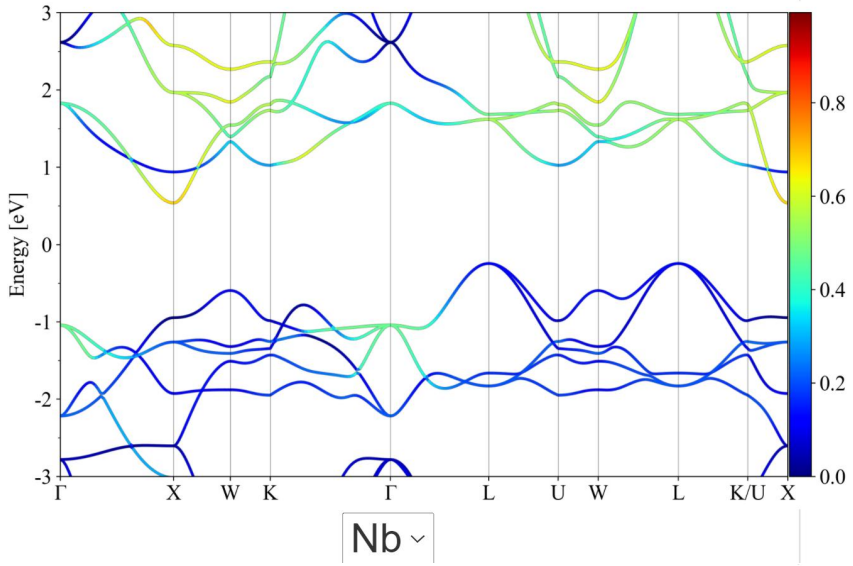

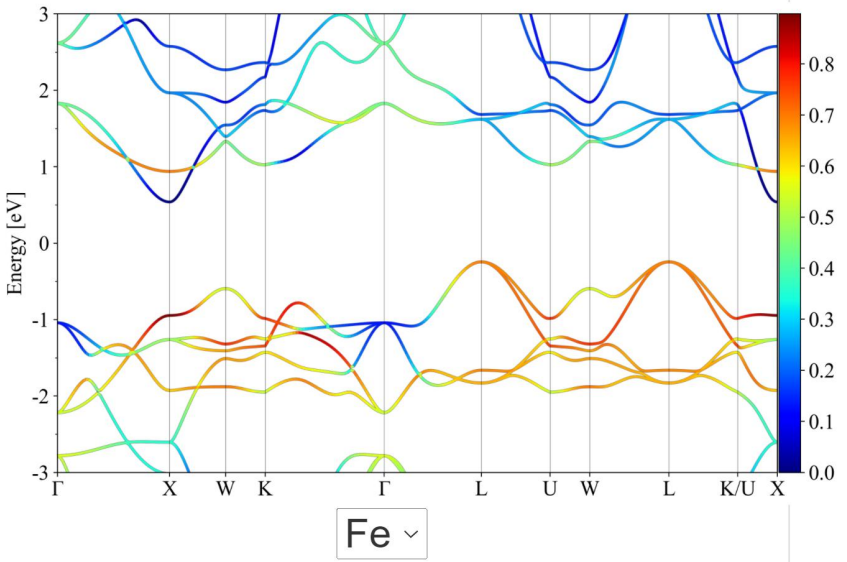

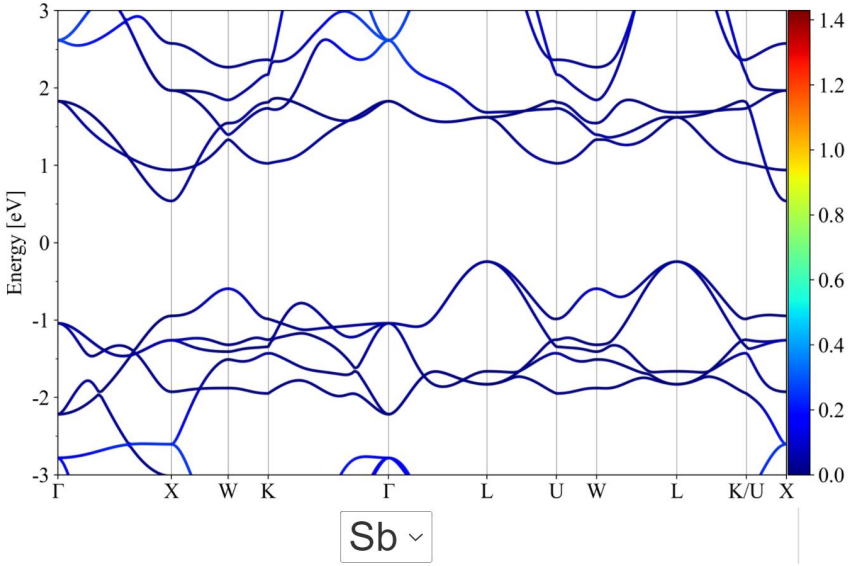

Property	Value
Band gap	0.78 eV
Band degeneracy(CBM)	3.00
Band degeneracy(VBM)	8.00

能带简并度

能带简并度

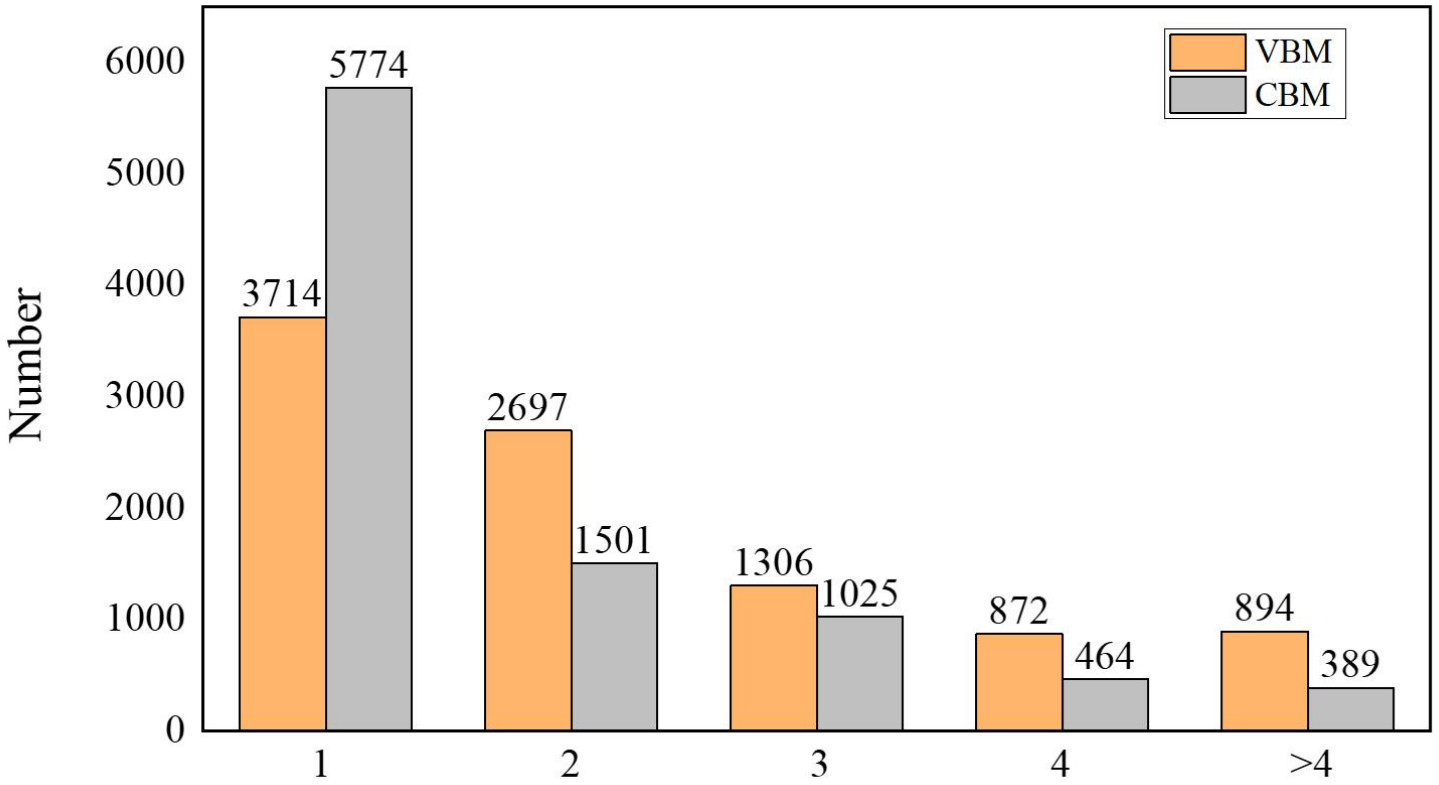

k点简并(Nv_k)：4

能带简并 (Nv_band)：2

实际简并度(Nv_total)=Nv_k*Nv_band=8

热电输运性质

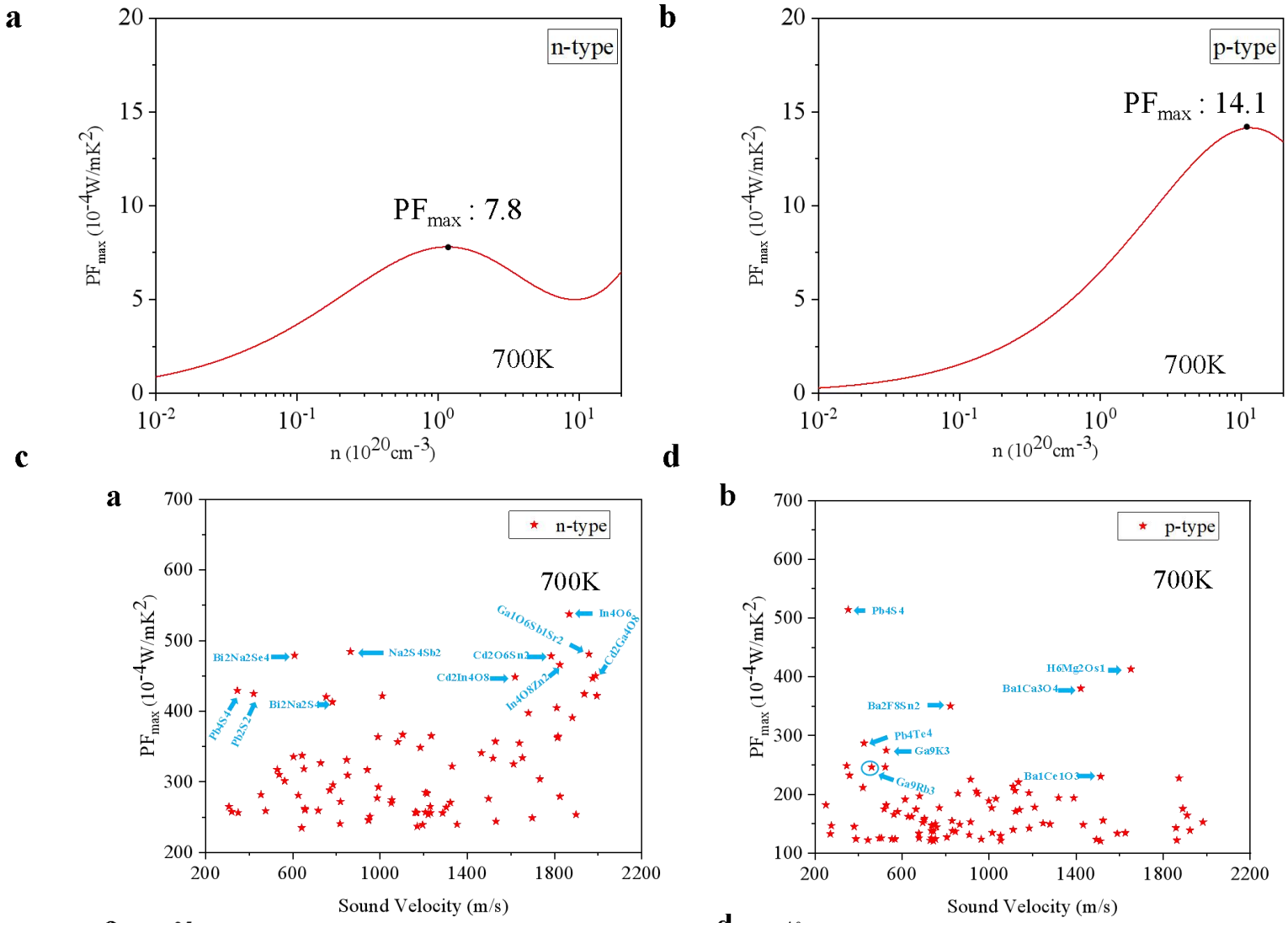
a
n-type
PF$_{max}$: 7.8
700K
PF$_{max}$ (10^{-4}W/mK^2)
n (10^{20}cm^{-3})
b
p-type
PF$_{max}$: 14.1
700K
PF$_{max}$ (10^{-4}W/mK^2)
n (10^{20}cm^{-3})
c
a
n-type
700K
Bi2Na2Se4
Na2S4Sb2
Cd2O6Sn2
Ga1O6Sb1Sr2
In4O6
Cd2Ga4O8
Cd2In4O8
In4O8Zn2
Bi2Na2S4
Pb4S4
Pb2S2
PF$_{max}$ (10^{-4}W/mK^2)
Sound Velocity (m/s)
b
p-type
700K
Pb4S4
H6Mg2Os1
Ba1Ca3O4
Ba2F8Sn2
Pb4Te4
Ga9K3
Ba1Ce1O3
Ga9Rb3
PF$_{max}$ (10^{-4}W/mK^2)
Sound Velocity (m/s)

类金刚石硫族热电材料高通量筛选

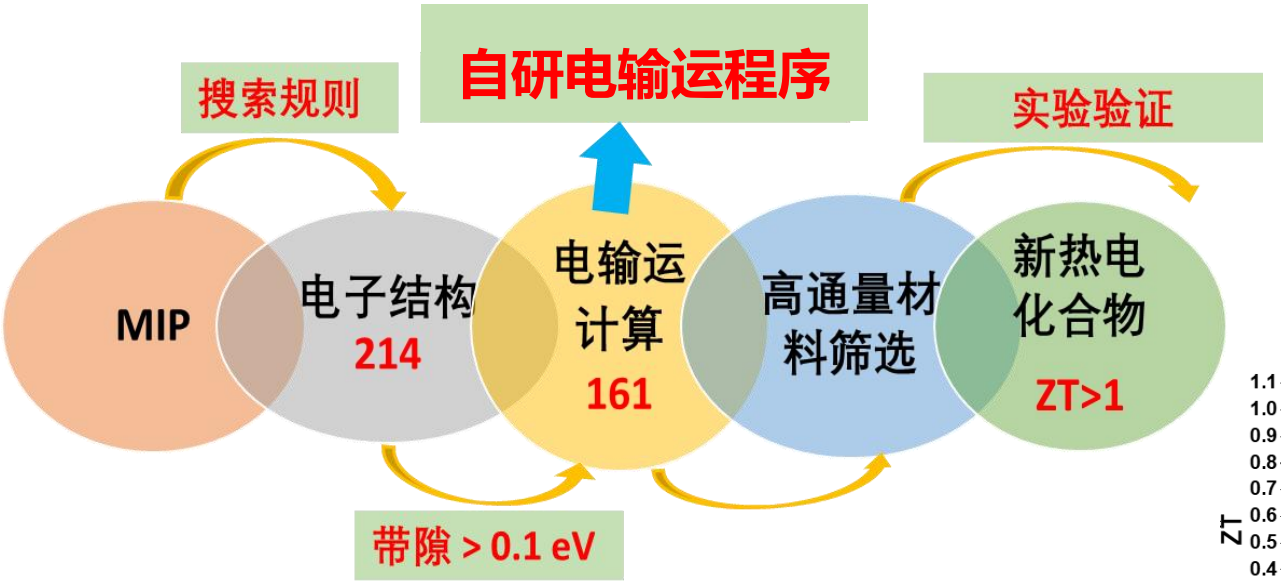

热电材料筛选工作流

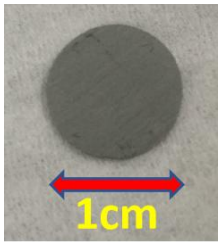

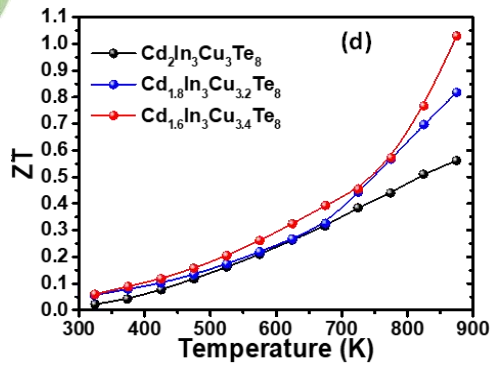

- 热电筛选工作流结合实验验证，发现了一类新型高性能热电材料$Cd_2Cu_3In_3Te_8$

Xi, Yang, Luo, Zhang et al., J. Am. Chem. Soc. 140, 10785 (2018)

ABX_2硫族与磷族热电材料高通量筛选

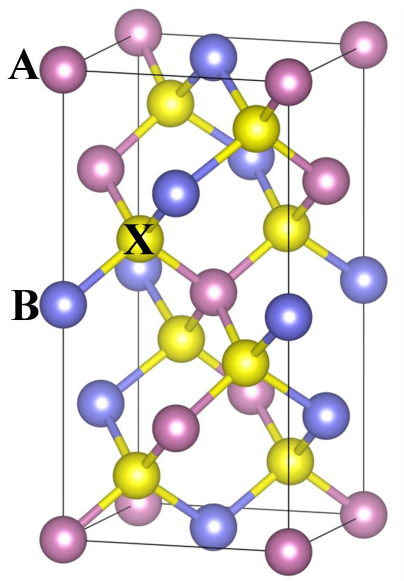

A B
IA, IIA, IIIA, IVA, VA,
IB, IIB, VB, VIII

X
IIIA,VA, VIA, VIIA

ABX_2:I-42d

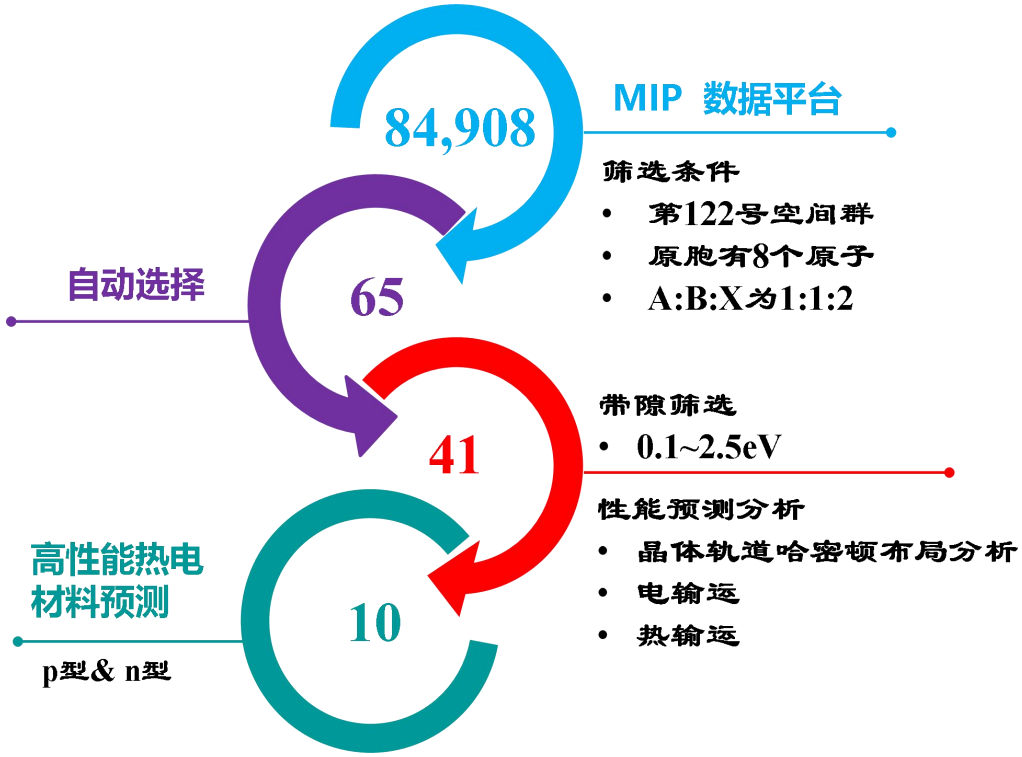

- 开发了热输运算法EPHC，运用于1:1:2类金刚石热电材料的热电优值预测。

Li, Xi, Yang, Zhang, ACS Appl. Mater. Inter. 11, 24859 (2019)

主动学习进行热电功率因子预测

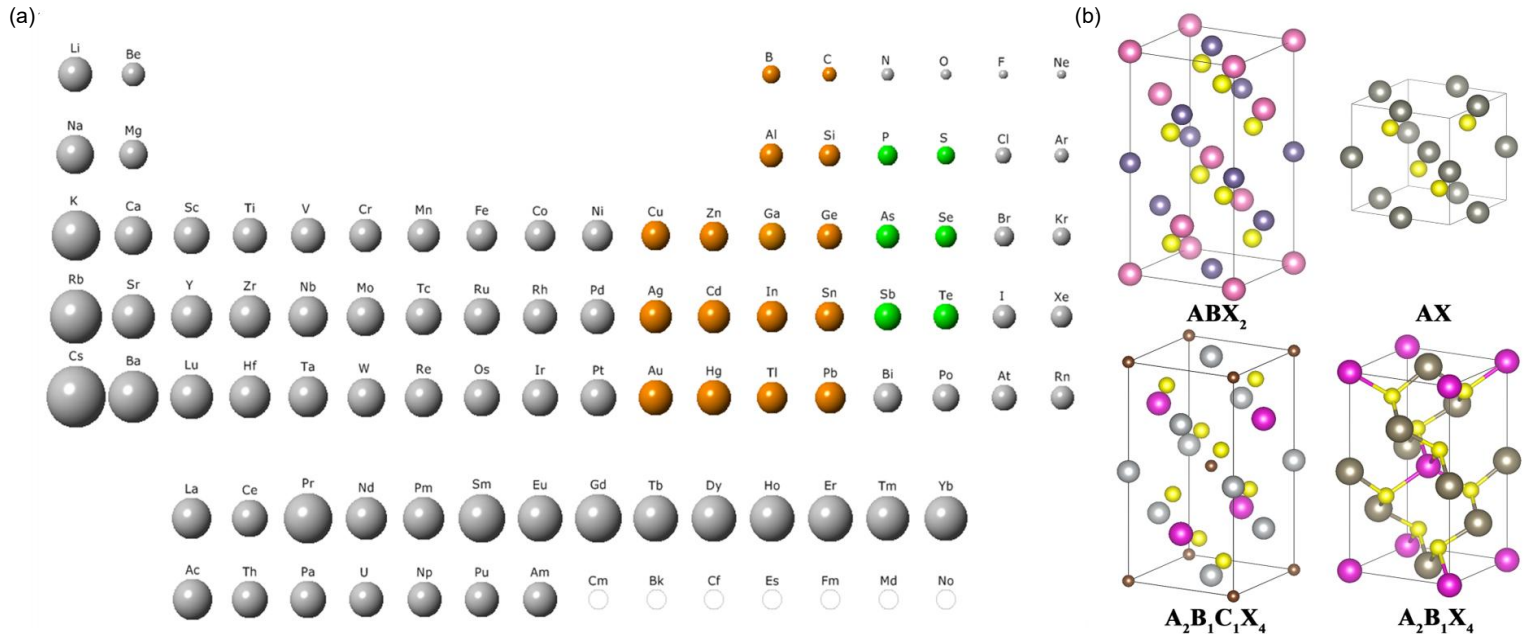

- DFT database--JACS 2018 and ACS AMI 2019 (158 entries)
- Search space--all possible combinations of cations and anions (chalcogenides and pnictides, 482 entries)
- Target--p-type maximum power factors @ 700 K

Pridiction power!

迭代式主动学习

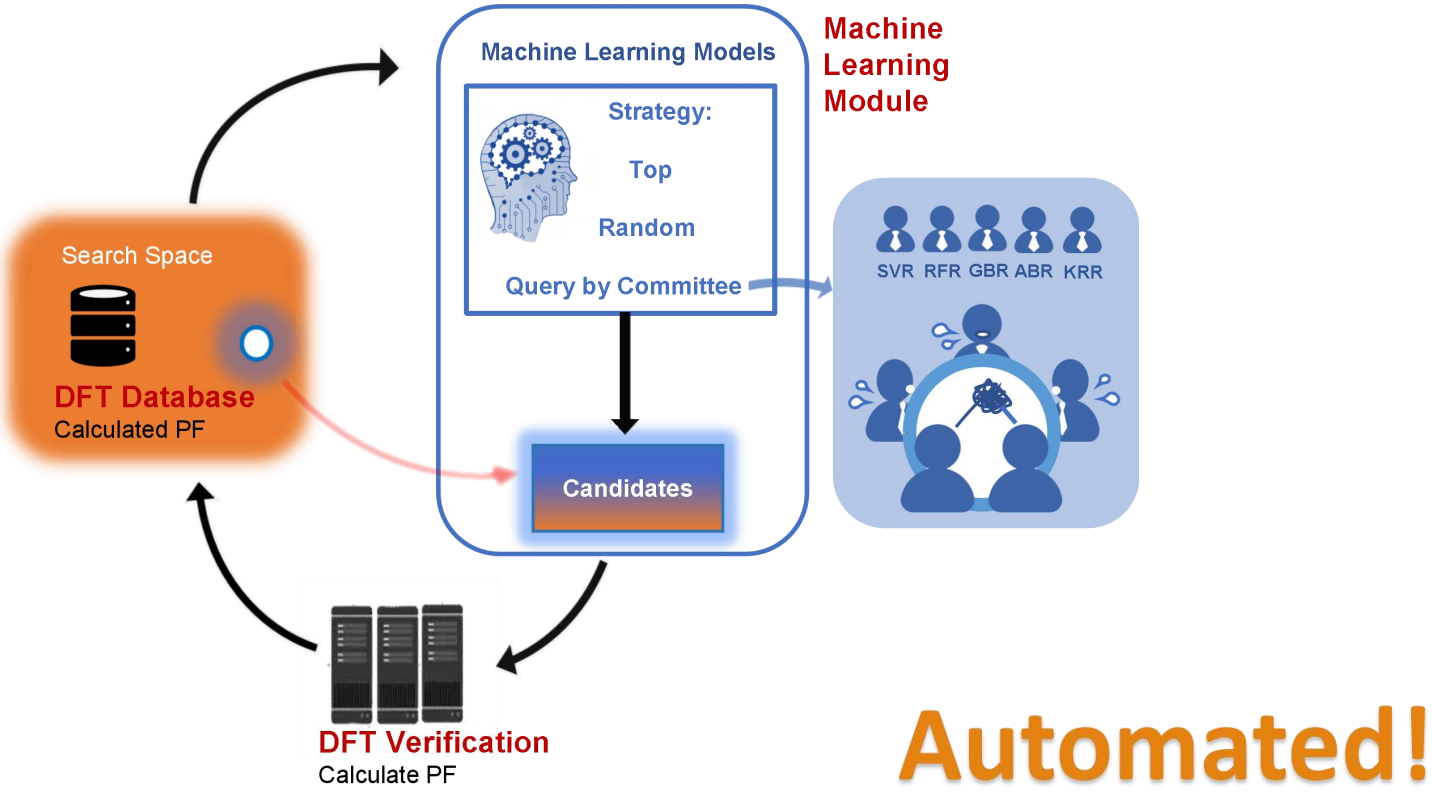

- Overall loop: Based on the DFT Database, the ML module picks uncalculated compounds (candidates) from the Search space, and have them calculated by DFT and added into the DFT Database.
- Three strategies for the picking of candidates

主动学习结果

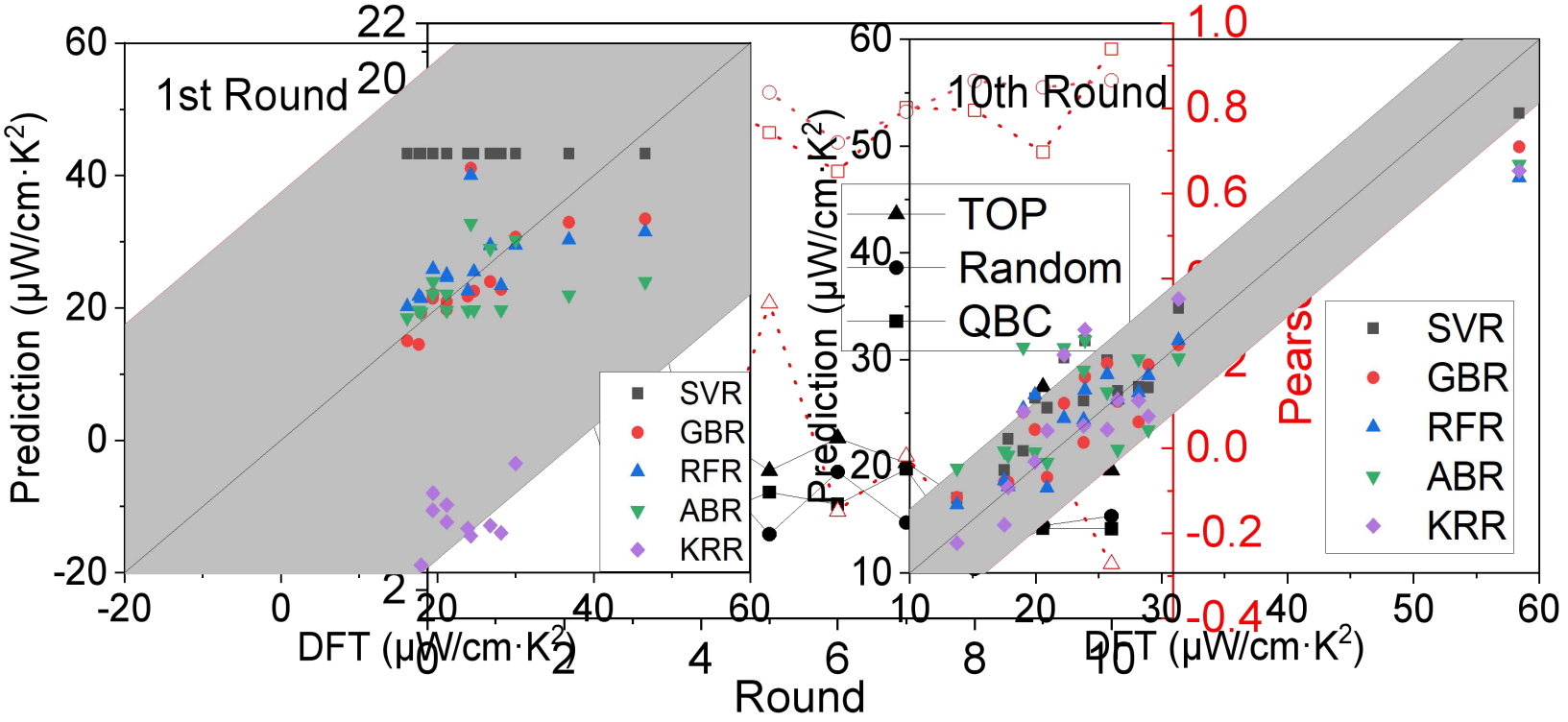

- After 10 rounds, the prediction accuracy on candidates' PFs is enhanced greatly.

功率因子预测及物理分析

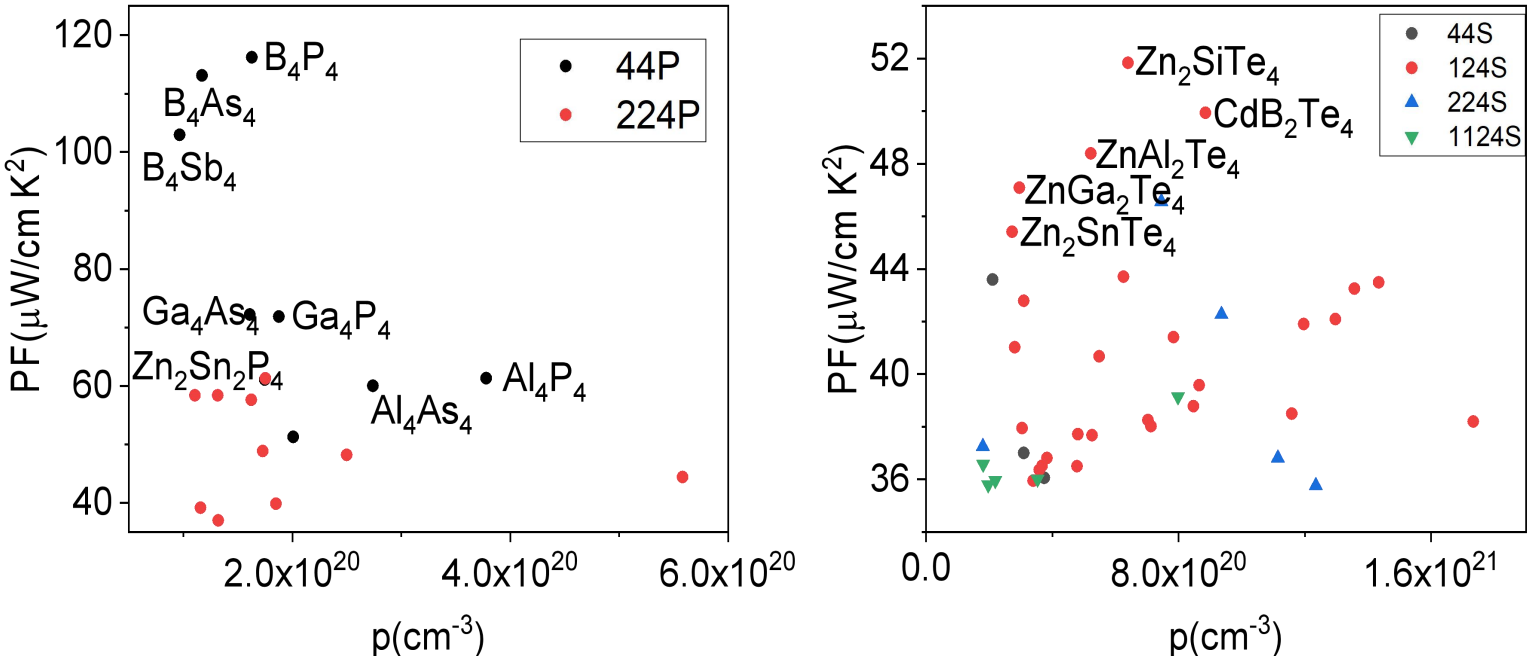

- The PFs of pnictides are generally larger.
- The PFs of chalcogenides in IIB_1:$IIIA_2$:VIA_4 atomic ratio are relatively large.
- Small atomic radius elements (such as Si or B) usually induce larger PFs.

Sheng, Yang, Zhang, et al., NPJ Comput. Mater. 6, 171 (2020)

功率因子预测及物理分析

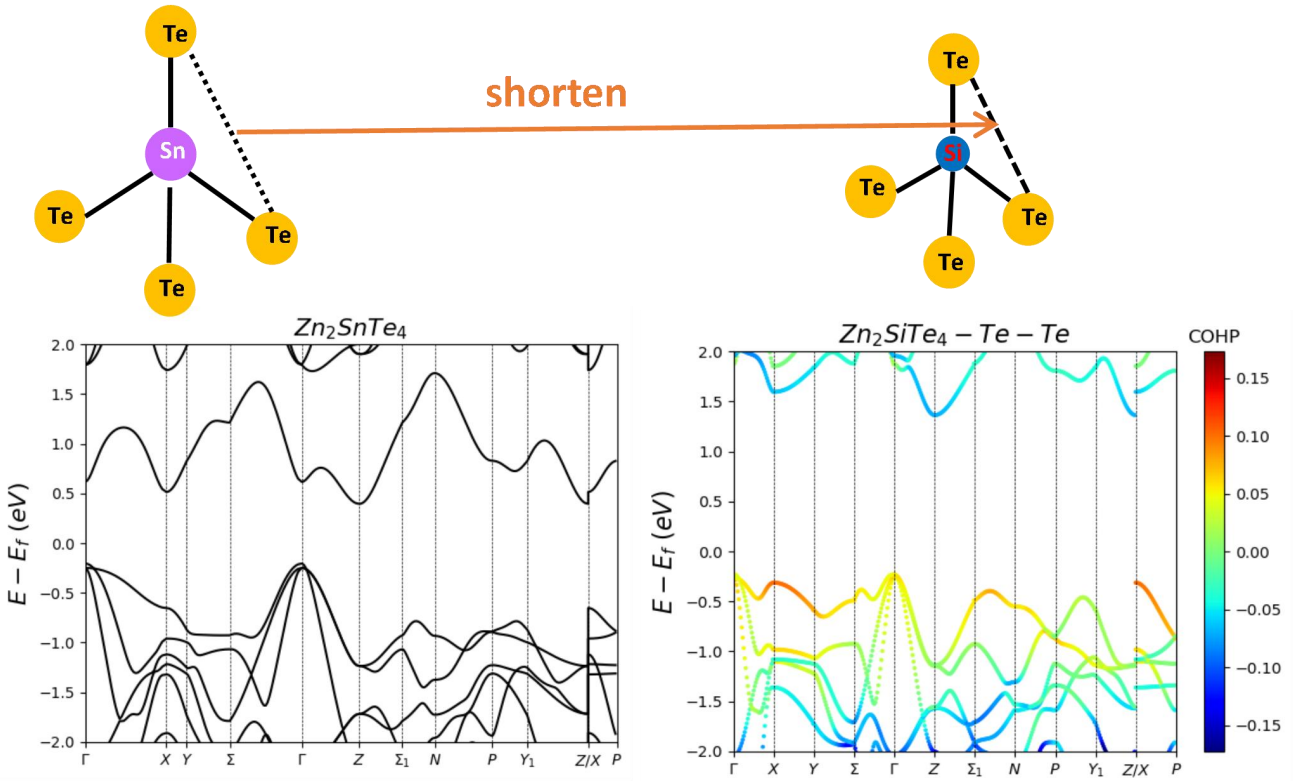

- Small cations induce the anions getting closer.
- The antibonding between otherwise nonbonding anions causes higher energy at X point.

Sheng, Yang, Zhang, et al., NPJ Comput. Mater. 6, 171 (2020)

热输运性质

- 热导率基本概念及传统模型
- 声子及三声子计算
- 最新方向

热导率范围

热导率范围（室温下）

10^{-1} ~ 10^{3} W/mK

金属：电子热导率为主

本征半导体与绝缘体：晶格热导率为主

重掺杂半导体：取决于电导率

物质	态	导热率 $W \cdot m^{-1} \cdot K^{-1}$
石墨烯	固态	(4840±440) - (5300±480)
钻石	固态	900 - 2320
银	固态	420
铜	固态	401
黄金	固态	318
铝	固态	237
白金	固态	70
铁	固态	60
钢	固态	60
铅	固态	35
汞	液态	8.34
冰	固态	2
陶瓷	固态	1.22
玻璃	固态	1.1
水	液态	0.6
聚乙烯	固态	0.3
尼龙	固态	0.2
石蜡油	液态	0.2
石棉	固态	0.2
聚苯乙烯	固态	0.08
软木塞	固态	0.05
采用在标准状况下的数据。对于气体，值是对应于 c_p。		

晶格热导率

$$\kappa_L = \frac{1}{3} C_V \mathbf{v_q} l_\mathbf{q}$$

$$l_\mathbf{q} = \mathbf{v_q} \tau_\mathbf{q}, \quad \kappa_L = \frac{1}{3} C_V \mathbf{v_q^2} \tau_\mathbf{q}$$

$$\kappa_L = \frac{1}{3\Omega N_q} \sum_{\lambda=1,3N} c_{\lambda,\mathbf{q}} \mathbf{v}^2_{\lambda,\mathbf{q}} \tau_{\lambda,\mathbf{q}}$$

$$= \frac{1}{3\Omega \mathrm{N_q}} \int_0^{\omega_m} N(\omega) c \mathbf{v}^2 \tau d\omega$$

与电导率非常类似，考虑所有声子对晶格热导率的贡献

声子驰豫时间

三声子相互作用　　点缺陷散射　　共振散射

$$\frac{1}{\tau_{\mathbf{q}}}=\frac{1}{\tau_{p-p}}+\frac{1}{\tau_B}+\frac{1}{\tau_{PD}}+\frac{1}{\tau_{e-p}}+\frac{1}{\tau_R}$$

晶界散射　　电声相互作用

声子驰豫时间由多种散射机制所决定；
其中三声子相互作用为最重要的本征散射机制

热导率几大因素的关系

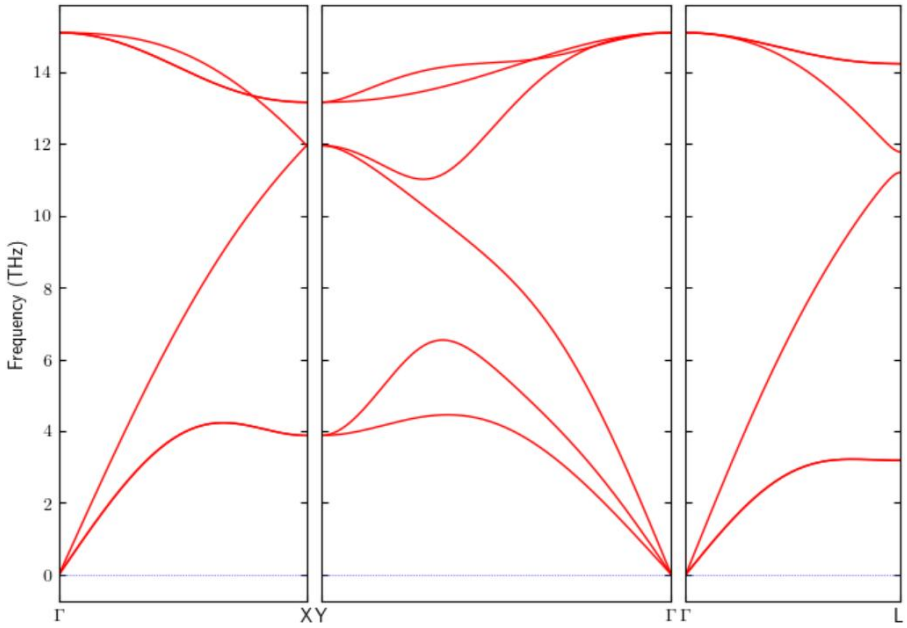

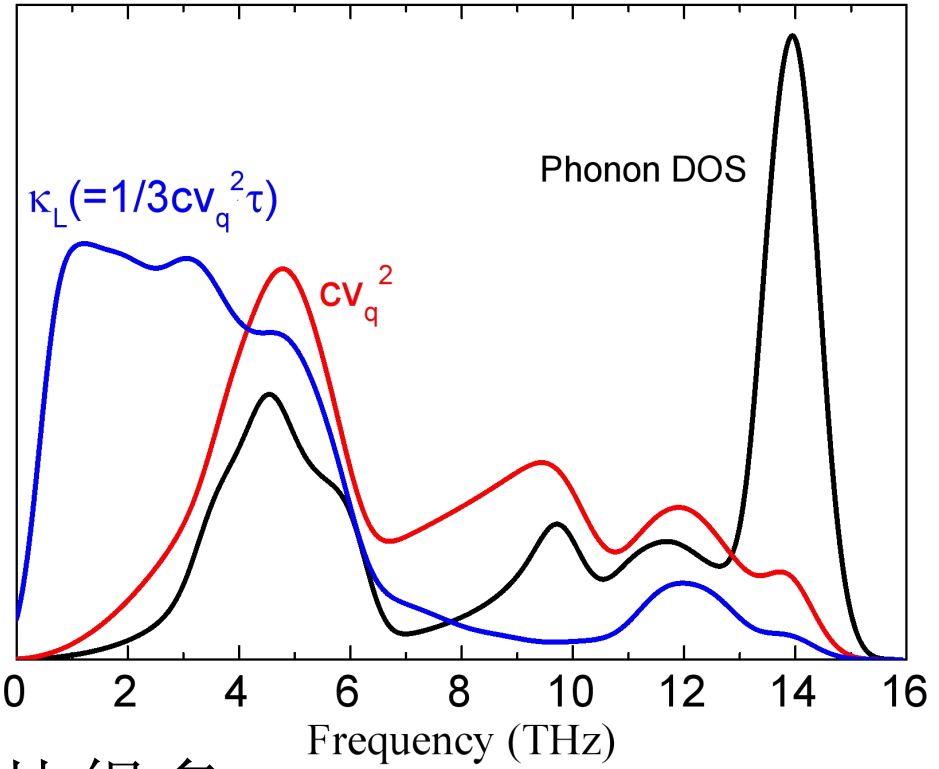

声学声子在晶格热导率中占比很多：

- 声学声子声速大
- 声学声子频率范围内态密度低，不易被散射

Debye-Callaway Model for κ_L

$$\kappa_i = \frac{1}{3} C_i T^3 \left\{ \int_0^{\Theta_i/T} \frac{\tau_c^i(x) x^4 e^x}{(e^x-1)^2} dx + \frac{\left[\int_0^{\Theta_i/T} \frac{\tau_c^i(x) x^4 e^x}{\tau_N^i (e^x-1)^2} dx \right]^2}{\int_0^{\Theta_i/T} \frac{\tau_c^i(x) x^4 e^x}{\tau_N^i \tau_U^i (e^x-1)^2} dx} \right\}$$

$$\frac{1}{\tau_N^{\mathrm{LA}}(x)} = \frac{k_B^3 \gamma_{\mathrm{LA}}^2 V}{M \hbar^2 v_{\mathrm{LA}}^5} \left(\frac{k_B}{\hbar} \right)^2 x^2 T^5$$

$$\frac{1}{\tau_N^{\mathrm{TA/TA'}}(x)} = \frac{k_B^4 \gamma_{\mathrm{TA/TA'}}^2 V}{M \hbar^3 v_{\mathrm{TA/TA'}}^5} \frac{k_B}{\hbar} x T^5$$

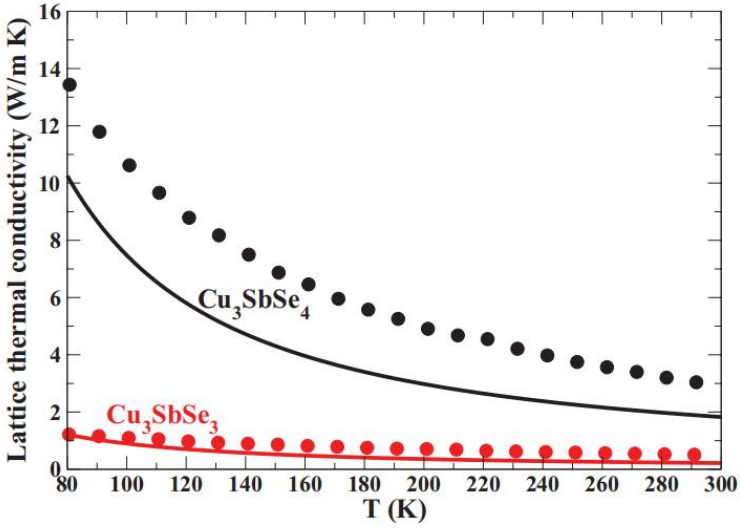

Callaway, Phys. Rev. 113, 1046 (1959)

Zhang et al., Phys. Rev. B 85, 054306 (2012)

Slack Model

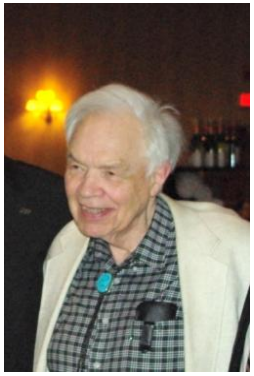

$$\kappa = A \cdot \frac{\overline{M}\theta^3\delta}{\gamma^2 T n^{2/3}}$$

Preconditions:

1. Near or above Debye temperature
2. Only acoustic phonons contribute

Slack, J. Phys. Chem. Solids 34, 321 (1973)
Morelli and Slack, "High lattice thermal conductivity solids" in *High Thermal conductivity Materials*, 2005, p.37
Snyder et al., Nat. Mater. 7, 105 (2008)
Toberer et al., J. Mater. Chem., 21, 15843 (2011)

Utilizations of the Slack model in high-throughput

$$\kappa = A \cdot \frac{\overline{M}\theta^3\delta}{\gamma^2 T n^{2/3}}$$

$\{c_{ij}\}$

ABO_3 thermal barrier coating materials

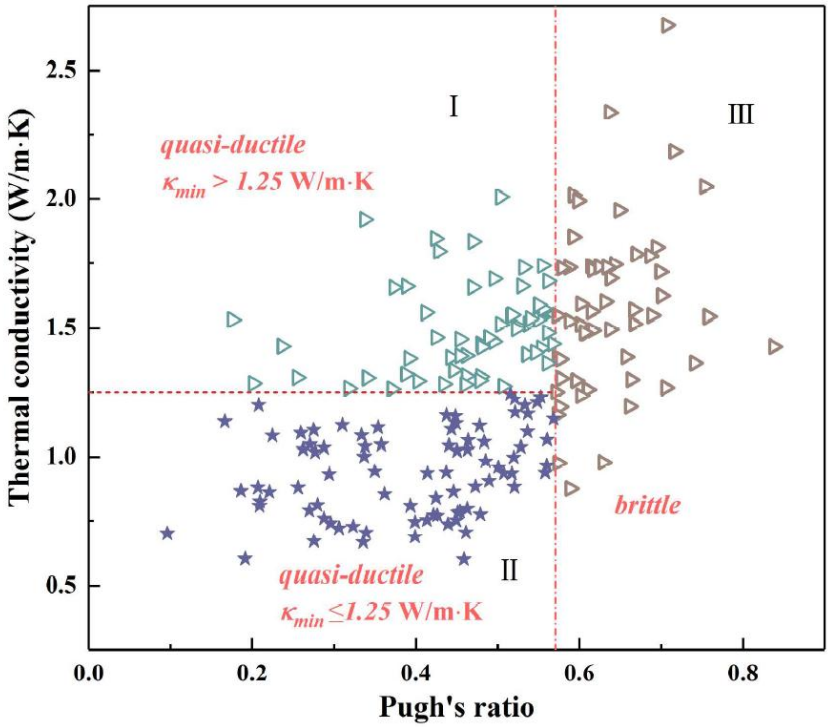

Sun et al., J. Am. Ceram. Soc., 99, 2442 (2016)

Liu, Yang, Zhou et al., Materials Research Letters, 7, 145 (2019)

Utilizations of the Slack model in high-throughput

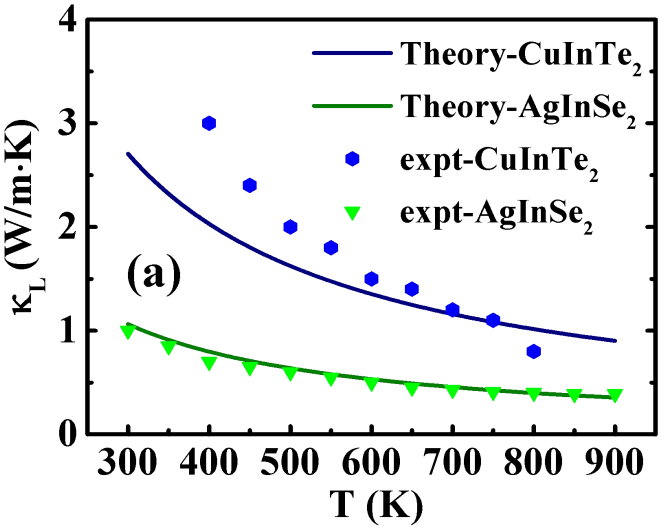

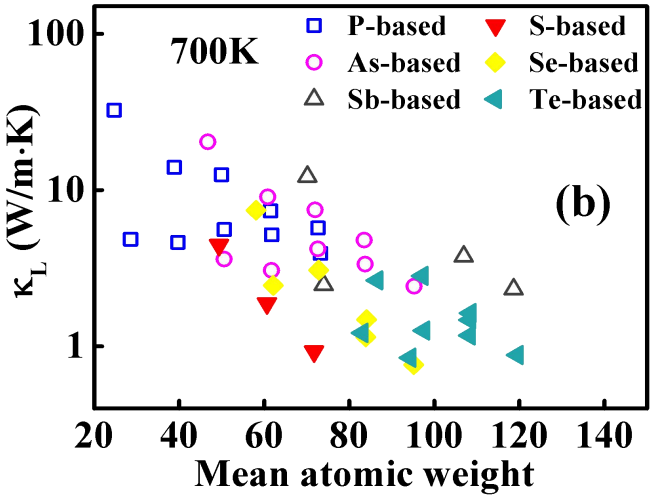

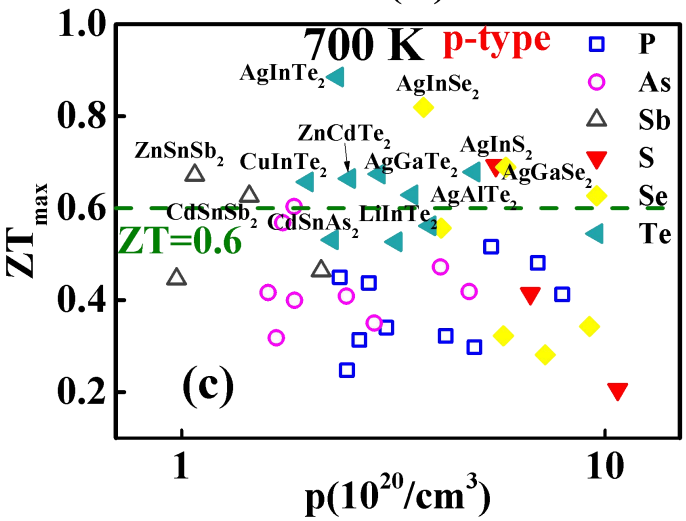

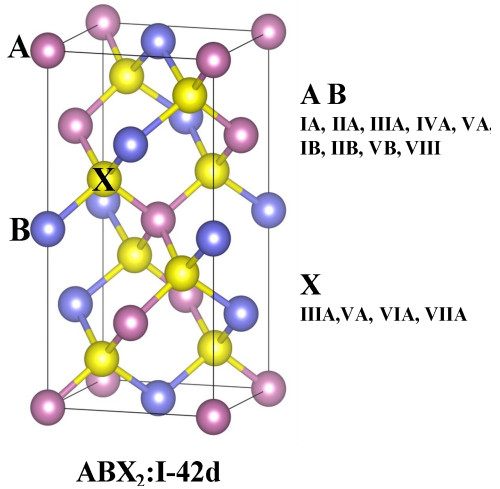

Li, Xi, Yang, Zhang, et al., ACS Appl. Mater. Inter., 11, 24859 (2019)

热输运性质

- 热导率基本概念及传统模型
- 声子及三声子计算
- 最新方向

Direct calculation of κ_L

$$\kappa_L = \frac{1}{3NV}\sum_{\mathbf{q}s} c_{\mathbf{q}s}\mathbf{v}_{g\,\mathbf{q}s}^2\tau_{\mathbf{q}s}$$

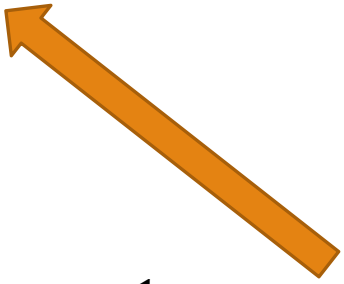

$$H = U_0 + \frac{1}{2}\sum_{ij\alpha\beta}\boldsymbol{\Phi}_{ij}^{\alpha\beta}u_i^\alpha u_j^\beta + \frac{1}{3!}\sum_{ijk\alpha\beta\gamma}\boldsymbol{\Phi}_{ijk}^{\alpha\beta\gamma}u_i^\alpha u_j^\beta u_k^\gamma + \cdots$$

Broido et al., APL, 91, 231922 (2007)
Lindsay et al., PRB, 87, 165201 (2013)

Phonon dispersion and group velocity

$$\kappa_L = \frac{1}{3NV}\sum_{\mathbf{q}s} c_{\mathbf{q}s}\mathbf{v}_{g\,\mathbf{q}s}^2\tau_{\mathbf{q}s}$$

$$H = U_0 + \frac{1}{2}\sum_{ij\alpha\beta}\boldsymbol{\Phi}_{ij}^{\alpha\beta}u_i^\alpha u_j^\beta + \frac{1}{3!}\sum_{ijk\alpha\beta\gamma}\boldsymbol{\Phi}_{ijk}^{\alpha\beta\gamma}u_i^\alpha u_j^\beta u_k^\gamma + \cdots$$

$$D_{ij}^{\alpha\beta}(\mathbf{q}) = \sum_l \frac{\boldsymbol{\Phi}_{i,jl}^{\alpha\beta}}{\sqrt{m_i m_j}} exp\left[i\mathbf{q}\cdot\left(\boldsymbol{r}_i - \boldsymbol{r}_{jl}\right)\right]$$

$$\sum_{j\alpha} D_{ij}^{\alpha\beta}(\mathbf{q})e^\alpha(i,\mathbf{q}s) = \omega_{\mathbf{q}s}^2 e^\alpha(i,\mathbf{q}s)$$

$$\mathbf{v}_{g\mathrm{q}s} = \frac{\mathrm{d}\omega_{\mathbf{q}s}}{\mathrm{d}\mathbf{q}}$$

Phonopy

Togo et al., APL, 108, 1 (2015)

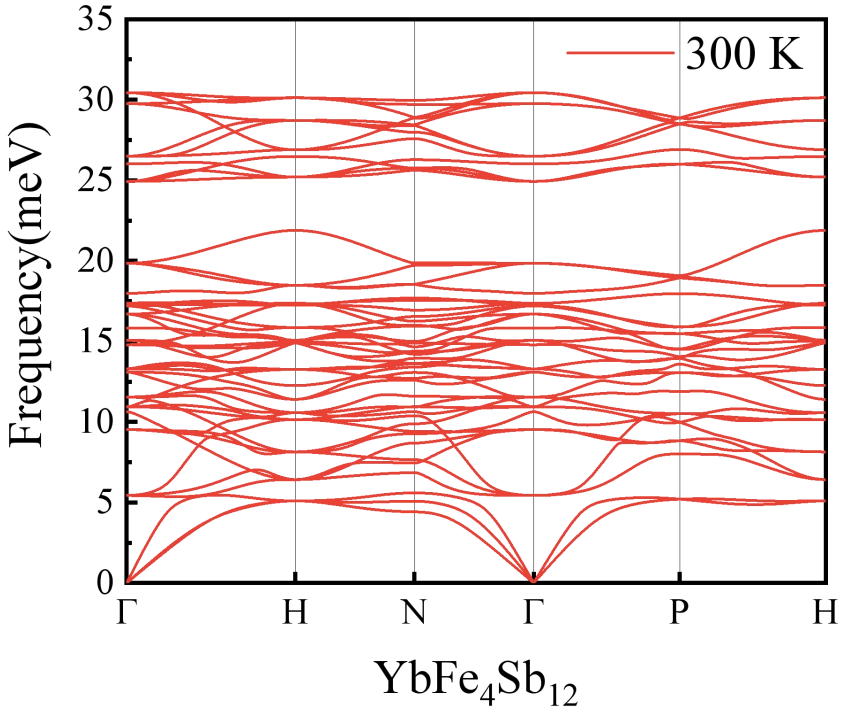

Phonon number and heat capacity

$$E_{qs} = \left(n_{\mathbf{q}s} + \frac{1}{2}\right)\hbar\omega_{\mathbf{q}s} \qquad n_{\mathbf{q}s} = \frac{1}{\exp\left(\frac{\hbar\omega_{\mathbf{q}s}}{k_B T}\right) - 1}$$

Bose-Einstein distribution

$$C = \left(\frac{dU}{dT}\right) = \left(\frac{d\sum_{s\mathbf{q}} E_{\mathbf{q}s}}{dT}\right) = \sum_{s\mathbf{q}} c_{\mathbf{q}s}$$

$$n_{\mathbf{q}s} = \frac{1}{\exp\left(\frac{\hbar\omega_{\mathbf{q}s}}{k_B T}\right) - 1} \sim \frac{k_B T}{\hbar\omega_{\mathbf{q}s}}$$

High-temperature limit

$c_{\mathbf{q}s} \sim k_B, \quad C \sim 3N_A k_B$

$$\mathrm{U}_{\mathrm{cart}}(j,T) = \frac{\hbar}{2Nm_j}\sum_{\mathbf{q},\nu}\omega_\nu(\mathbf{q})^{-1}(1+2n_\nu(\mathbf{q},T))\mathbf{e}_\nu(j,\mathbf{q})\otimes\mathbf{e}_\nu^*(j,\mathbf{q})$$

Phonon-phonon interaction

$$\kappa_L = \frac{1}{3NV}\sum_{\mathbf{q}s} c_{\mathbf{q}s}\mathbf{v}_{g\,\mathbf{q}s}^2\tau_{\mathbf{q}s}$$

$$H = U_0 + \frac{1}{2}\sum_{ij\alpha\beta}\boldsymbol{\Phi}_{ij}^{\alpha\beta}u_i^\alpha u_j^\beta + \frac{1}{3!}\sum_{ijk\alpha\beta\gamma}\boldsymbol{\Phi}_{ijk}^{\alpha\beta\gamma}u_i^\alpha u_j^\beta u_k^\gamma + \cdots$$

$$\boldsymbol{\Phi}_{\lambda\lambda'\lambda''} = \sum_{ijk}\sum_{\alpha\beta\gamma}\frac{e^\alpha(i,\lambda)e^\beta(j,\lambda')e^\gamma(k,\lambda'')}{\sqrt{m_i m_j m_k}\sqrt{\omega_\lambda\omega_{\lambda'}\omega_{\lambda''}}}\boldsymbol{\Phi}_{ijk}^{\alpha\beta\gamma}e^{i(q\cdot r_i + q'\cdot r_j + q''\cdot r_k)}$$

Scattering strength

$$\tau_\lambda^{-1}(\omega) = \frac{\hbar\pi}{8}\sum_{\lambda',\lambda''}|\boldsymbol{\Phi}_{\lambda\lambda'\lambda''}|^2[(n_{\lambda'}+n_{\lambda''}+1)\delta(\omega-\omega_{\lambda'}-\omega_{\lambda''}) + 2(n_{\lambda'}-n_{\lambda''})\delta(\omega-\omega_{\lambda'}+\omega_{\lambda''})]\Delta_{\boldsymbol{qq'q''}}$$

Scattering phase space

$$\begin{cases}\hbar\omega_\lambda \pm \hbar\omega_{\lambda'} = \hbar\omega_{\lambda''} \\ \boldsymbol{q}+\boldsymbol{q}' = \boldsymbol{q}'' + \boldsymbol{G}\end{cases}$$

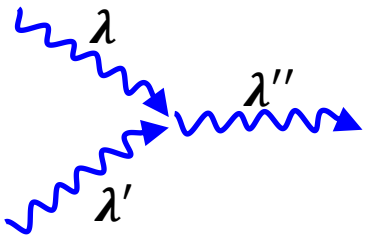

$$n_{\mathbf{q}s} \sim \frac{k_B T}{\hbar\omega_{\mathbf{q}s}}$$

ShengBTE

Phono3py

Li et al., PRB, 185, 1747 (2014)

Togo et al., PRB, 91, 094306 (2015)

Role of scattering phase space

Filled skutterudites Yb(Ba)Fe_4Sb_{12}

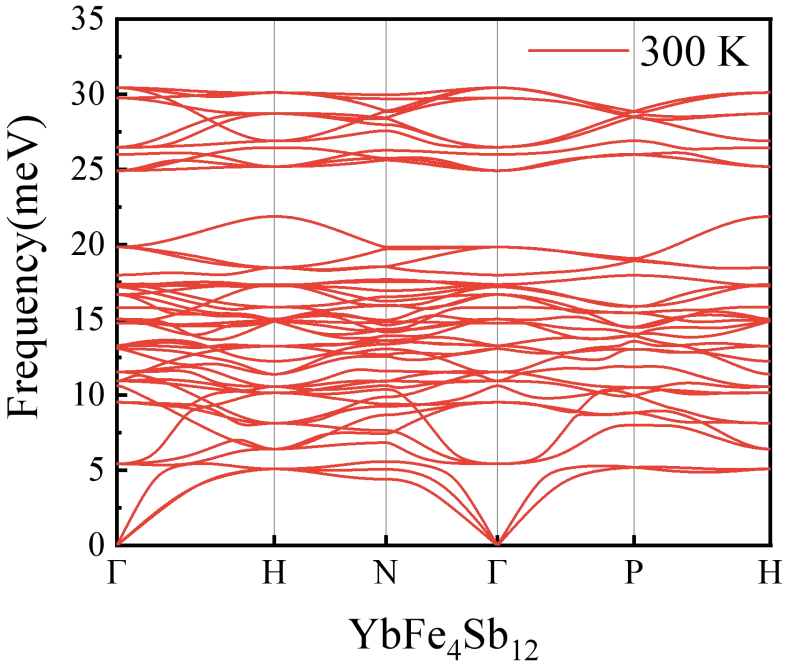

The avoided-crossing filler modes greatly enhance the scattering phase space of $YbFe_4Sb_{12}$.

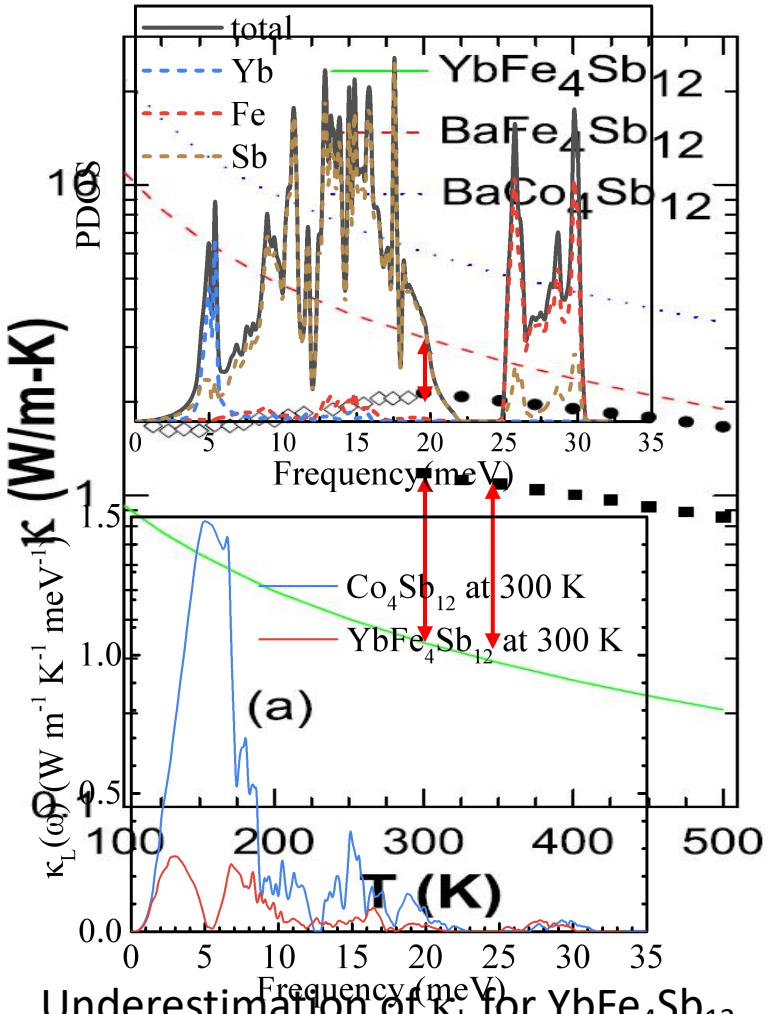

- Underestimation of κ_L for $YbFe_4Sb_{12}$
- Incorrect temperature dependence of κ_L

Li et al., PRB, 91, 144304 (2015)

Direct calculation of κ_L for V_2VI_3

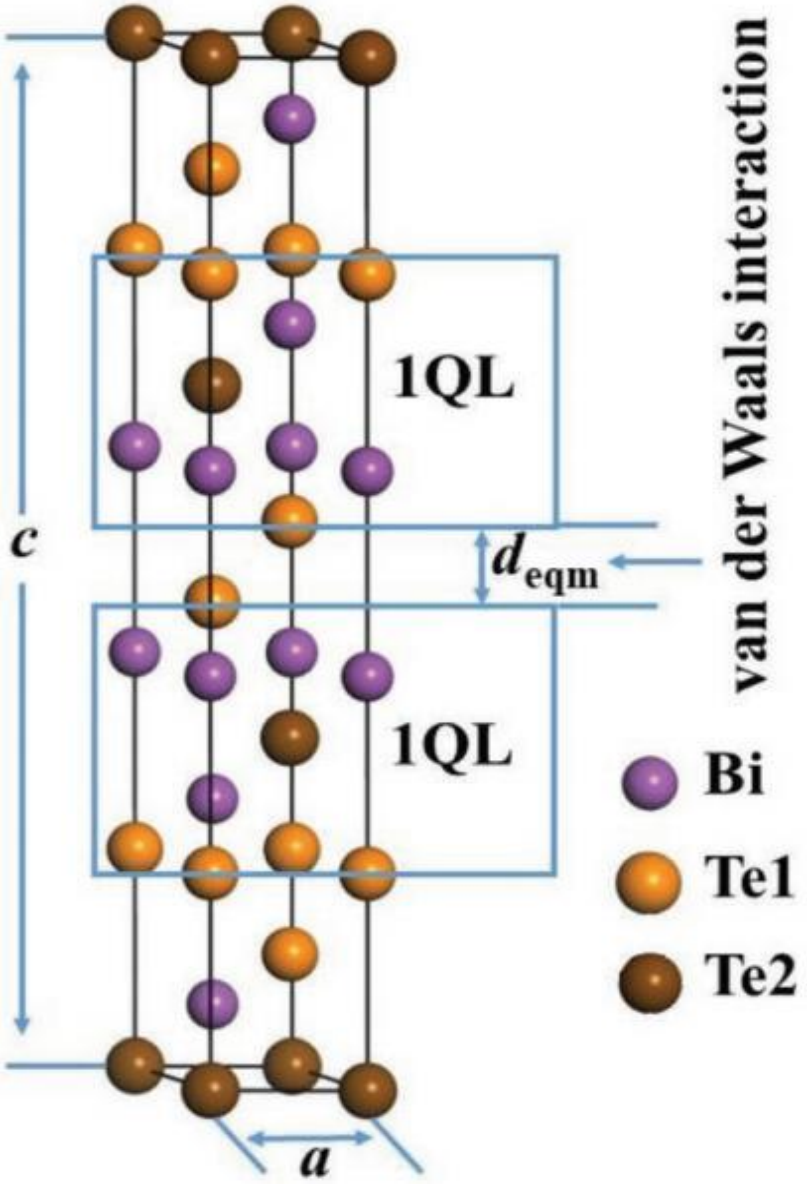

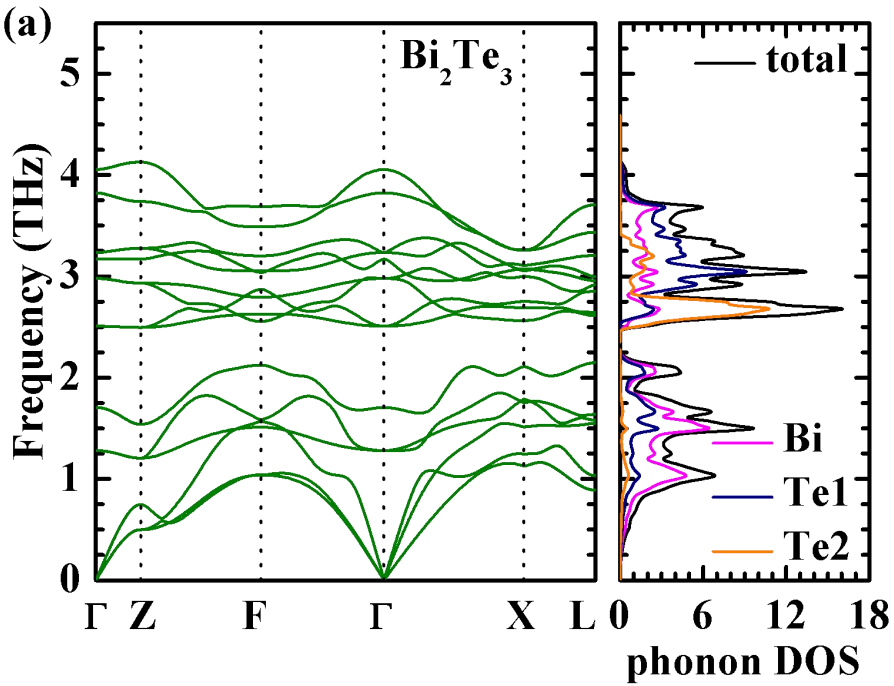

- *Ab initio* molecular dynamics (AIMD)
- 300 K
- $\Phi^{\alpha\beta}$ and $\Phi^{\alpha\beta\gamma}$ are obtained by fitting the potential energy in AIMD.

TDEP

Hellman et al., PRB, 88, 144301 (2013)

Fang, Yang, Zhao, Zhu, et al., Adv. Funct. Mater., 29, 1900677 (2019)

Direct calculation of κ_L for V_2VI_3

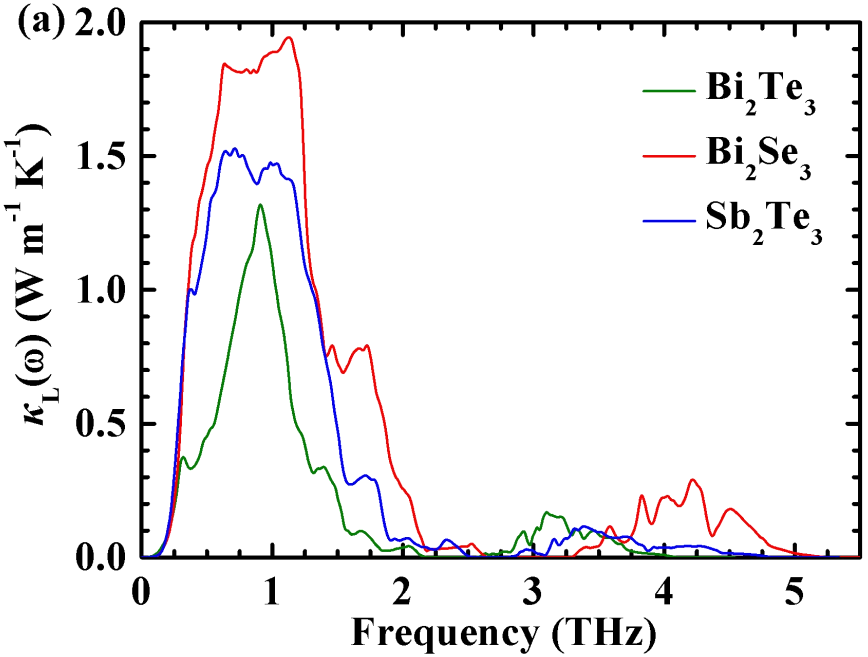

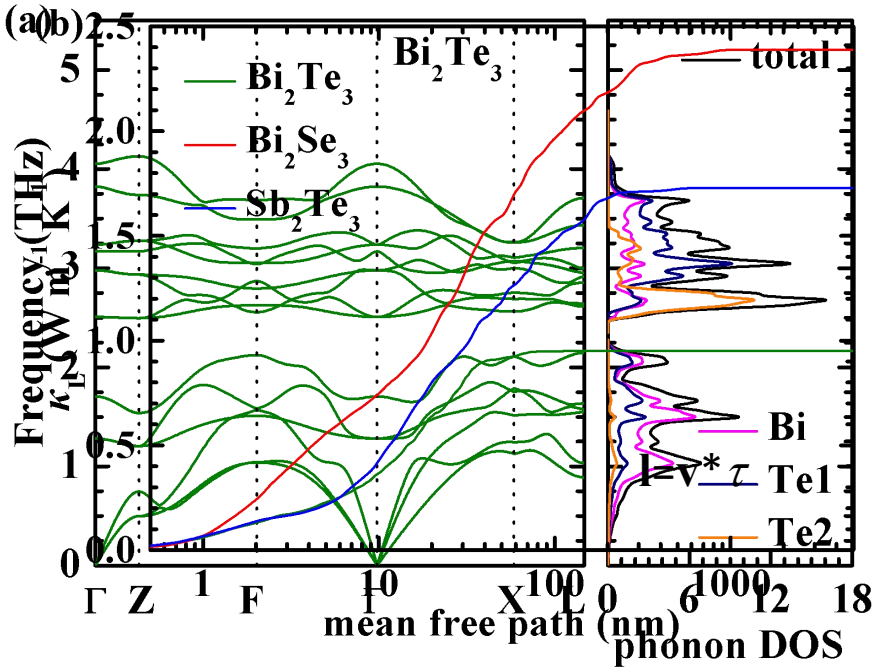

- The phonons contribute most of the κ_L are around 1 THz in V_2VI_3.
- Grain size within tens of nanometers is necessary to reduce the κ_L of V_2VI_3.

Fang, Yang, Zhao, Zhu, et al., Adv. Funct. Mater., 29, 1900677 (2019)

Direct calculation of κ_L for Mg_3Sb_2

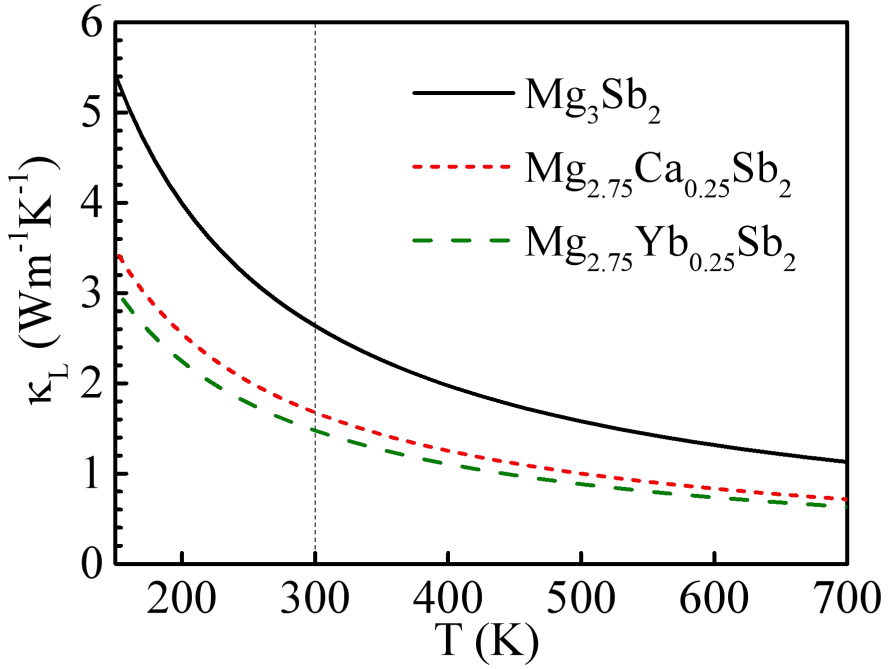

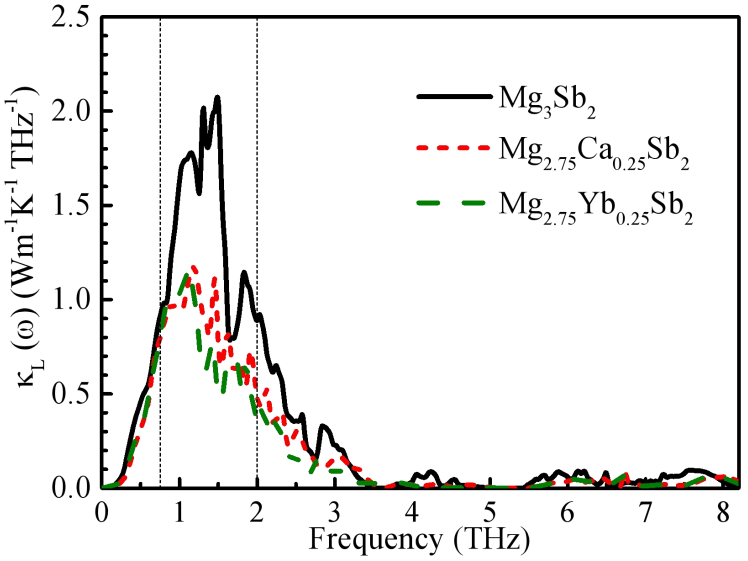

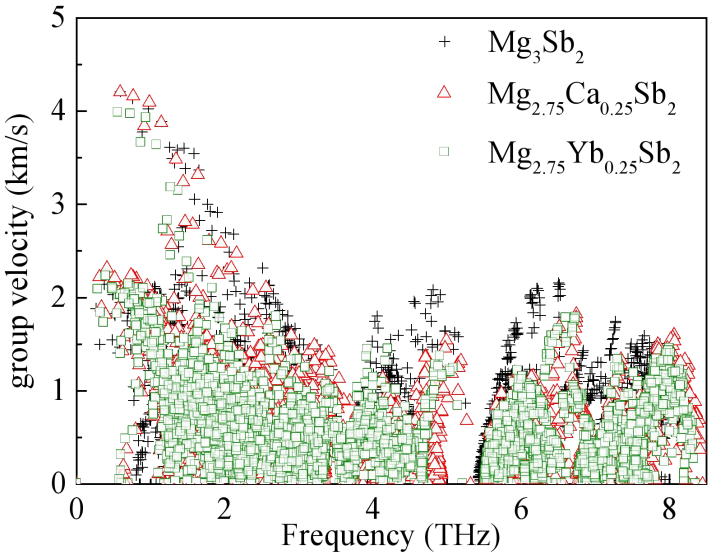

- Dopants in Mg_3Sb_2 reduce the phonon group velocities within 0.75 ~ 2 THz.

Sun, Dronskwoski, Yang, Zhang, et al., J. Comput. Chem., 40, 1693 (2019)

热输运性质

- 热导率基本概念及传统模型
- 声子及三声子计算
- 最新方向
  - 声子重整化
  - 其他散射机制（电声相互作用等）
  - 更高阶声子相互作用
  - 机器学习势函数用于热输运

$$\Phi^{\alpha\beta}(T) \qquad \Phi^{\alpha\beta\gamma}(T)$$

Temperature Dependent IFCs

Crystal structure of Mg_3Sb_2

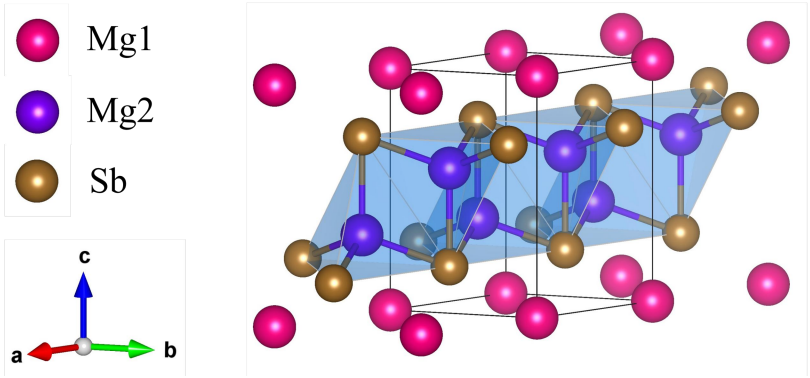

Zintl compound Space group $p\bar{3}m1$

Mg1 coordination

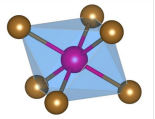

Mg^{2+} ionic layer

Octahedral site

Mg2 coordination

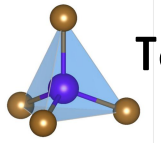

$[Mg_2Sb_2]^{2-}$ Covalent layer

Tetrahedral site

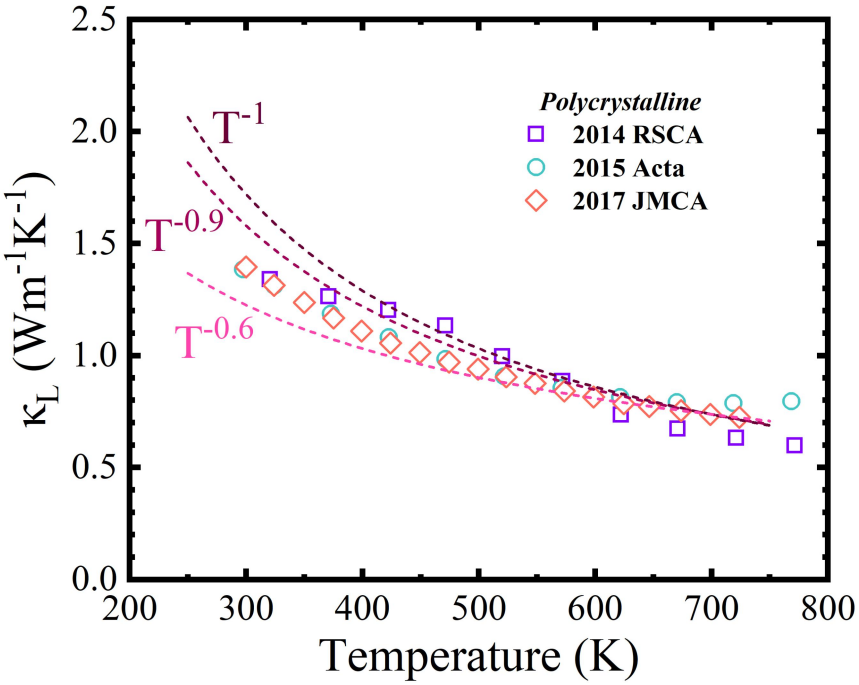

Thermal expansion

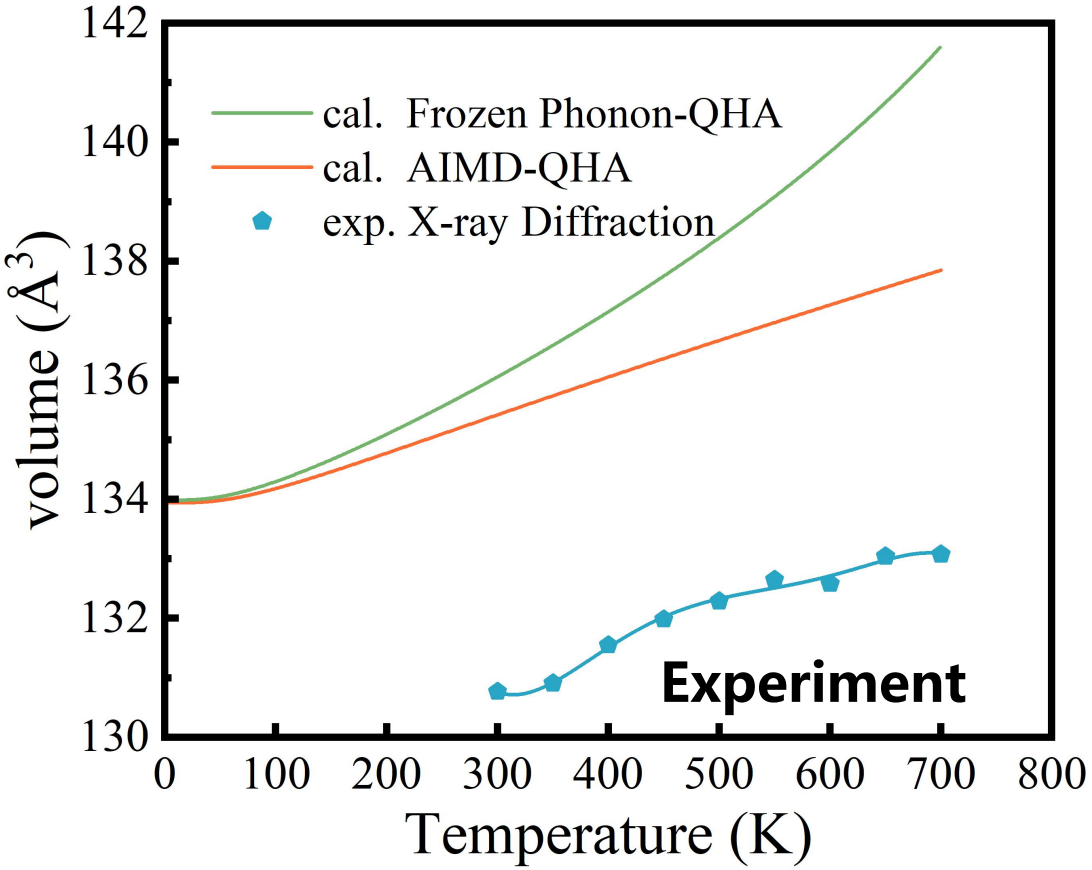

- Thermal expansion obtained from AIMD is more consistent with experiment.

Thermal conductivity

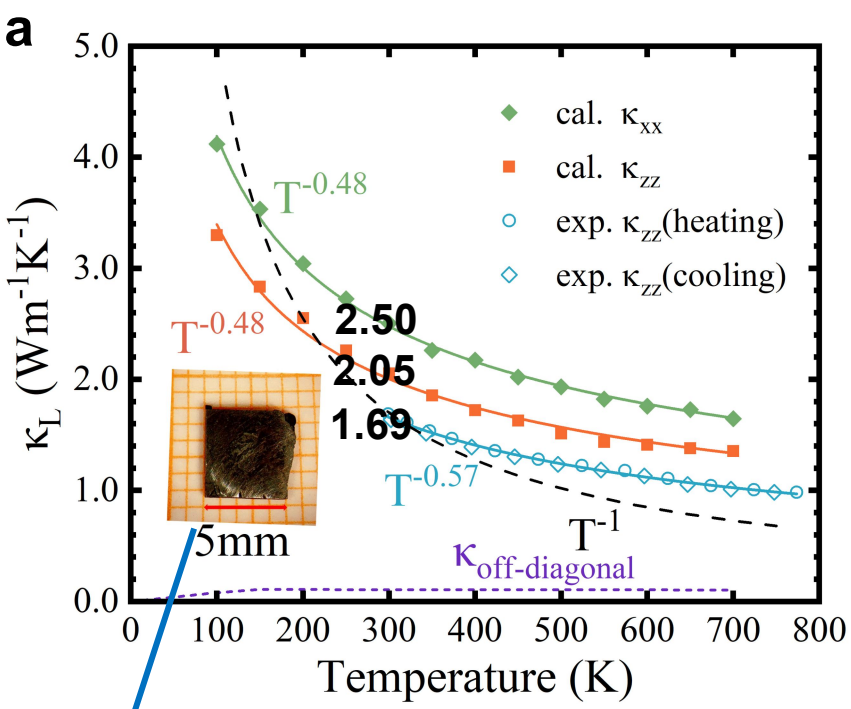

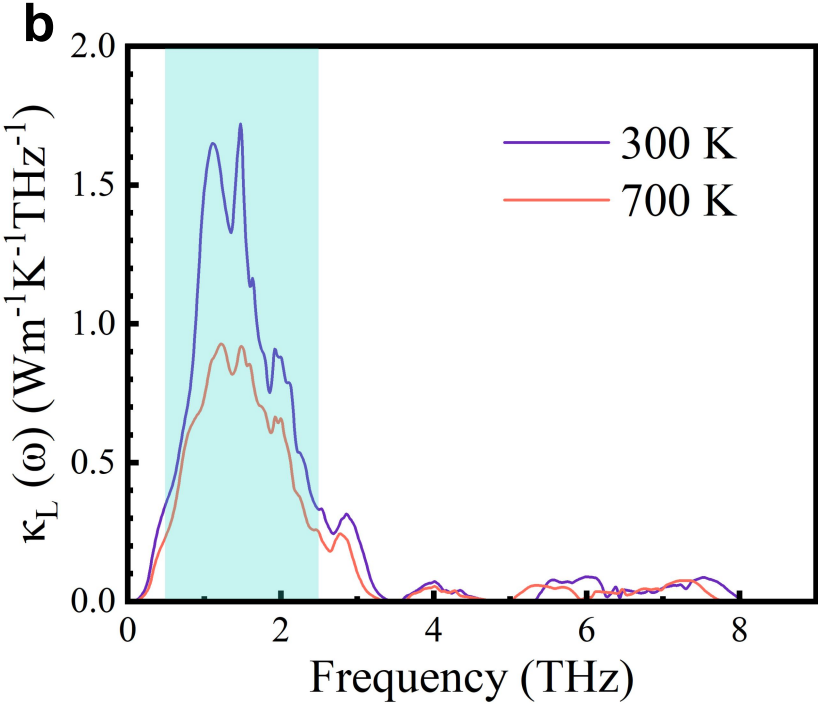

Mg_3Sb_2 Single Crystal

- Weak temperature depdendent κ_L of Mg_3Sb_2 in both calculations and experiments.

Renormalization on 2nd-order force constant

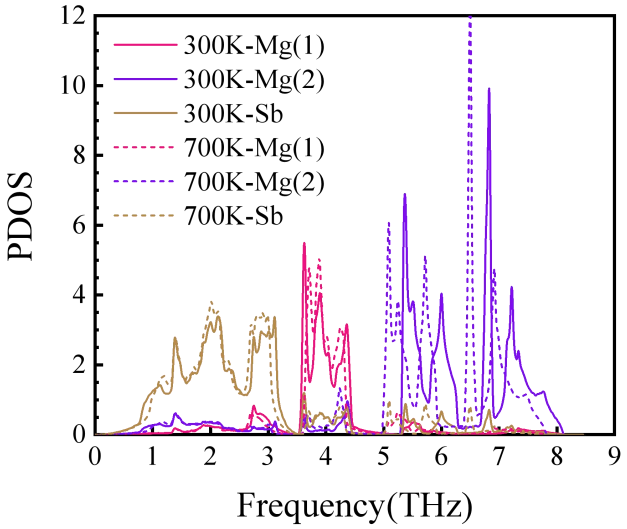

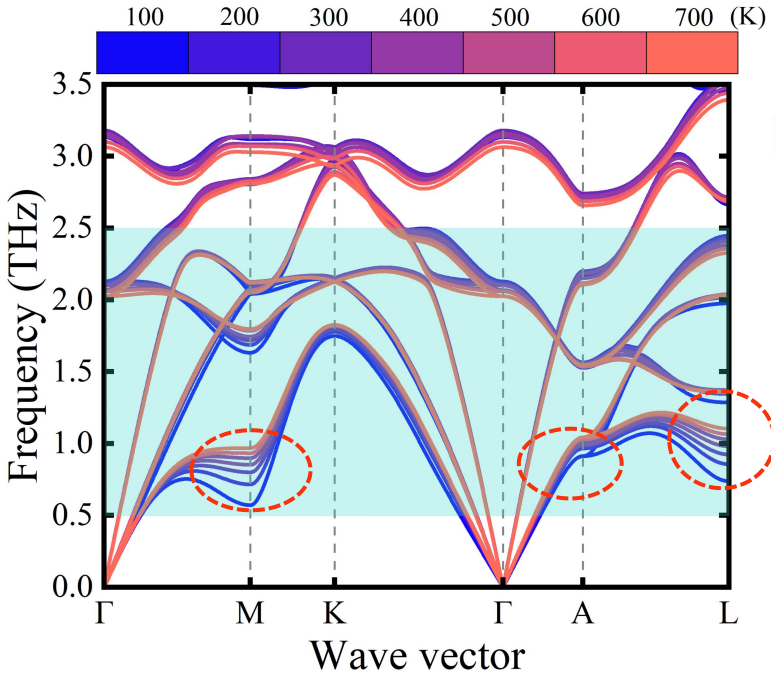

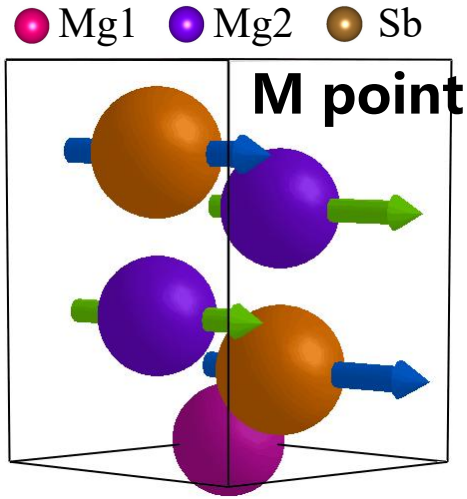

- Hardening effect on lower frequency phonons due to the head-to-head motions at BZ boundary

Scattering rate

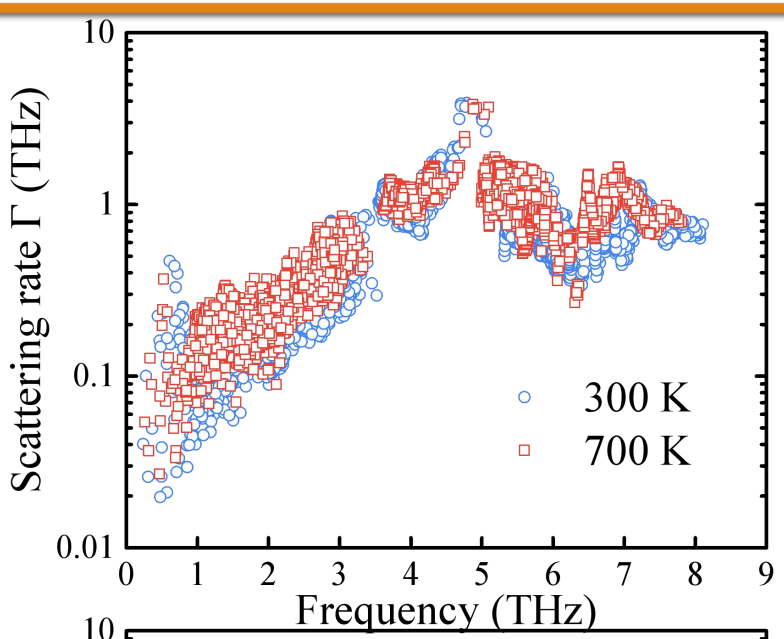

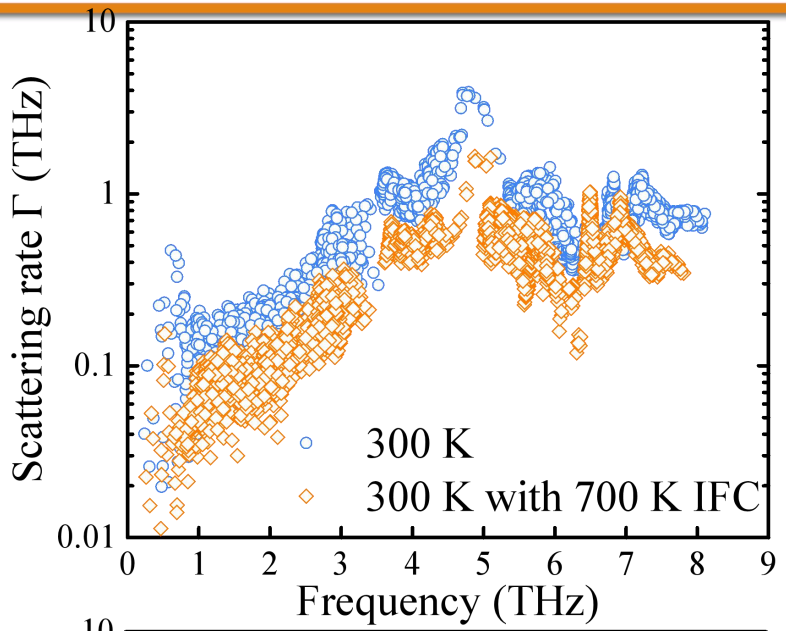

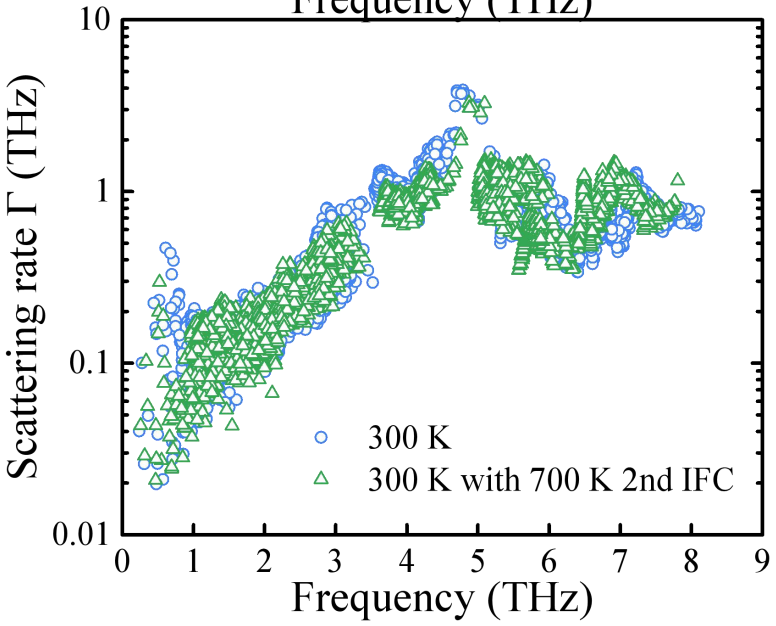

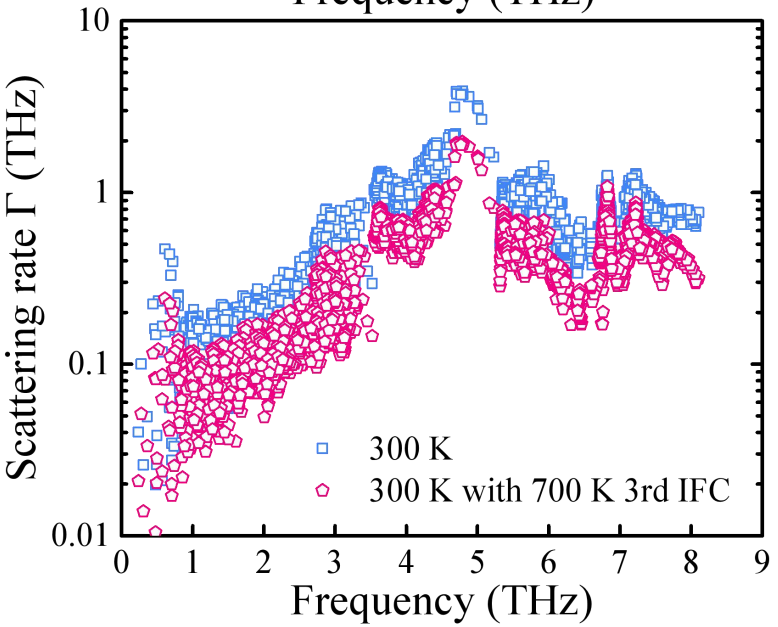

Gruneisen parameter

$$\gamma_{\mathbf{q}s} = -\frac{1}{6\omega_{\mathbf{q}s}^2} \sum_{ijk\alpha\beta\gamma} \frac{\epsilon_{\mathbf{q}s}^{i\alpha\dagger} \epsilon_{\mathbf{q}s}^{j\beta}}{\sqrt{m_i m_j}} r_k^{\gamma} \Phi_{ijk}^{\alpha\beta\gamma} e^{i\mathbf{q}\cdot\mathbf{r}_j}$$

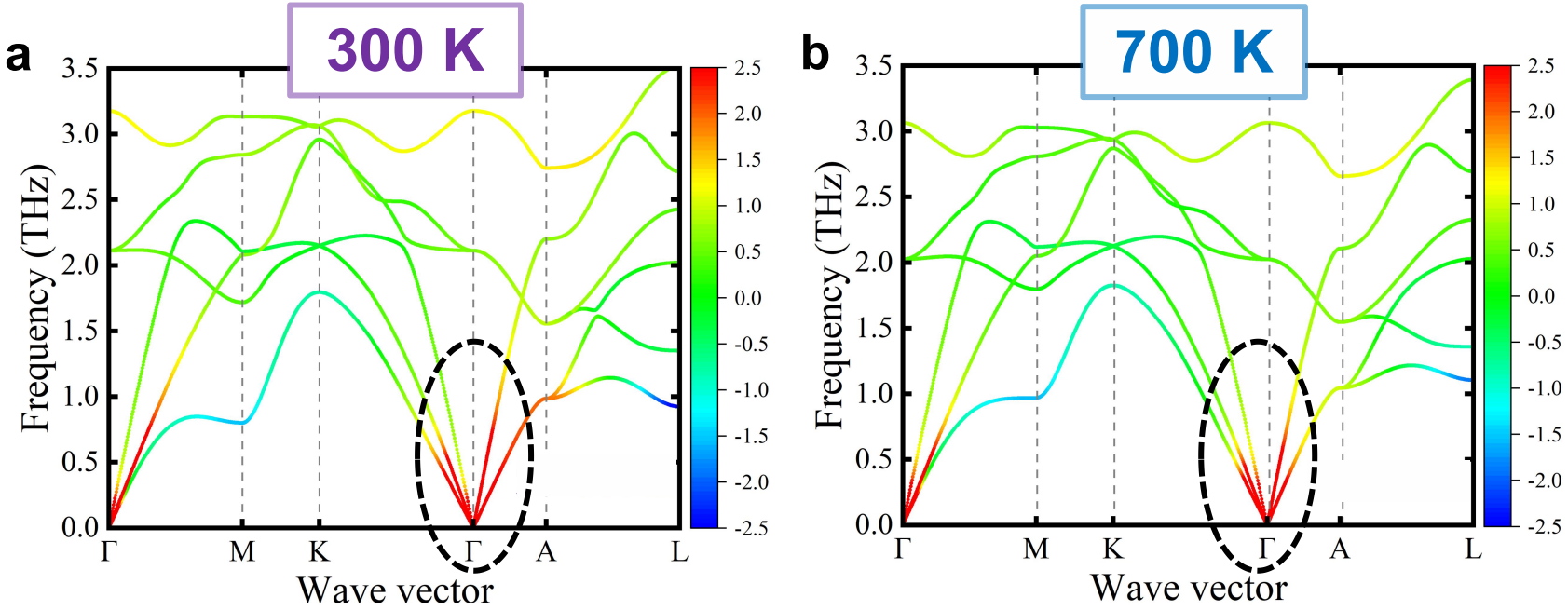

- Large Gruneisen parameters at BZ boundary.
- Lower Gruneisen parameters at higher temperatures → lower anharmonicity and 3rd-force constants

Renormalization of 3rd-order force constants

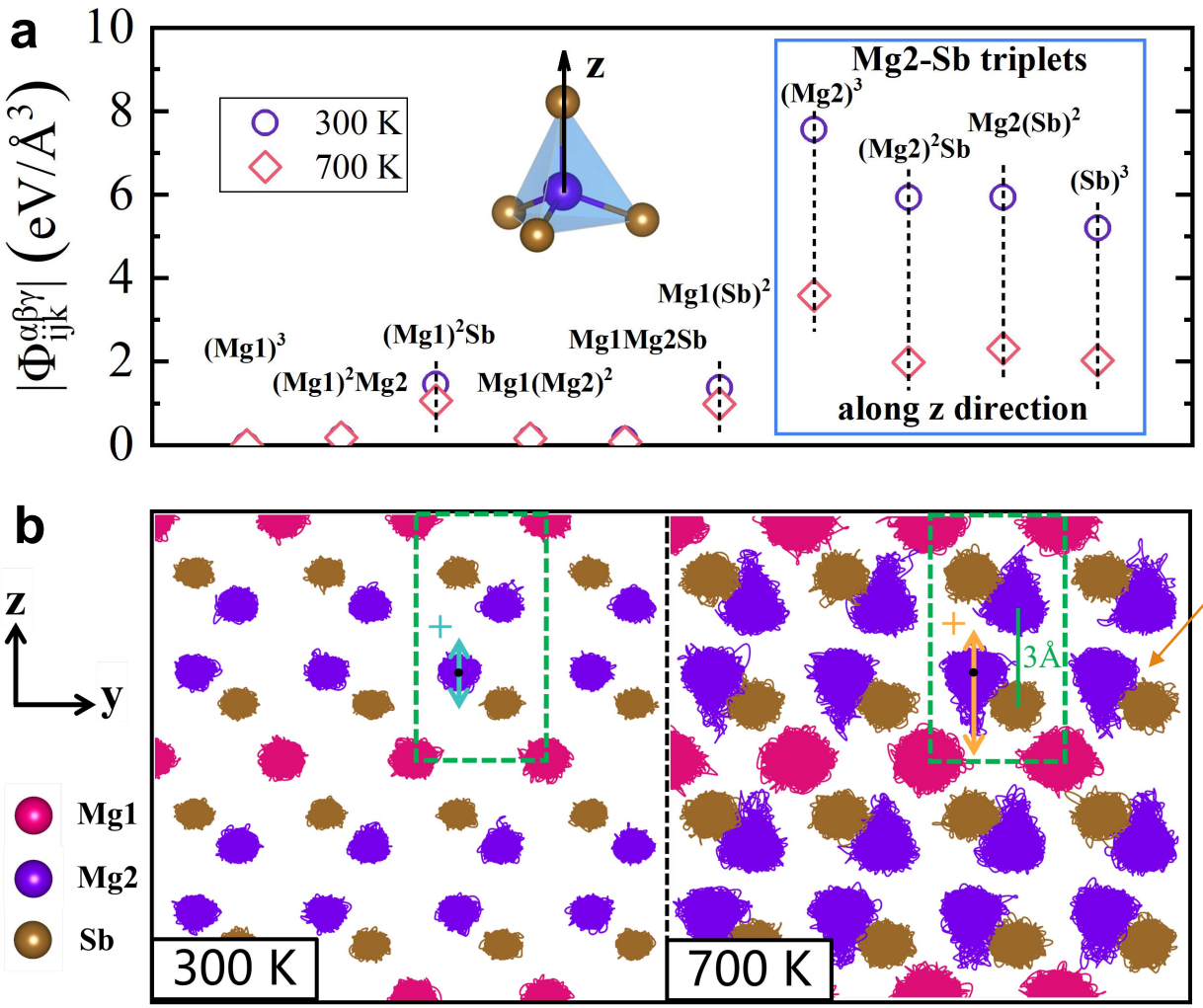

Asymmetrical vibrations of Mg2 at high temperatures

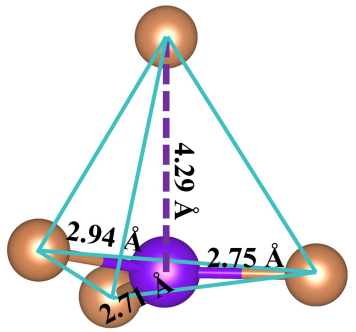

Zhu, Yang, Fu, Zhang et al., Research, 2020, 4589786 (2020)

Explicit El-ph interaction in Ph-trans

$$\frac{1}{\tau^{\mathrm{EP}}_{\mathbf{q}\lambda}} = \frac{2\pi}{\hbar} \sum_{mn,\ \mathbf{k}} |g_{mn\lambda}(\mathbf{k},\mathbf{q})|^2 \left(f_{n\mathbf{k}} - f_{m\mathbf{k+q}}\right)\delta\left(\varepsilon_{n\mathbf{k}} - \varepsilon_{m\mathbf{k+q}} - \hbar\omega_{\mathbf{q}\lambda}\right)$$

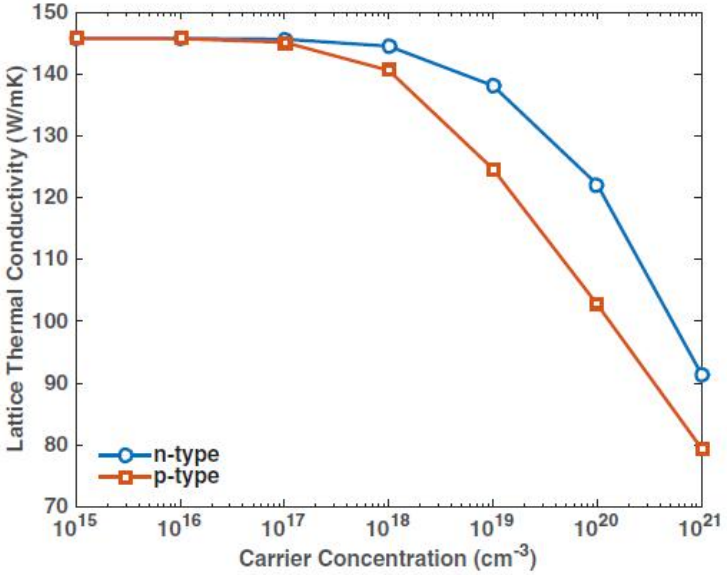

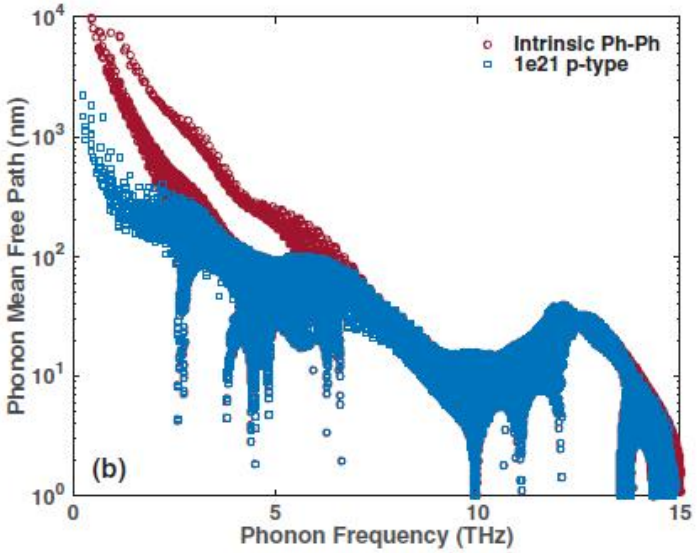

Liao et al., PRL, 114, 115901 (2015) **Fan et al., J. Mater. Chem. A, 6, 12125 (2018)**

Influences of el-ph on Ph-trans

$$\tau_{EP}^{-1} = \frac{4nm^* v_F L_e \omega^2}{15dv^2} \quad \text{for} \quad qL_e << 1$$

$$\tau_{EP}^{-1} = \frac{\pi nm^* v_F \omega}{6dv} \quad \text{for} \quad qL_e >> 1$$

$$\frac{1}{\tau_{\mathbf{q}}} = \frac{1}{\tau_U} + \frac{1}{\tau_{e-p}}$$

$$\frac{1}{\tau_{\mathbf{q}\lambda}^{\mathrm{EP}}} = \frac{2\pi}{\hbar} \sum_{mn,\,\mathbf{k}} |g_{mn\lambda}(\mathbf{k},\mathbf{q})|^2 \left(f_{n\mathbf{k}} - f_{m\mathbf{k}+\mathbf{q}}\right) \delta\left(\varepsilon_{n\mathbf{k}} - \varepsilon_{m\mathbf{k}+\mathbf{q}} - \hbar\omega_{\mathbf{q}\lambda}\right)$$

- Less sensitive to temperature, comparing with U process
- The influence of EPI on phonon transport is determined by: Temperature; relative magnitude comparing with U process; EPI coupling matrix; band-related quantities (carrier, effective mass)

Case study—2D MoS_2, PtSSe

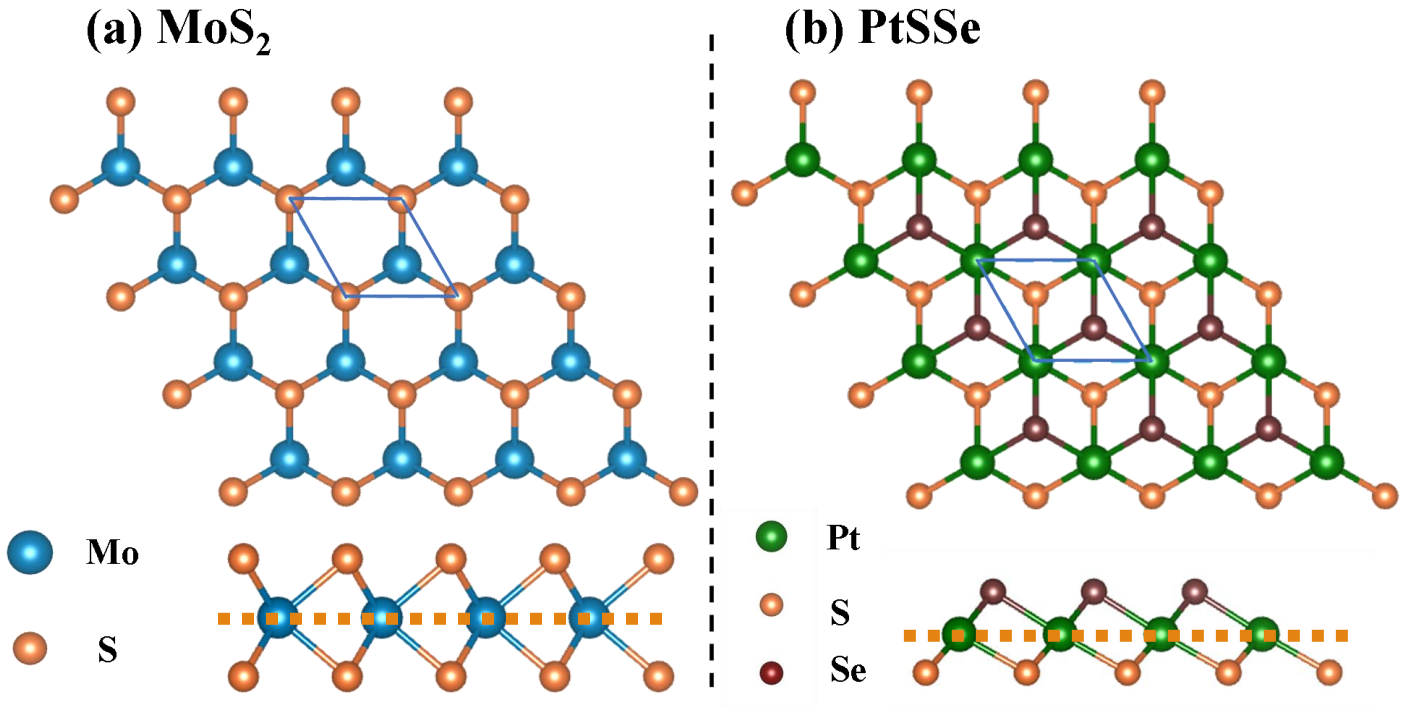

- MoS_2 has the horizonal mirror symmetry (σ_h symmetry), while PtSSe doesn't.

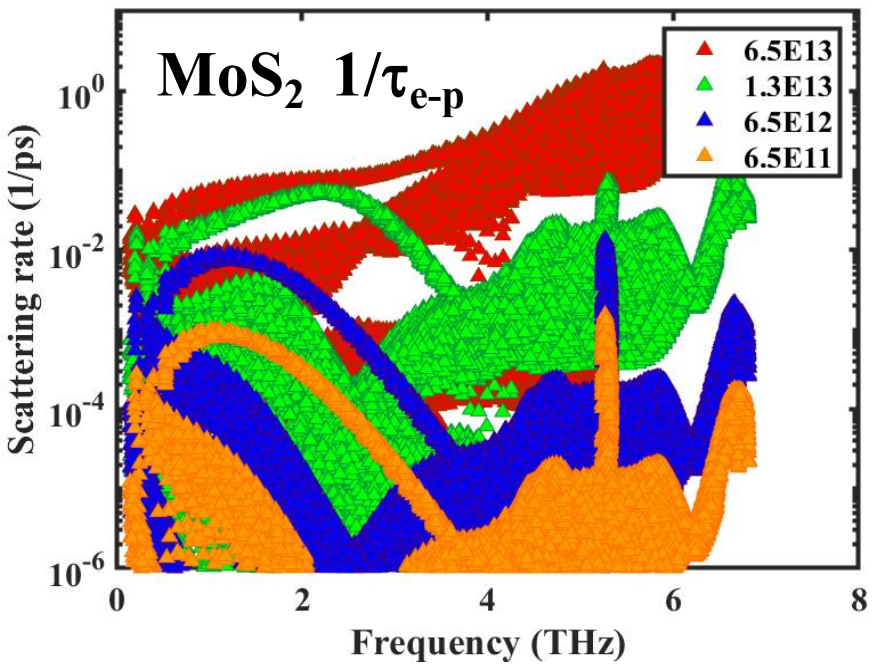
MoS2 1/τe-p
6.5E13
1.3E13
6.5E12
6.5E11
Scattering rate (1/ps)
Frequency (THz)

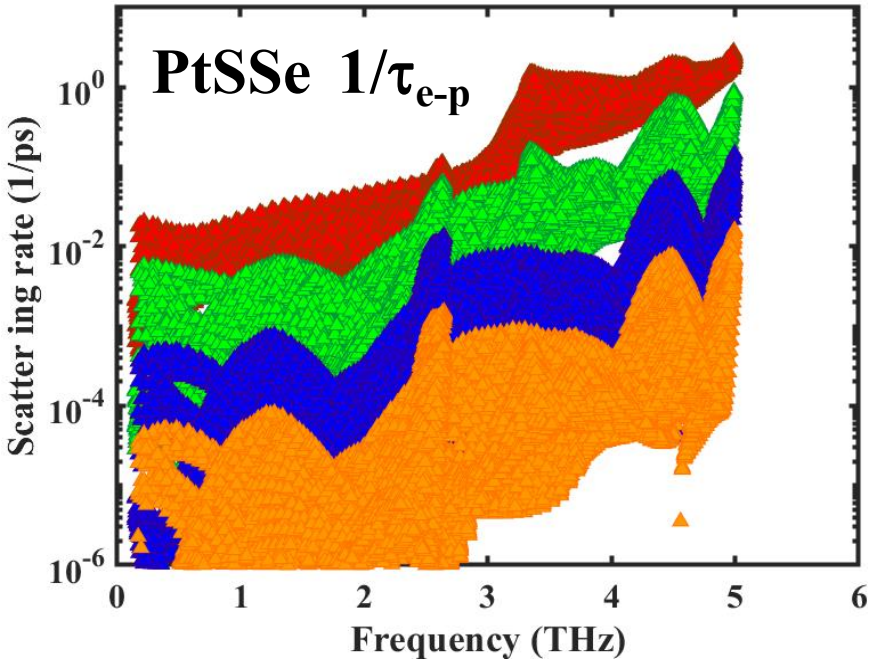
PtSSe 1/τe-p
Scatter ing rate (1/ps)
Frequency (THz)

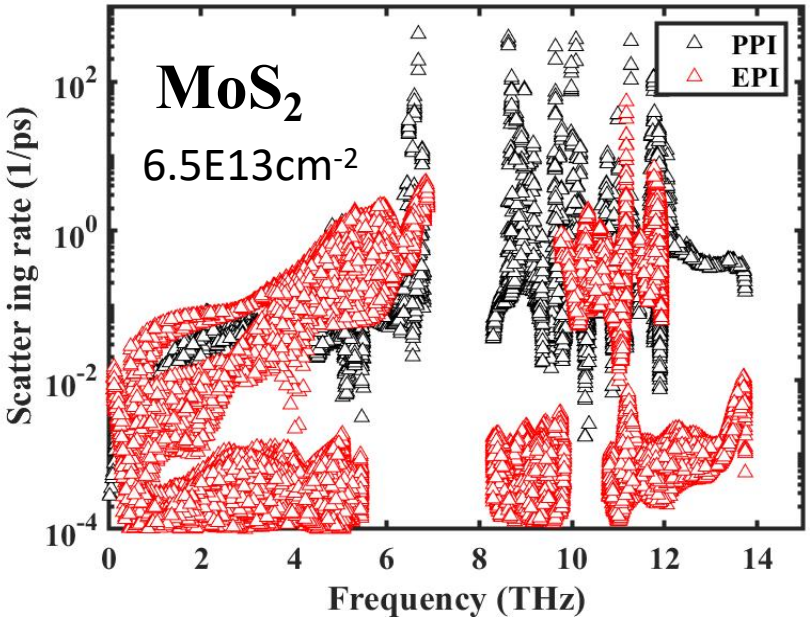
MoS2
6.5E13cm-2
PPI
EPI
Scatter ing rate (1/ps)
Frequency (THz)

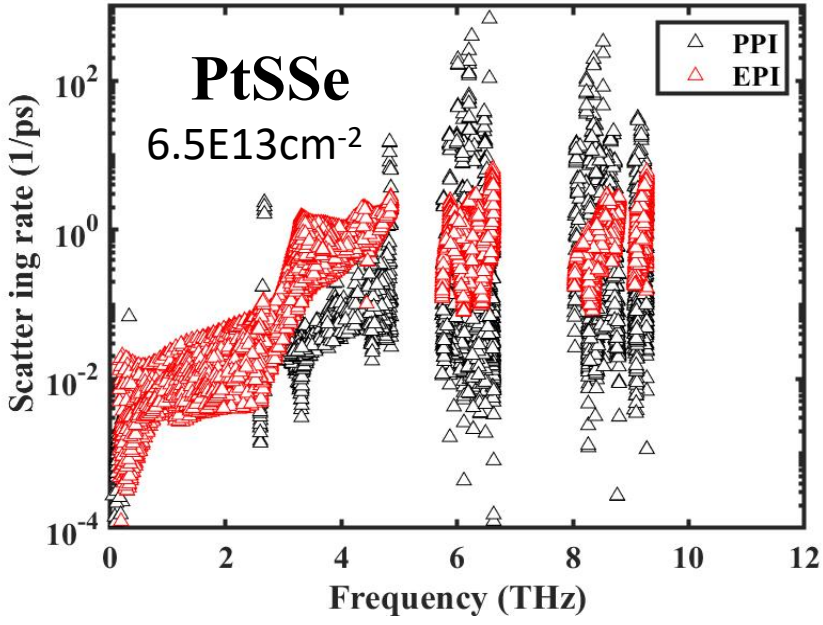
PtSSe
6.5E13cm-2
PPI
EPI
Scatter ing rate (1/ps)
Frequency (THz)

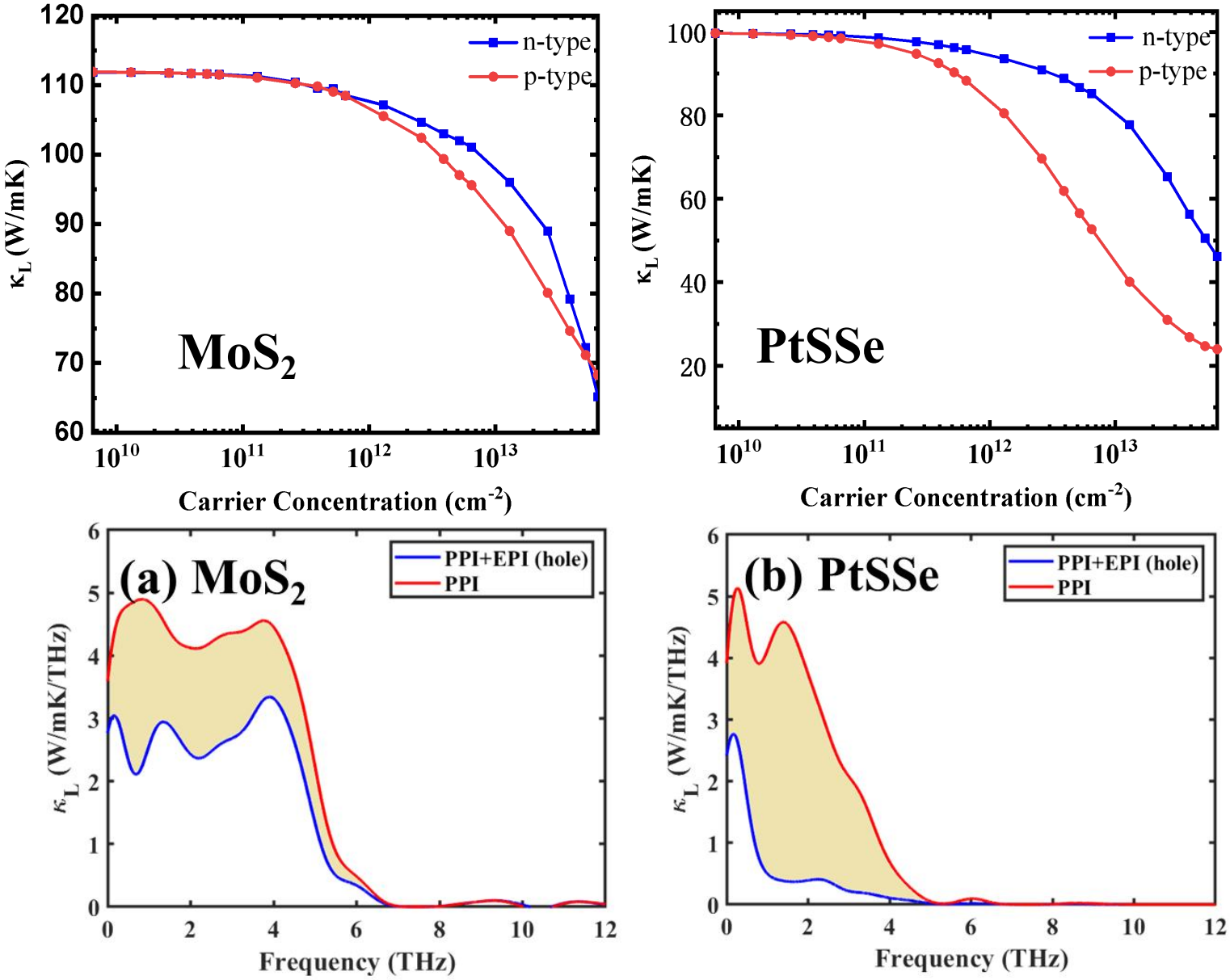

- At 300 K and 6.5*10^{13} cm^{-2}, the reduction of EPI is 39 % for MoS_2 and 78 % for PtSSe.

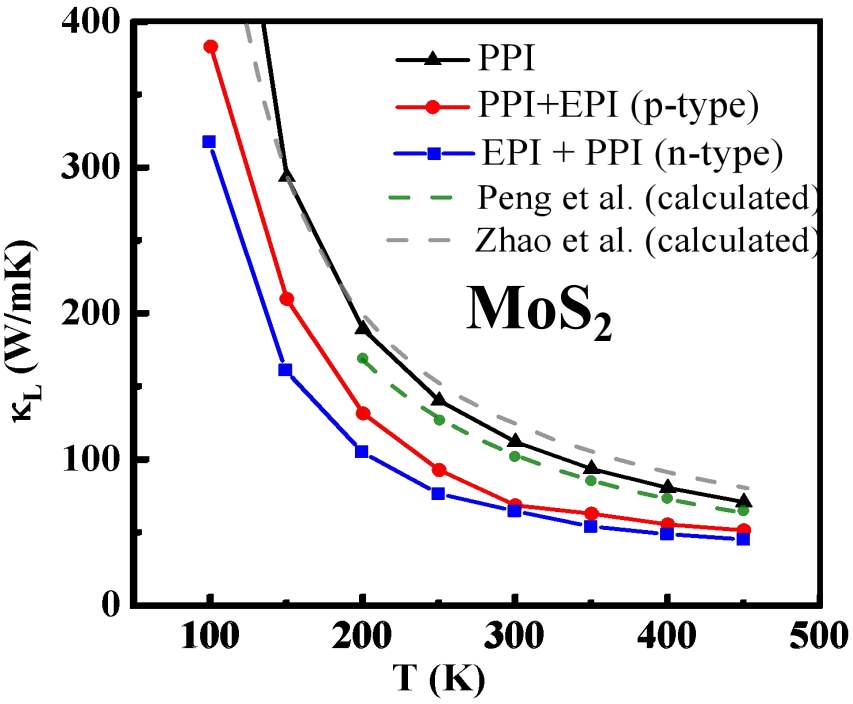

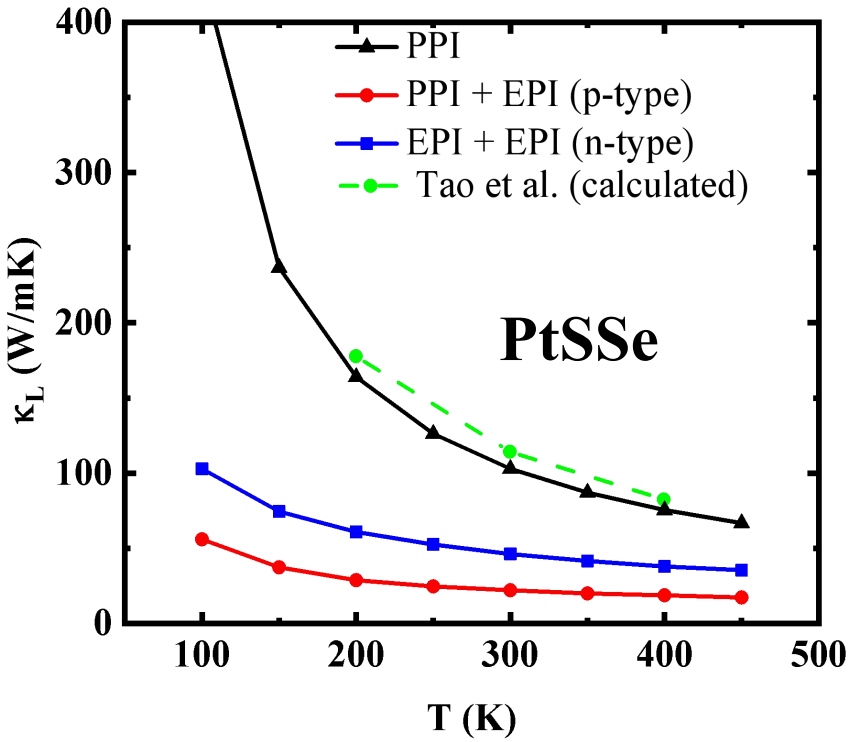

- The temperature dependence of κ_L due to both EPI (6.5E13 cm^{-2}) and PPI is reduced to $T^{-0.6}$ above 300 K for p-type.

Difference between MoS_2 and PtSSe

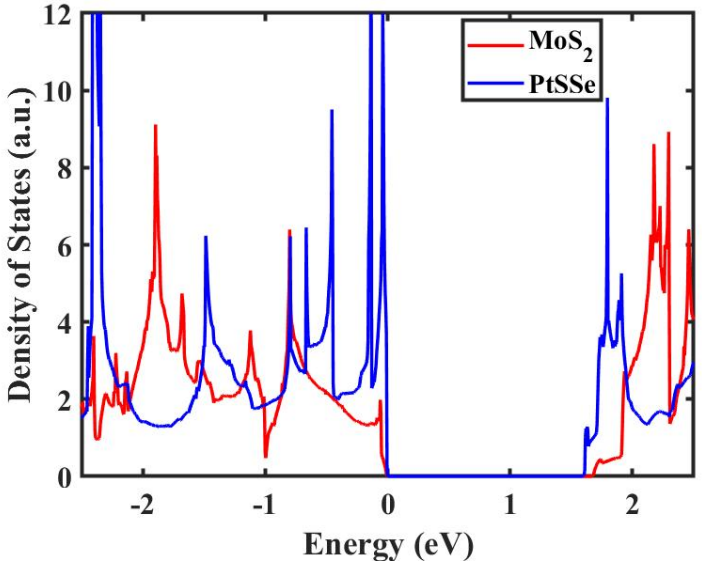

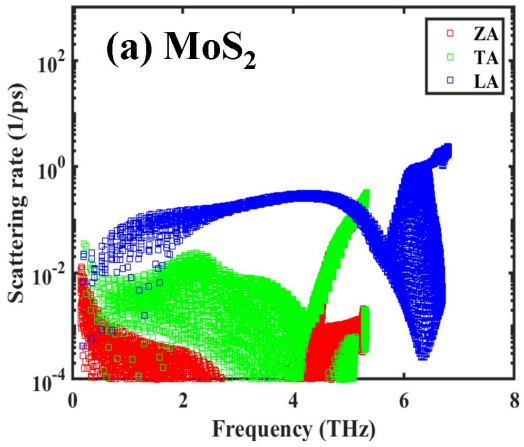

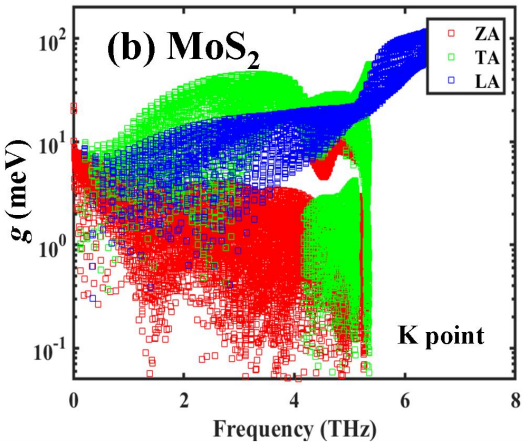

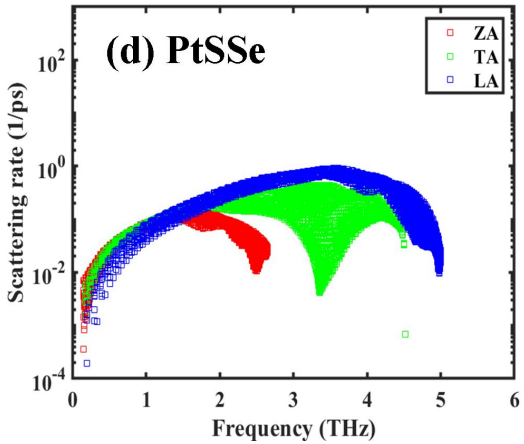

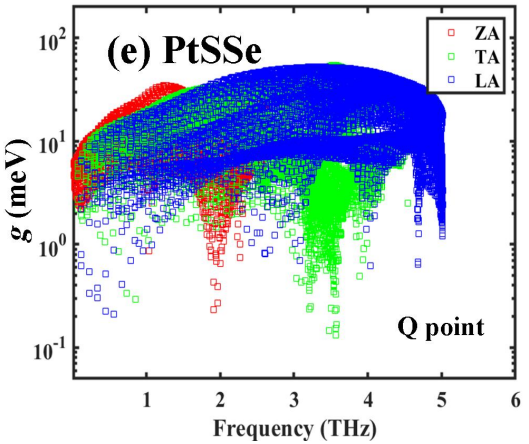

$$\frac{1}{\tau_{\mathbf{q}\lambda}^{\mathrm{EP}}} = \frac{2\pi}{\hbar} \sum_{mn,\,\mathbf{k}} |g_{mn\lambda}(\mathbf{k},\mathbf{q})|^2 \left(f_{n\mathbf{k}} - f_{m\mathbf{k}+\mathbf{q}}\right) \delta\left(\varepsilon_{n\mathbf{k}} - \varepsilon_{m\mathbf{k}+\mathbf{q}} - \hbar\omega_{\mathbf{q}\lambda}\right)$$

- PtSSe has higher band edge DOS.
- PtSSe has higher g for ZA, due to the broken of the σ_h symmetry.*

*PRL, 17, 1133, 1988

Liu, Yao, Yang, Xi, Ke, Mater. Today Phys. 15, 100277 (2020)

电热输运程序只是手段；

想明白做什么才是关键！